THE DARK SIDE
OF THE UNIVERSE

Istituto Nazionale di Fisica Nucleare
Sezione di Cagliari

Matteo Cadeddu
On behalf of the **DarkSide Cagliari group**
Mini-Simposio Fisica Alte Energie
Cagliari, 11 November 2019

The Dark Matter paradigm

Velocity dispersion of spiral galaxies

In the 1970s, Ford and Rubin discovered that rotation curves of galaxies are flat.

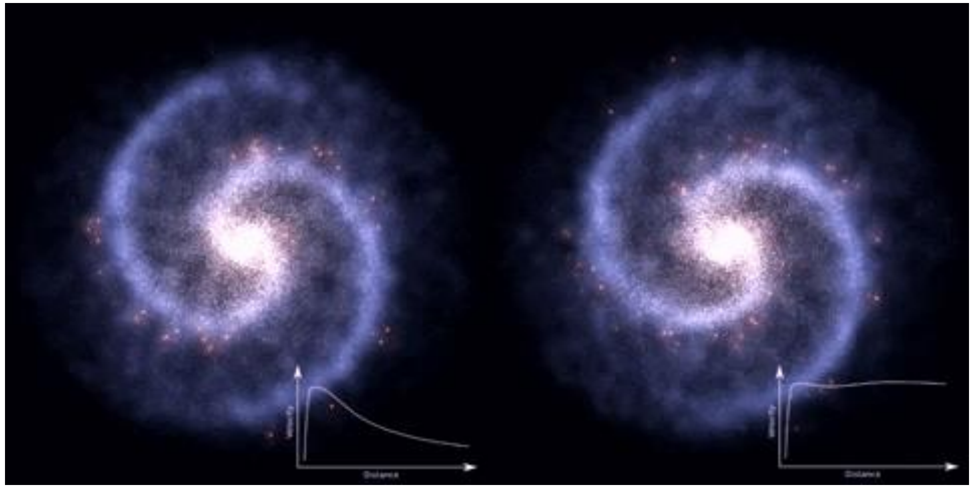

Cosmic Microwave Background

CMB temperature and power spectrum

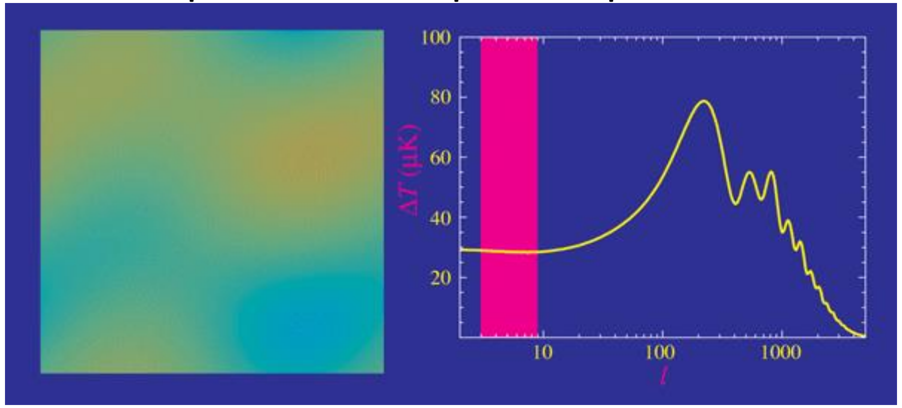

Bullet cluster and gravitational lensing

Lensing and optical observation of two galaxy clusters collision.

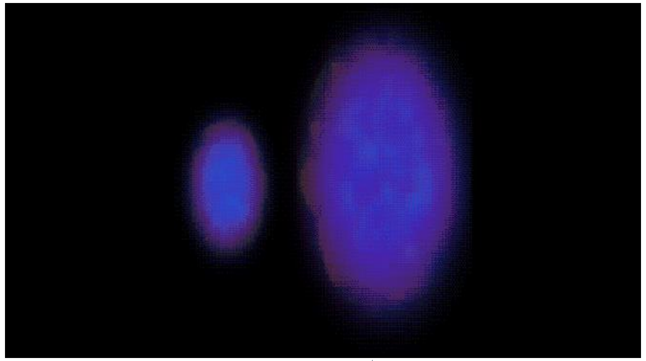

ΛCDM model ?

Detection of Dark Matter

The most searched candidate is a **Weakly Interacting Massive Particle (WIMP)**

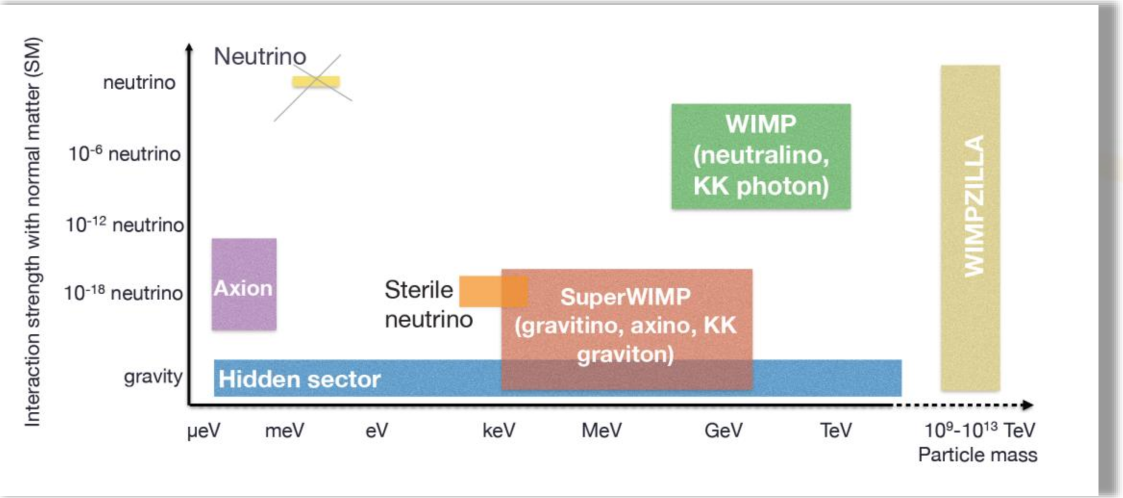

Direct detection

Nuclear recoils from elastic scattering

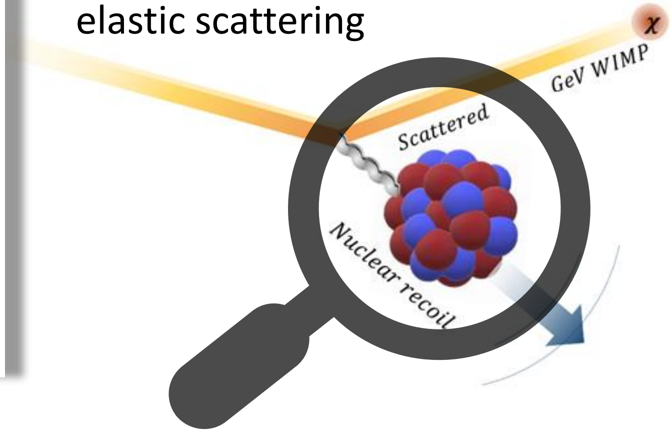

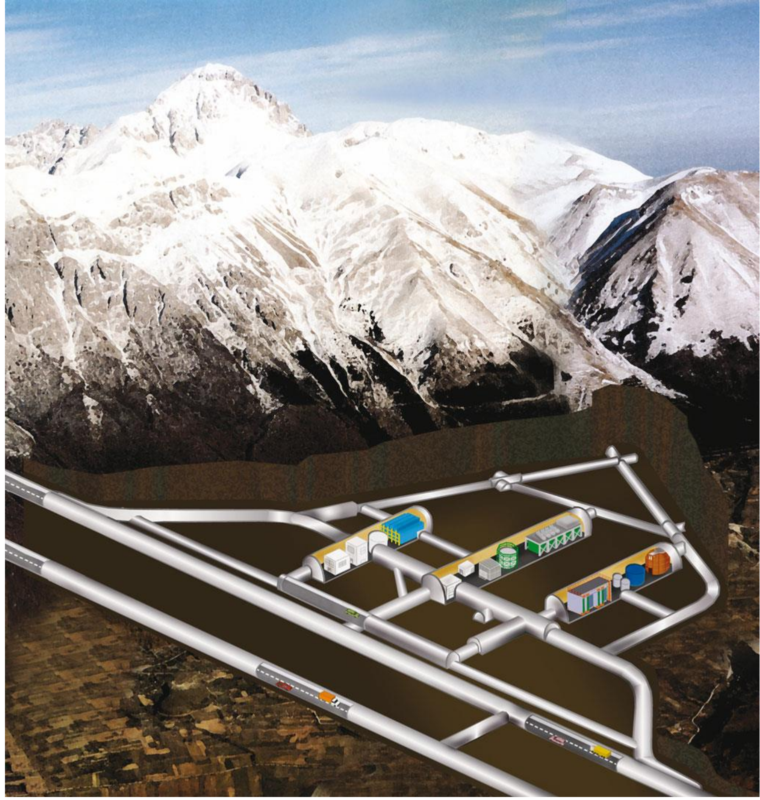

Accelerator searches

Missing ET, mono-'objects', etc…
Can it establish that the new particle is the DM?

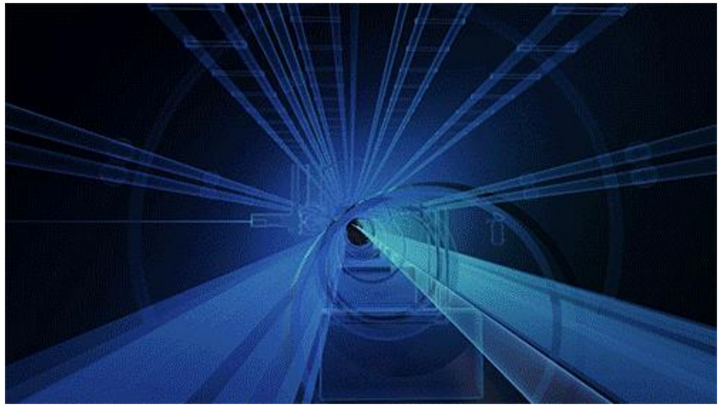

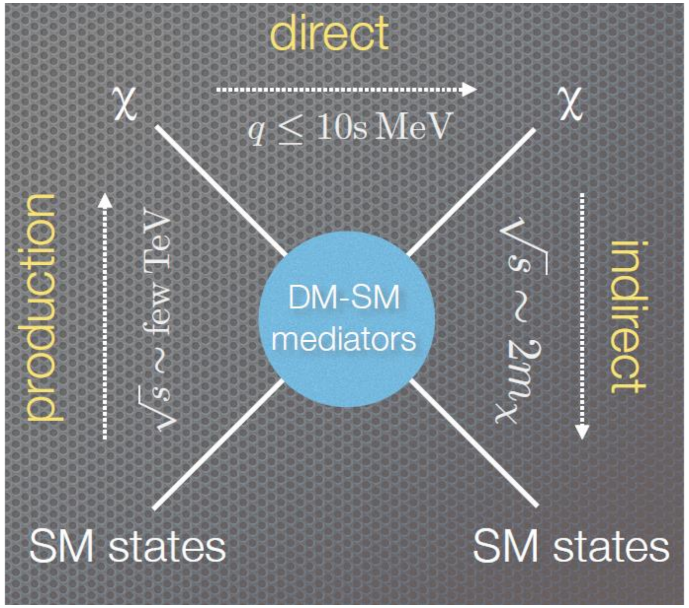

Indirect detection

High-energy neutrinos, gammas look at over-dense regions in the sky. Astrophysical backgrounds are difficult to model

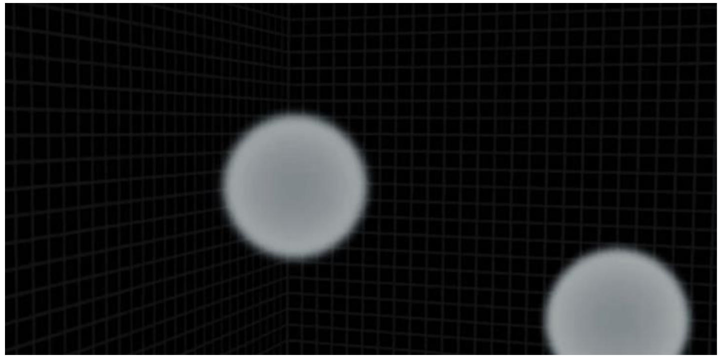

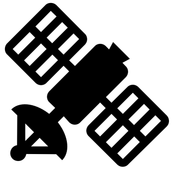

The DarkSide Program

2011 2012 2013 2014 2015 2016 2017 2018 2019 2020 2021 2022

Past — Present — Future

DarkSide-10

Technical prototype
No Dark Matter goal

DarkSide-50

Sensitivity to WIMP-nucleon cross section 10^{-44} cm^2 for a WIMP mass of 100 GeV/c^2

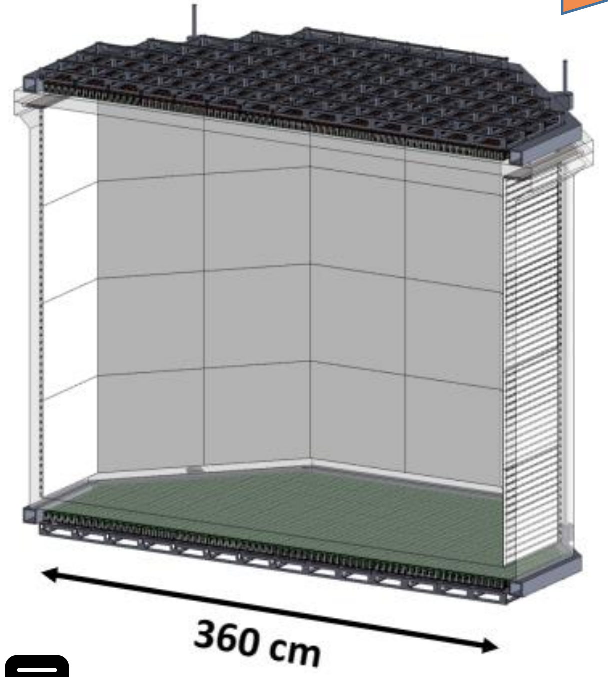

DarkSide-20k

Sensitivity to WIMP-nucleon cross section 10^{-48} cm^2 (10^{-47} cm^2) for a WIMP mass of 100 GeV/c^2 (1 TeV/c^2)

Dual-phase argon TPC: working principle

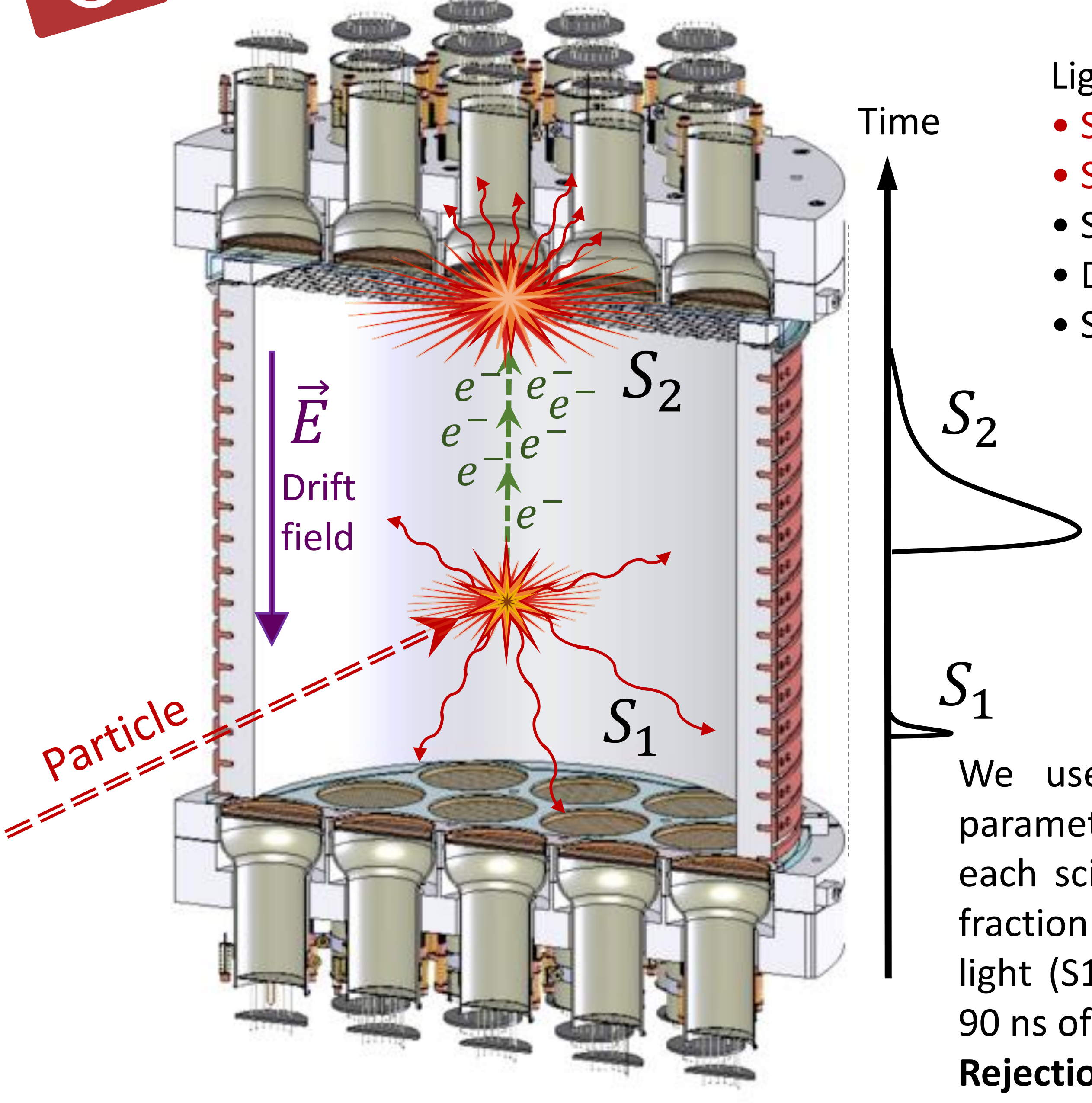

Light collected by top and bottom PMT arrays

- S1 = Primary scintillation in liquid Ar
- S2 = Secondary scintillation in Ar gas pocket
- S1 & S2 -> full energy deposition
- Drift time -> vertical (z) position
- S2 Channel light pattern -> xy position

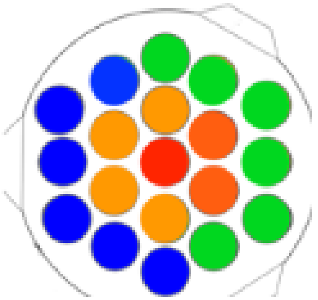

S2 pattern on top PMTs

Pulse Shape Discrimination (PSD)

Argon has a fast component with a 7 ns decay time, or a slower component with 1.6 µs decay time depending on the nature of incident particle.

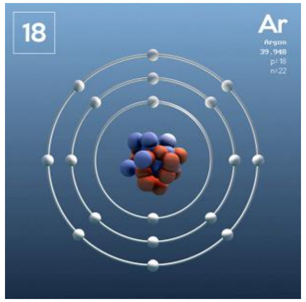

We used the discrimination parameter **f90**, defined for each scintillation event as the fraction of primary scintillation light (S1) collected in the first 90 ns of the pulse.

Rejection power >10^8

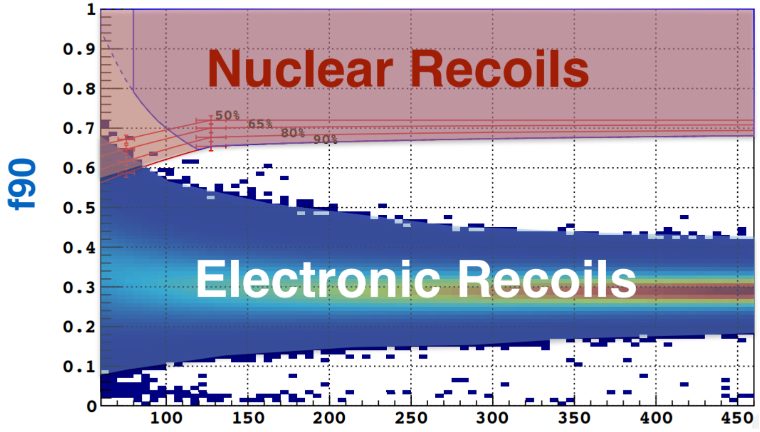

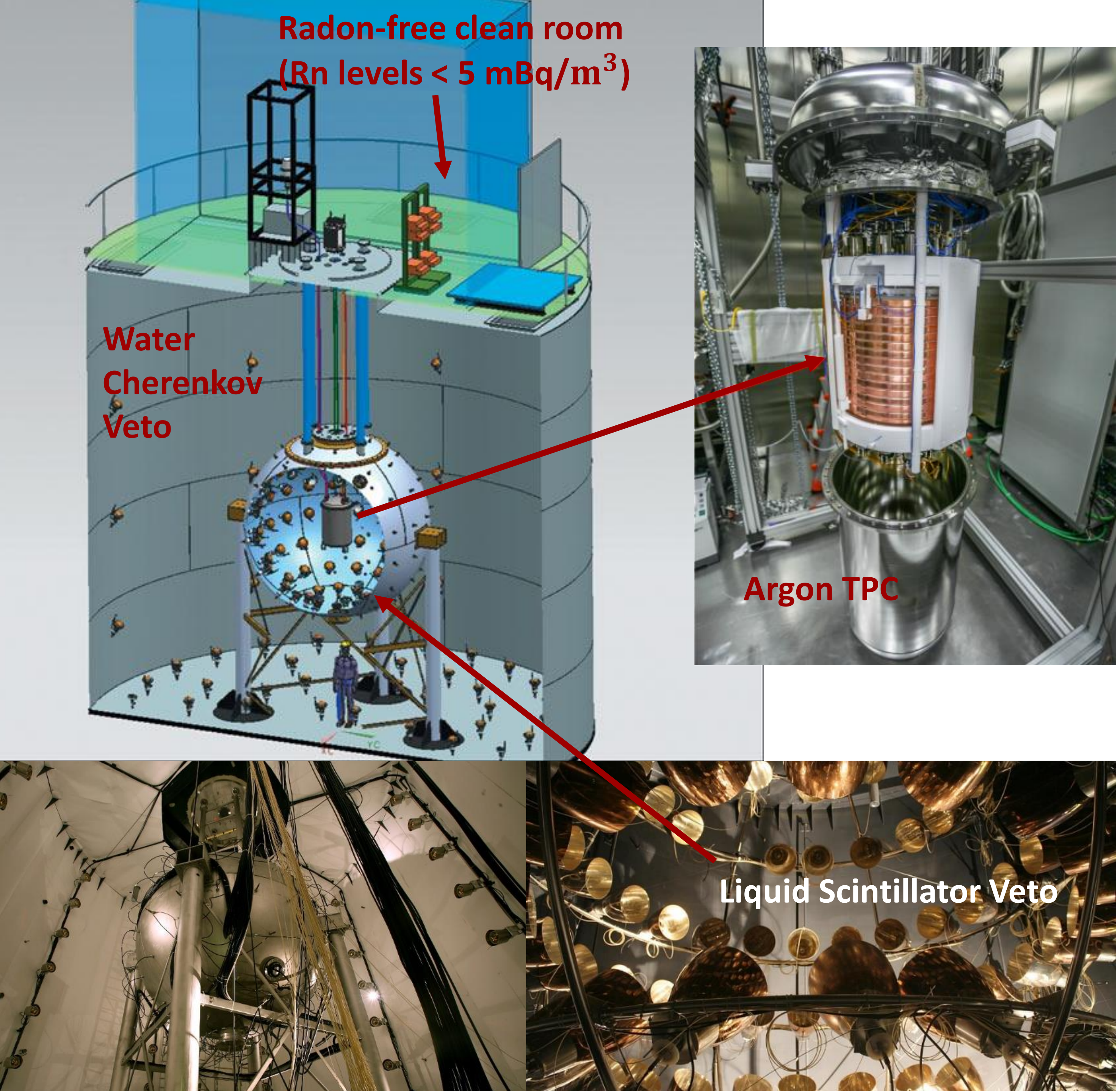

The DarkSide-50 detector

- Current detector has ~50 kg active mass.
  - Challenge: intrinsic ^{39}Ar ß-decay

(T1/2: 269 yr, Q: 565 keV). ~1 Bq/kg in atmospheric argon.

Solution: extract low radioactivity argon from underground source (^{39}Ar depletion factor >1400)

TPC was previously loaded with atmospheric argon, now loaded with low radioactive underground argon

Active shielding:

- Neutron and $\gamma's$ Veto: 4 m diameter filled with 30-tonne boron-loaded liquid scintillator with veto efficiency above 99.8 %

- Muon Veto (Water Cherenkov Detector 1,000-tonne cosmic ray veto) with efficiency >99.5%

- Designed to be background-free (<0.1 background events in the nominal exposure) with various active techniques to reject backgrounds

Results

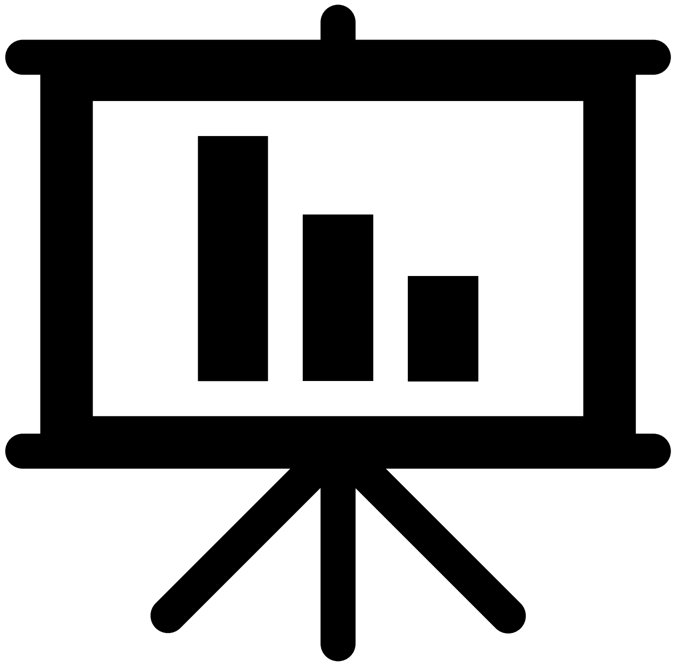

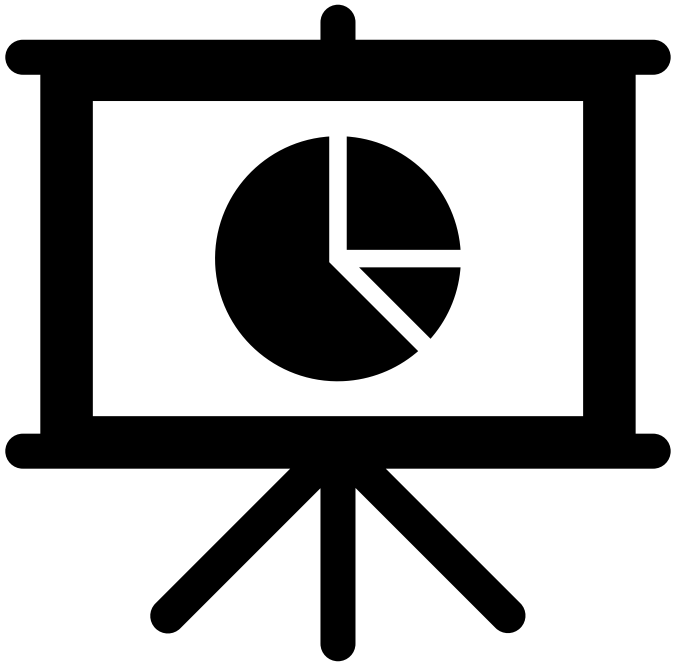

High-Mass Search: A blind analysis of 532 days of data

f_{90} = the fraction of S1 light collected in the first 90 ns

Blinding box (red outline) shown with 71-day data
PRD **93**, 081101 (2016)

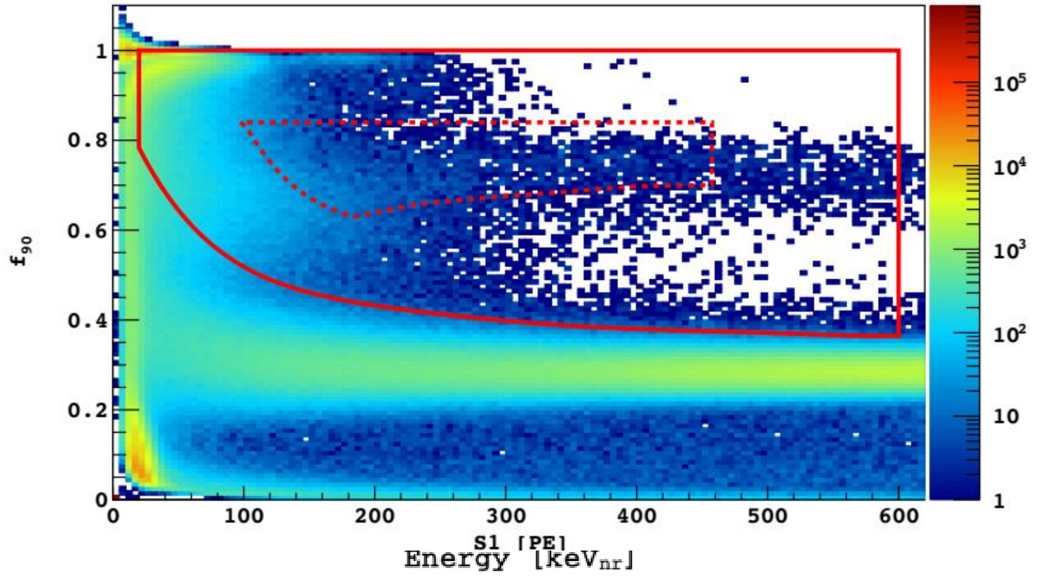

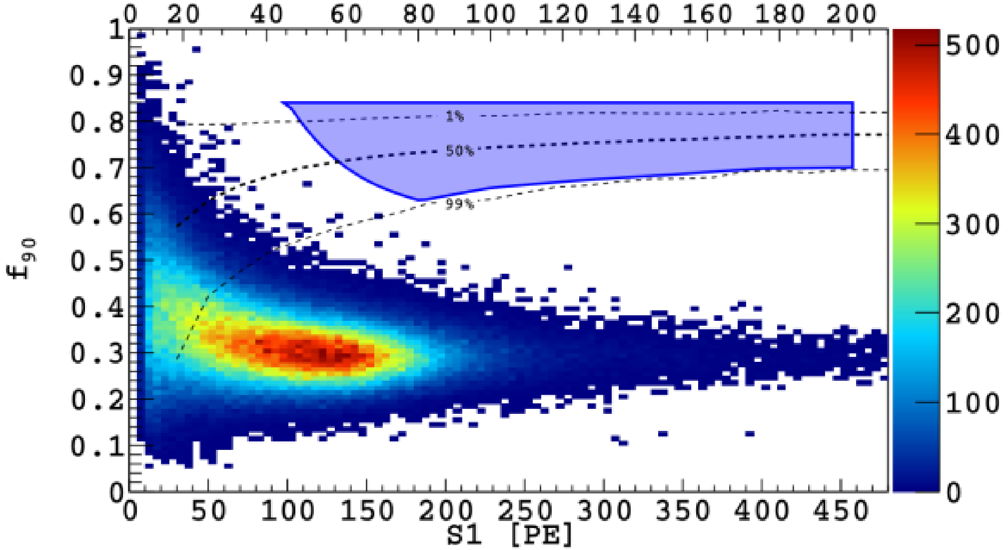

Summary of NR and ER backgrounds

Background	Est. Survive
Surface a decays	0.001
Cosmogenic n	<0.0003
Radiogenic n	<0.005
ER S1+Cherenkov	0.08*
Total	**0.09±0.04**

Goal: **design an analysis that will have <0.1 events of background** in the to be-designed search box. (Final box chosen: dashed red)

DarkSide-50 532-day dark matter search with low-radioactivity argon

P. Agnes *et al.* (DarkSide Collaboration)
Phys. Rev. D **98**, 102006 – Published 16 November 2018

Using S1+S2 signals

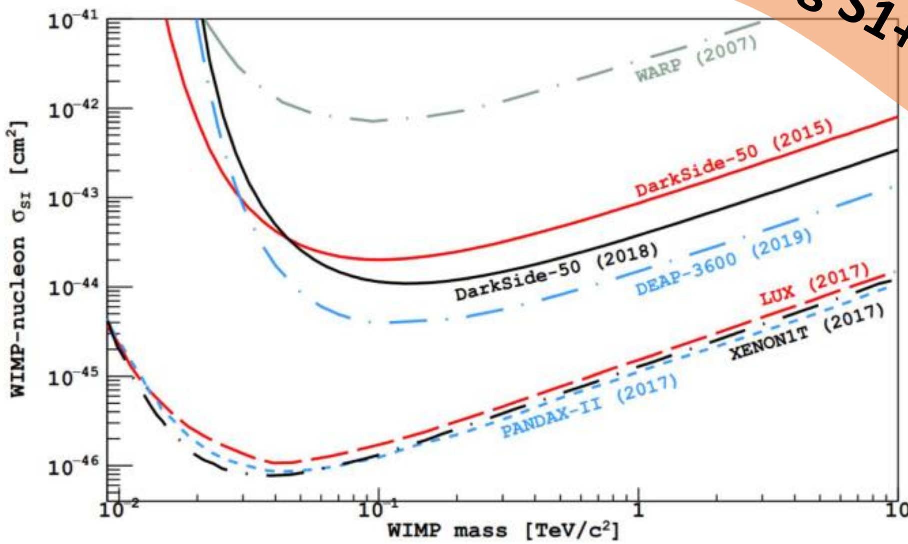

World best results for low mass WIMPs

Using only S2

Great effort here in Cagliari to study the «single electron background»

Unexplained excess of ionization electron events

Data (points) and total MC background estimate (histogram)

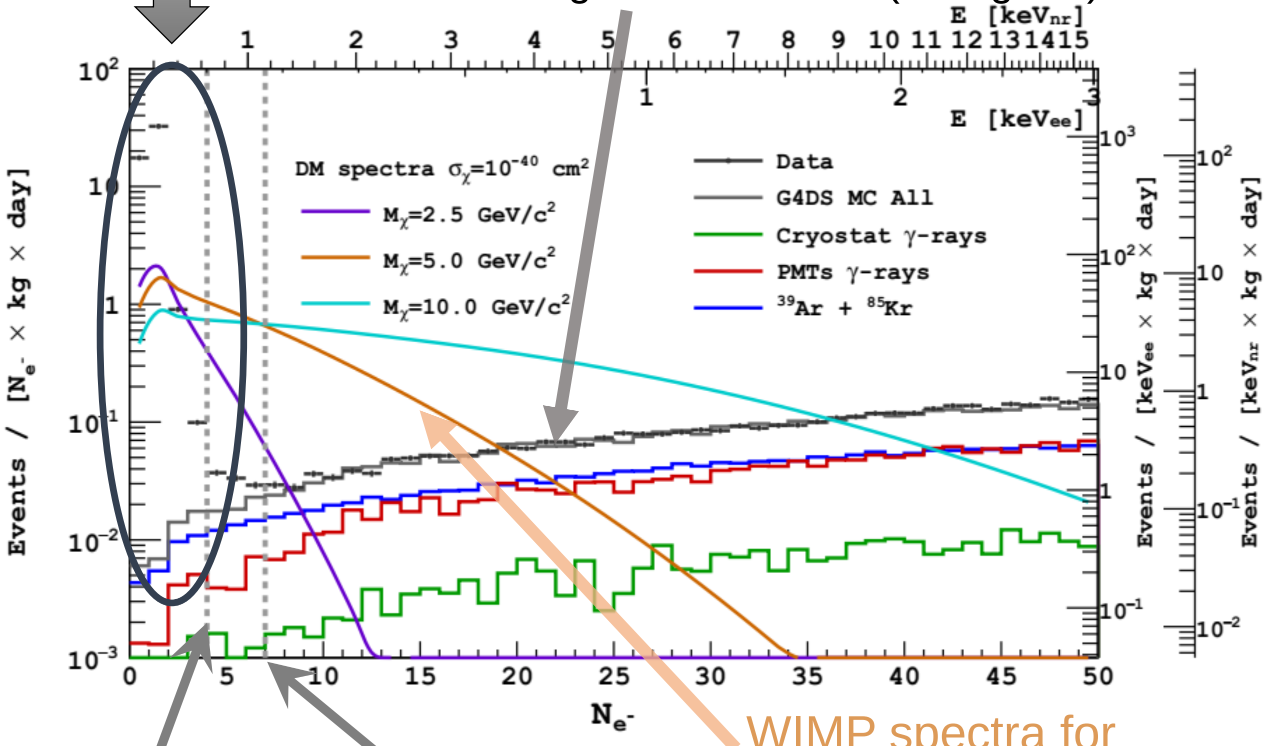

Analysis thresholds

WIMP spectra for different masses

Editors' Suggestion

Low-Mass Dark Matter Search with the DarkSide-50 Experiment

P. Agnes *et al.* (DarkSide Collaboration)
Phys. Rev. Lett. **121**, 081307 – Published 23 August 2018

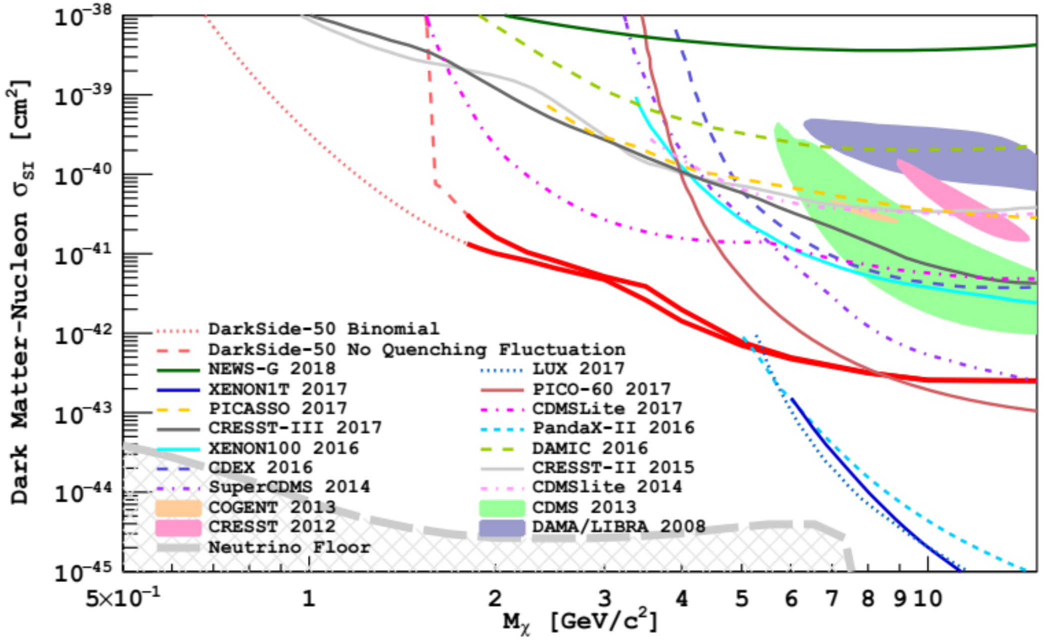

Profile Likelihood Method is used

- Uncertainties from both WIMP signals (NR ionization yield, single electron yields) and BG spectrum (rates, ER ionization yield).

Interpretation for DM-electron scattering

Using only S2

Constraints on Sub-GeV Dark-Matter–Electron Scattering from the DarkSide-50 Experiment

P. Agnes *et al.* (The DarkSide Collaboration)
Phys. Rev. Lett. **121**, 111303 – Published 12 September 2018

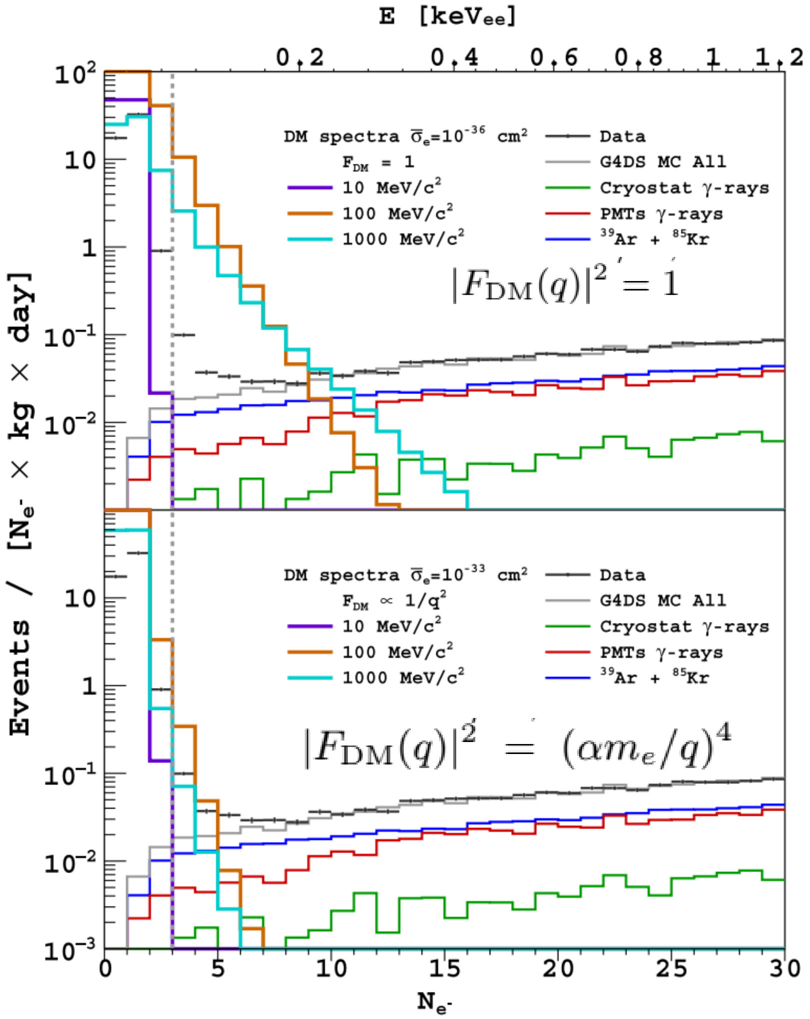

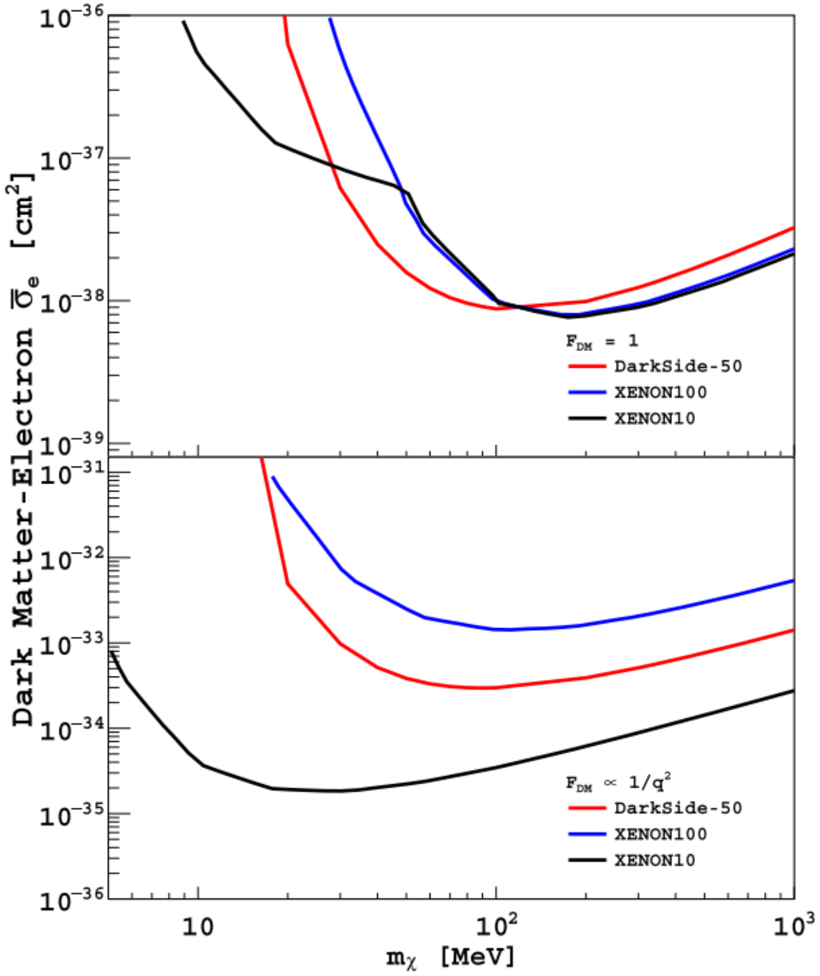

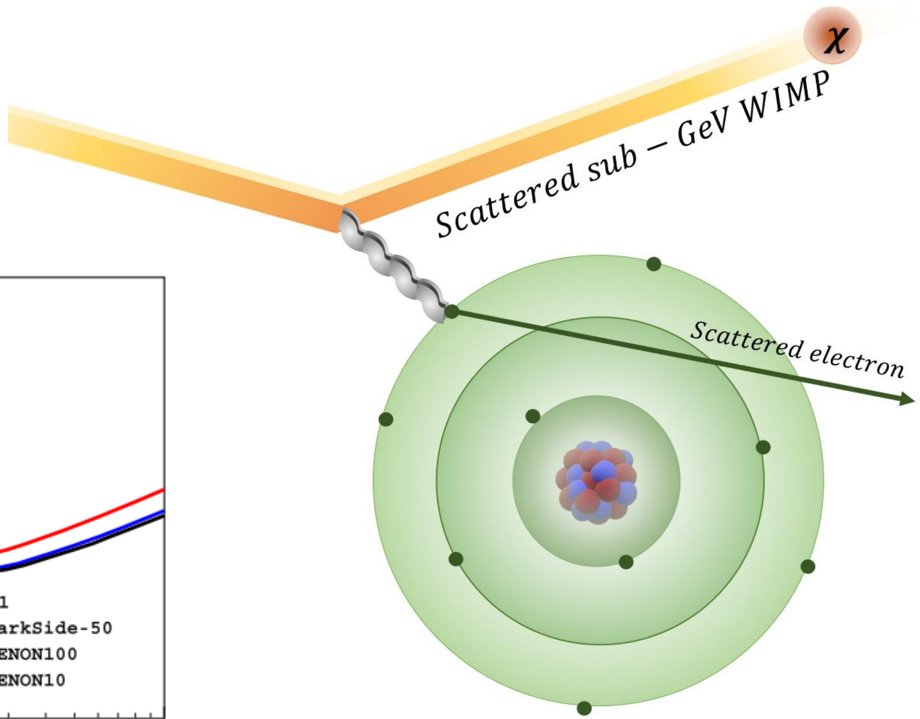

Both the theoretical formalism, and the simulation of the predicted signal have been developed here in Cagliari.

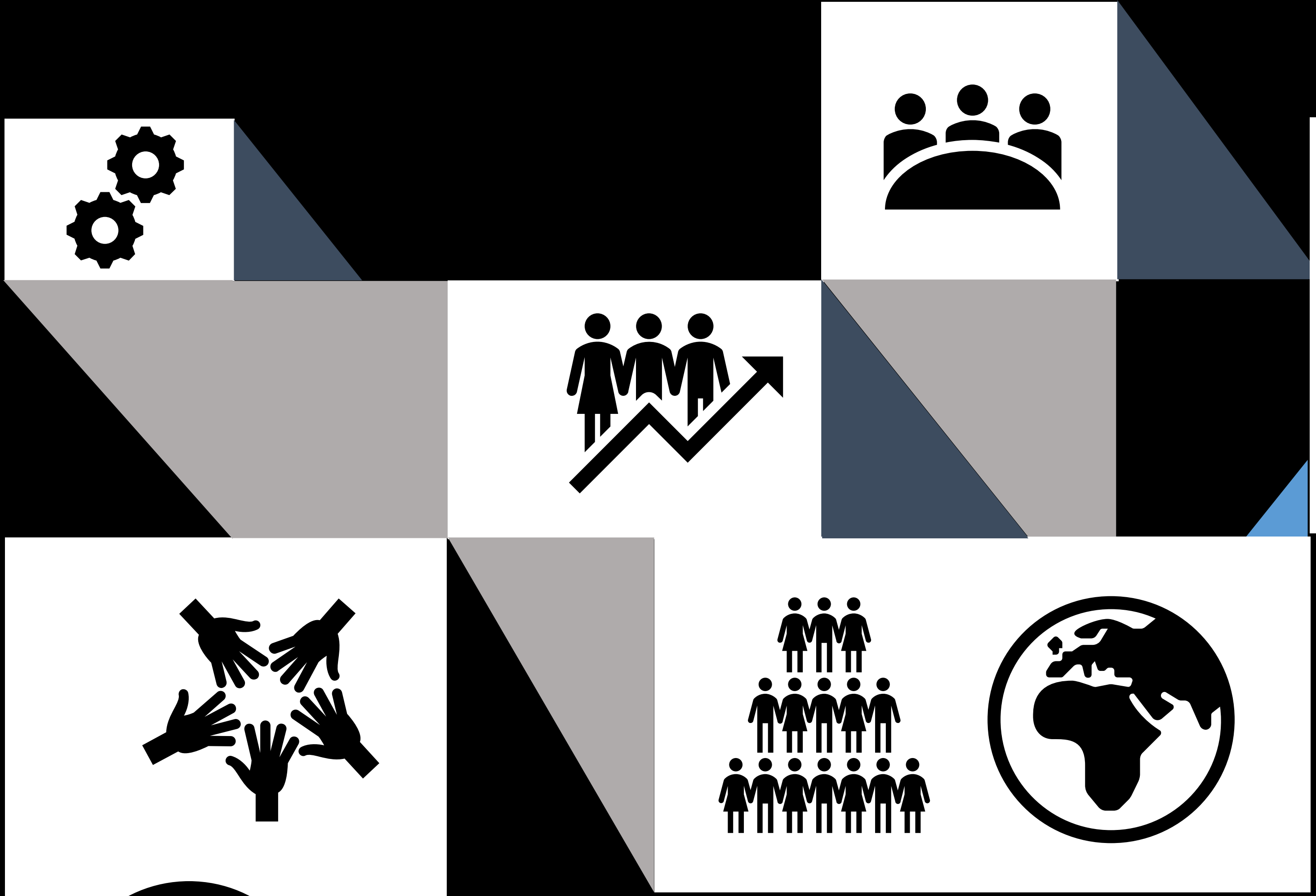

Global Argon Dark Matter Collaboration (GADMC)

GADMC Collaboration

- In 2017, the ArDM,DEAP, MiniCLEAN and DarkSide collaborations joined forces to form The Global Argon Dark Matter Collaboration (GADMC). This has united the major experiment programs using argon
- DarkSide-20k is the first experiment in this global program
- As of August 2019, GADMC includes scientists from 14 Countries: Brazil, Canada, China, France, Greece, Italy, Mexico, Poland, Romania, Russia, Spain, Switzerland, United Kingdom, United States of America

Five new key technologies enabling DarkSide-20k

- **Urania:** for high through-put extraction of low radioactivity underground argon (UAr) [Colorado, USA]
- **Aria:** for high through-put purification of the UAr [Sardinia, Italy]
- **DArT**: Assessing the content of ^{39}Ar of UAr [Canfranc, Spain]
- **SiPM-based PhotoDetector Modules:** for enhanced light-detection and reduced radioactivity [LNGS, Italy]
- **Membrane Cryostat:** as developed in the ProtoDUNE projects [CERN, France/Switzerland]

DArT: Assessing the content of ^{39}Ar of UAr.

Now approved; paper almost ready!

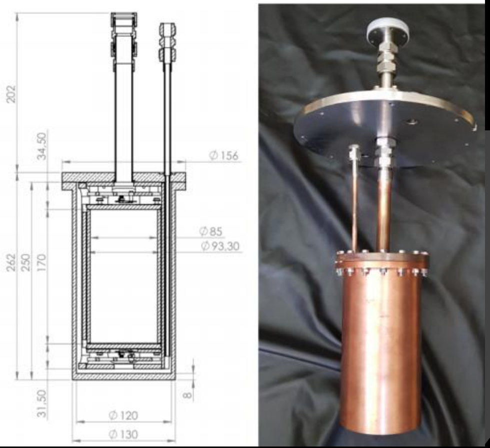

One board w/ new layout **developed in Cagliari**

A lot of involvement here in Cagliari

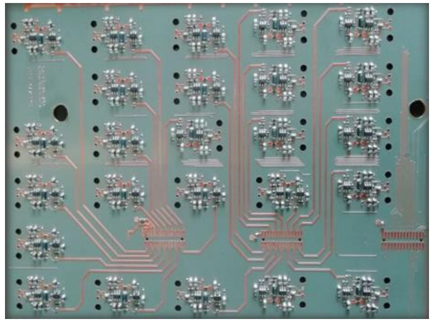

Optical receiver (DS-20K)

- **Receiver C** for DS-20K. To be hosted in the cryostat chimney.

A lot of involvement here in Cagliari to design the optical transmission of the signal

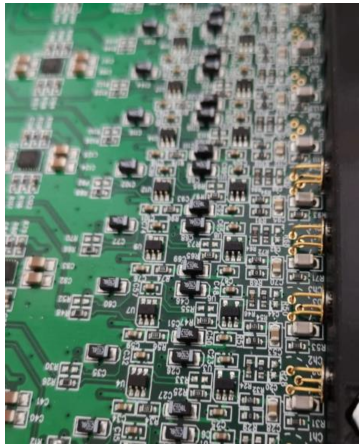

INFN CAGLIARI
Istituto Nazionale di Fisica Nucleare
Sezione di Cagliari

DarkSide-20k

Sealed acrylic TPC containing 50 t of UAr
- Membrane cryostat containing ~700 t of AAr
- 2% Gd-doped acrylic panels + AAr buffer as neutron veto
- SiPMs as photosensors: 8280 channels for TPC; ~3000 channels for Veto

Placed inside ProtoDUNE-like cryostat

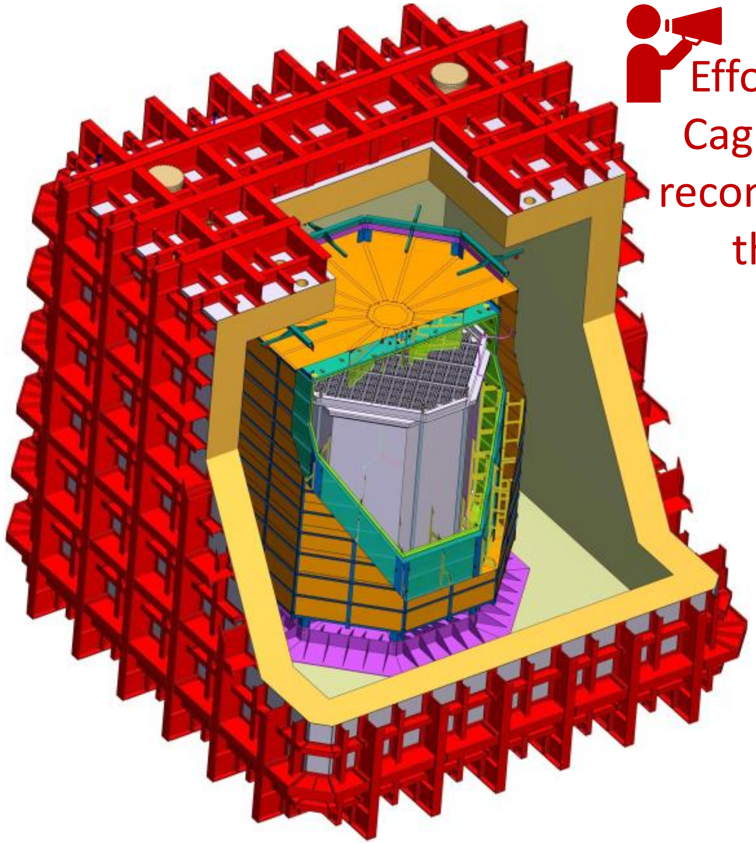

Efforts here in Cagliari for the reconstruction of the signal

90% CL WIMP-nucleon cross section sensitivity in cm^2

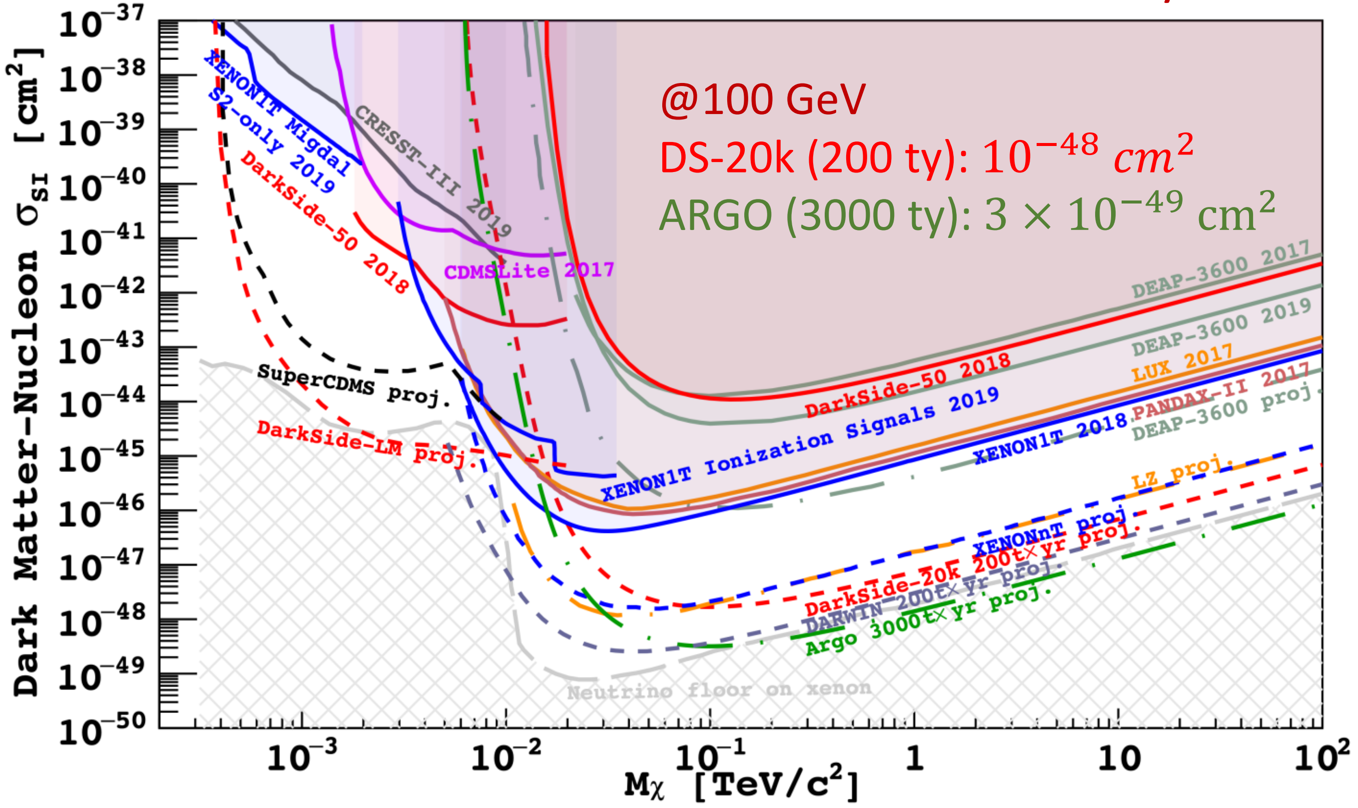

Background-free:< 0.1 instrumental background event in 200 tonne-year exposure

- **Coherent elastic neutrino nucleus scattering** (CEvNS)

~2.7 CEvNS background events (DS-20k 200 t)
~40 CEvNS background events (Argo 3000 t y)

«Neutrino floor» of the sensitivity

Irreducible background since CEvNS perfectly mimic WIMP events. Only two strategies
- Directionality of WIMPs and ν
- Charaterization of CEvNS

Leading contribution from the Cagliari group

WIMP directionality

V. Cataudella, A. de Candia, M. Cadeddu, M. Lissia, B. Rossi, G. Fiorillo C. Galbiati, "Directional modulation of electron-ion pairs recombination in liquid argon," JINST, 12, P12002, 2017.

*Cadeddu et al. **JCAP** 01 (2019) 014 «Directional dark matter detection sensitivity of a two-phase liquid argon detector.»*

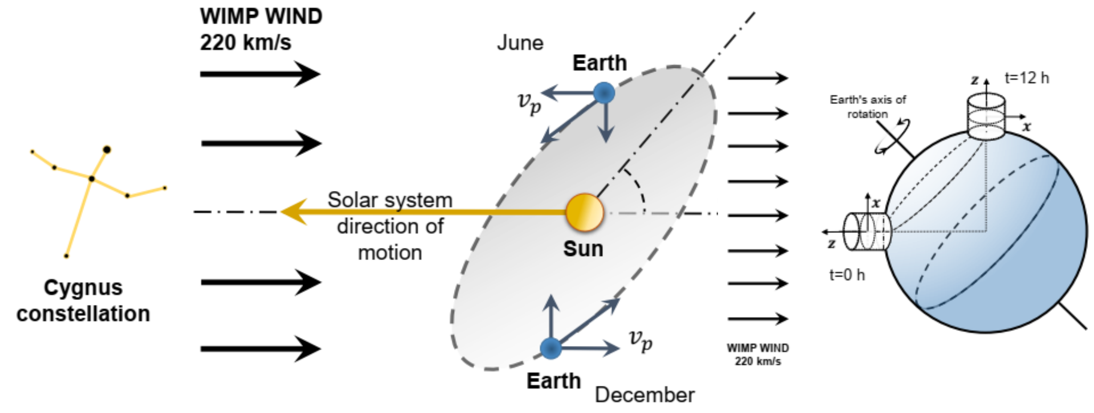

A lot of involvement from both phenomenological and experimental point of view of the Cagliari group.

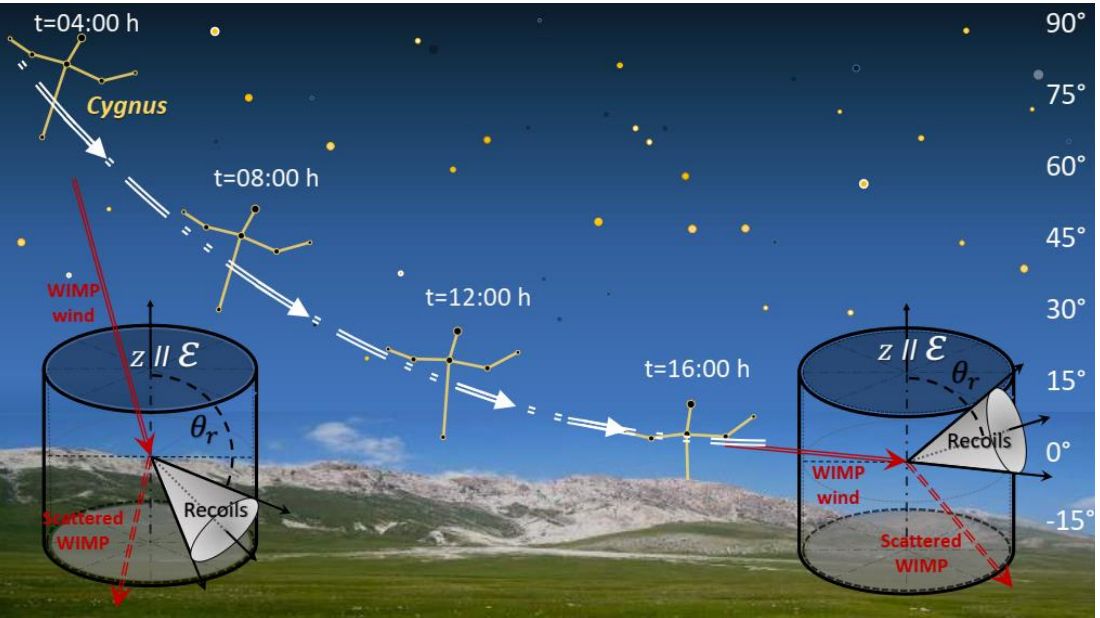

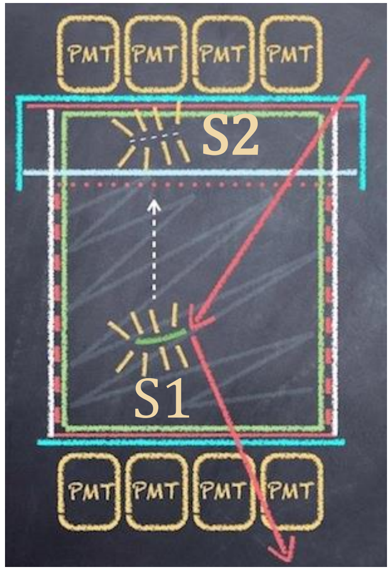

The basic idea of Columnar Recombination: *When a nuclear recoil is parallel to the electric field, there will be more electron-ion recombination since the electrons pass more ions as they drift through the chamber.*

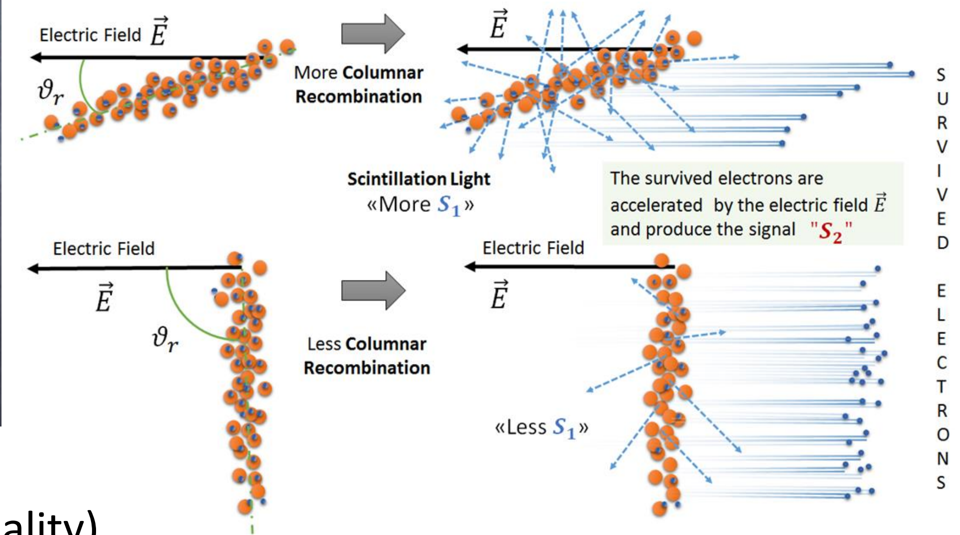

ReD (Recoil Directionality)

- 5x5x5 cm^2 TPC with 2 PDMs
- ✓ First test done!
- ✓ commissioning phase in Catania

2° goal scintillation efficiency of NR's

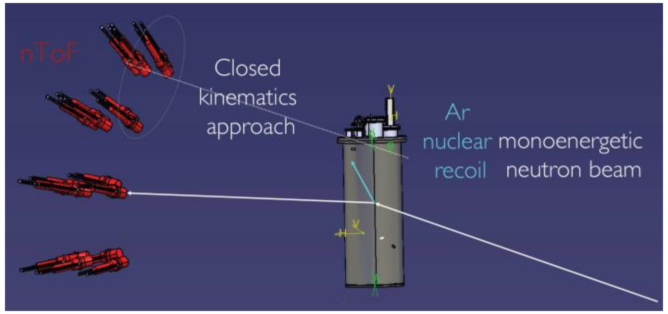

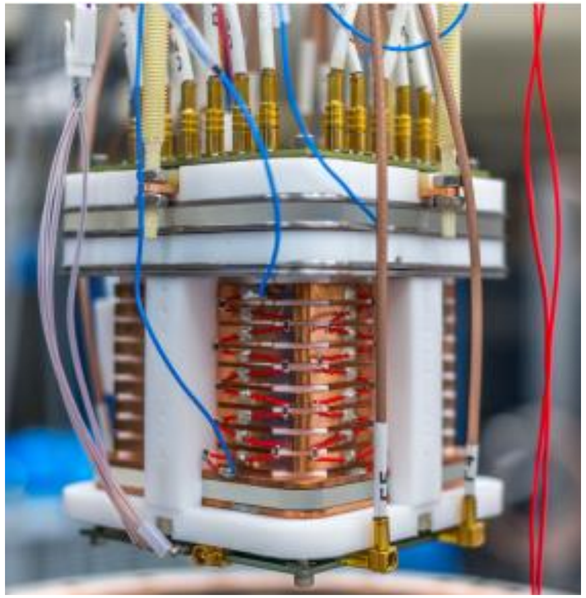

A lot of phenomenology…

*[D. Akimov et al. "Observation of Coherent Elastic Neutrino-Nucleus Scattering" **Science** 357 (2017)]*

CEvNS observed, at a 6.7σ CL, by the COHERENT Collaboration, using a low-background, 14.6-kg CsI scintillator exposed to the neutrino emissions from the Spallation Neutron Source at Oak Ridge National Laboratory.

Open Access

Average CsI Neutron Density Distribution from COHERENT Data

M. Cadeddu, C. Giunti, Y. F. Li, and Y. Y. Zhang
Phys. Rev. Lett. **120**, 072501 – Published 13 February 2018

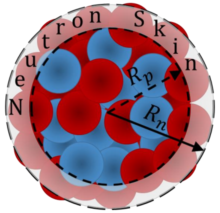

✓ First model-independent measurements of the average neutron radius of CsI, R_n^{CsI}, and its neutron skin ΔR_{np}^{Cs}.

Open Access

Reinterpreting the weak mixing angle from atomic parity violation in view of the Cs neutron rms radius measurement from COHERENT

M. Cadeddu and F. Dordei
Phys. Rev. D **99**, 033010 – Published 20 February 2019

✓ Using R_n^{Cs} from COHERENT we correct the previous determination of $\sin^2\theta_W^{APV}$ which was 1.5σ off the SM prediction at $Q^2 \approx 0$.

Editors' Suggestion **Open Access**

Neutrino charge radii from COHERENT elastic neutrino-nucleus scattering

M. Cadeddu, C. Giunti, K. A. Kouzakov, Y. F. Li, A. I. Studenikin, and Y. Y. Zhang
Phys. Rev. D **98**, 113010 – Published 26 December 2018

Constraint on the muon neutrino charge radius

$$-8 \times 10^{-32}\ \text{cm}^2 < \left\langle r_{\nu_\mu}^2 \right\rangle < 11 \times 10^{-32}\ \text{cm}^2\ @90\,\%\ \text{CL}$$

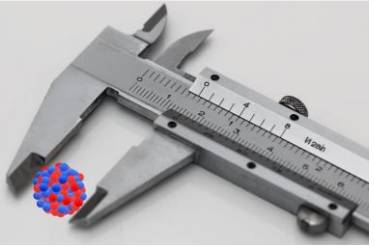

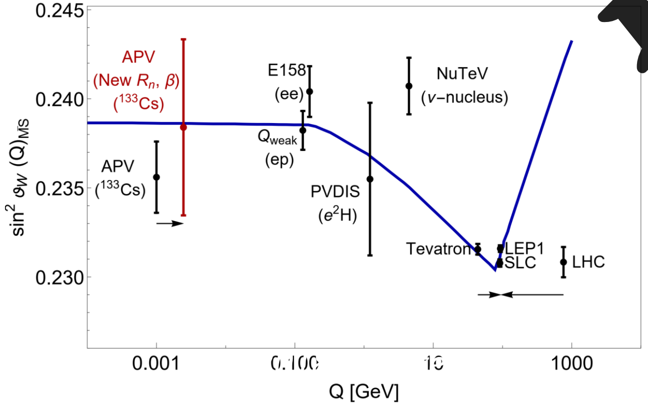

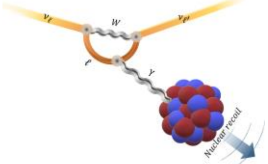

Result included in PDG

Spin-off: Coherency with the whole atom?

We propose an experimental setup to observe coherent elastic neutrino-atom scattering (CEvAS) using electron antineutrinos from tritium decay and a liquid helium target.

Potentialities of a low-energy detector based on ^{4}He evaporation to observe atomic effects in coherent neutrino scattering and physics perspectives

M. Cadeddu, F. Dordei, C. Giunti, K. A. Kouzakov, E. Picciau, and A. I. Studenikin
Phys. Rev. D **100**, 073014 – Published 29 October 2019

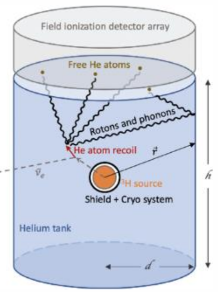

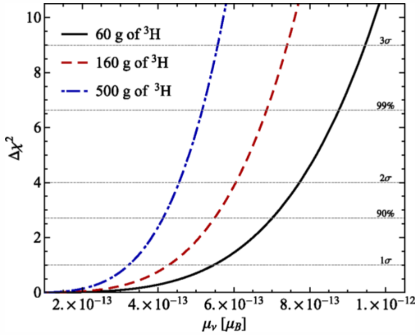

More than one order of magnitude smaller than the current experimental limit on ν magnetic moment

NEUTRINO CHARGE RADIUS SQUARED

We report limits on the so-called neutrino charge radius squared. While the straight-forward definition of a neutrino charge radius has been proven to be gauge-dependent and, hence, unphysical (LEE 77C), there have been recent attempts to define a physically observable neutrino charge radius (BERNABEU 00, BERNABEU 02). The issue is still controversial (FUJIKAWA 03, BERNABEU 03). A more general interpretation of the experimental results is that they are limits on certain nonstandard contributions to neutrino scattering.

VALUE (10^{-32} cm^2)	CL%	DOCUMENT ID		TECN	COMMENT
−2.1 to 3.3	90	[1] DENIZ	10	TEXO	Reactor $\overline{\nu}_e e$
−4 to 5.5	90	[2] CADEDDU	18		ν_μ coherent scat. on CsI
−0.53 to 0.68	90	[3] HIRSCH	03		$\nu_\mu e$ scat.
−8.2 to 9.9	90	[4] HIRSCH	03		anomalous $e^+e^- \to \nu\overline{\nu}\gamma$
−2.97 to 4.14	90	[5] AUERBACH	01	LSND	$\nu_e e \to \nu_e e$
−0.6 to 0.6	90	VILAIN	95B	CHM2	$\nu_\mu e$ elastic scat.
0.9 ±2.7		ALLEN	93	CNTR	LAMPF $\nu e \to \nu e$
< 2.3	95	MOURAO	92	ASTR	HOME/KAM2 ν rates
< 7.3	90	[6] VIDYAKIN	92	CNTR	Reactor $\overline{\nu} e \to \overline{\nu} e$
1.1 ±2.3		ALLEN	91	CNTR	Repl. by ALLEN 93
−1.1 ±1.0		[7] AHRENS	90	CNTR	$\nu_\mu e$ elastic scat.
−0.3 ±1.5		[7] DORENBOS...	89	CHRM	$\nu_\mu e$ elastic scat.
		[8] GRIFOLS	89B	ASTR	SN 1987A

[1] DENIZ 10 observe reactor $\overline{\nu}_e e$ scattering with recoil kinetic energies 3–8 MeV using CsI(Tl) detectors. The observed rate and spectral shape are consistent with the Standard Model prediction, leading to the reported constraint on $\overline{\nu}_e$ charge radius.

[2] CADEDDU 18 use the data of the COHERENT experiment, AKIMOV 18. The limit is $\langle r_\nu^2 \rangle$ for ν_μ obtained from the time-dependent data. Weaker limits were obtained for charge radii of ν_e and for transition charge radii. The published value was divided by 2 to conform to the convention of this table.

Ongoing works (many by students)

- ➢ Dark-Matter electron searches
- ✓ Emmanuele Picciau master thesis

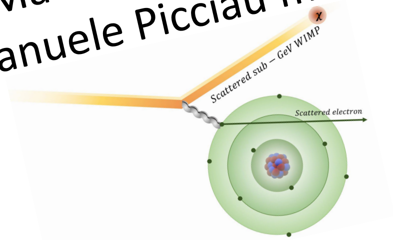

- ➢ Z' and darkphoton searches in DarkSide

Nicola Cargioli master thesis (just started..)

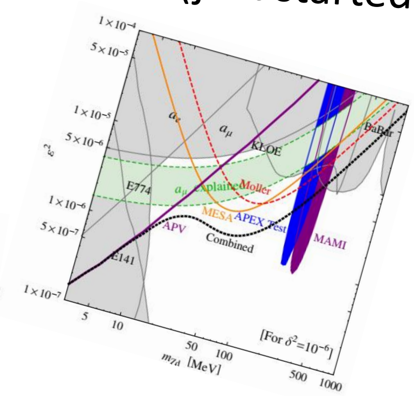

- ➢ Simulation of the solar reflection effect to search for low WIMP masses
- ✓ Nicola Cargioli bachelor thesis
- ✓ Mattia Atzori bachelor thesis

…more to come

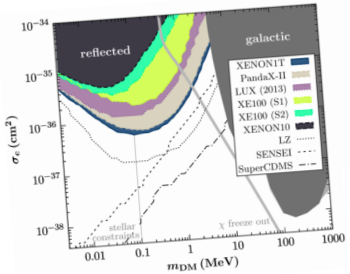

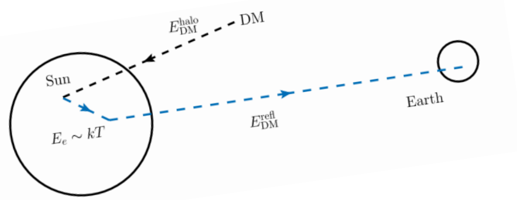

- ➢ Supernova neutrinos detection in DS20K and ARGO
- ➢ Multiple interacting darks matter particels in DEAP-3600
- ➢ X-Y reconstruction in DarkSide detectors
- ✓ Part of Michela Lai's PhD thesis.

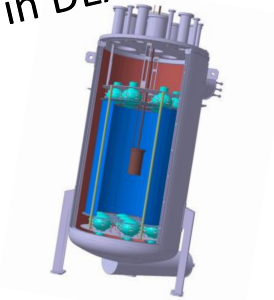

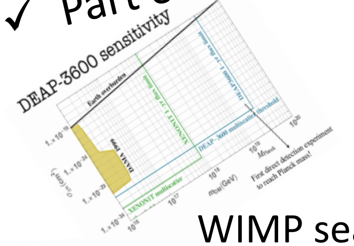

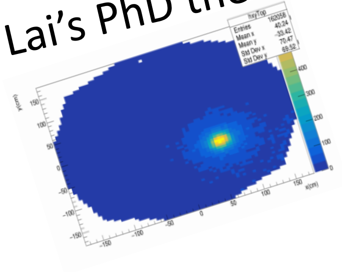

- ➢ Sensitivity to low mass WIMPs
- ✓ Part of Emmanuele Picciau's PhD thesis

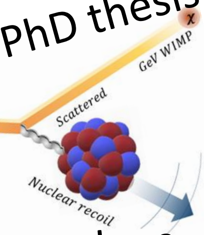

WIMP search with the DEAP-3600 and DS-50 detector.

- ➢ Standard WIMP analysis limits on different effective operators that may mediate WIMP-nucleon interactions

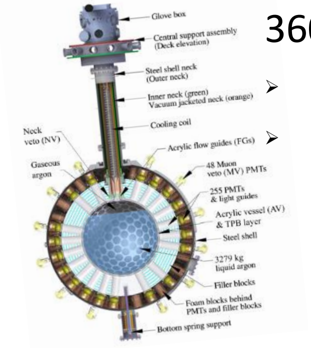

And many others topic and interested students….

- ➢ Role of Coherent elastic neutrino nucleus scattering from COHERENT data
- ✓ Part of Emmanuele Picciau's PhD thesis

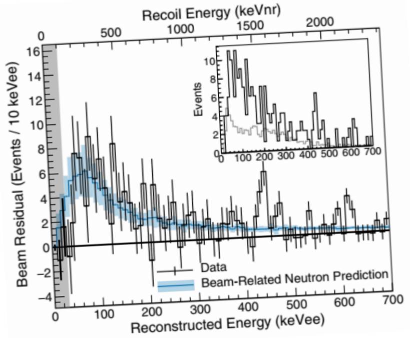

INFN
CAGLIARI
Istituto Nazionale di Fisica Nucleare
Sezione di Cagliari

Present members of the DarkSide Cagliari group

DARKSIDE



















BACKUP

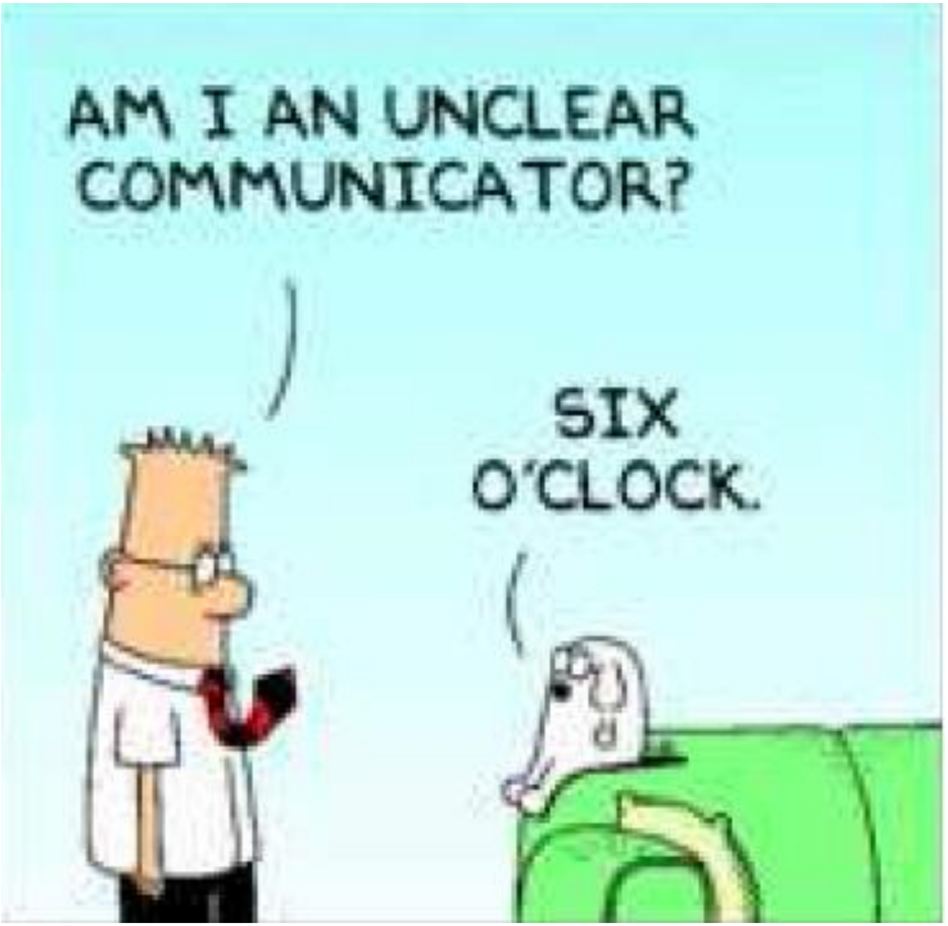

Photoelectronics for DS-20k

A lot of involvement here in Cagliari to design the optical transmission of the signal

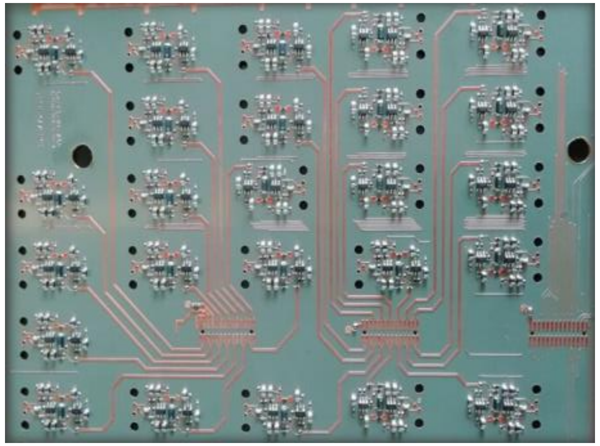

One board w/ new layout **now in Cagliari** (mounted @CERN, except connectors and LEDs)

Optical receiver (DS-20K)

- New revision of receiver A with both single ended and differential output for proto.
- Receiver C for DS-20K. To be hosted in the cryostat chimney. Differential output on KEL connectors directly connected to the flange of the cryostat

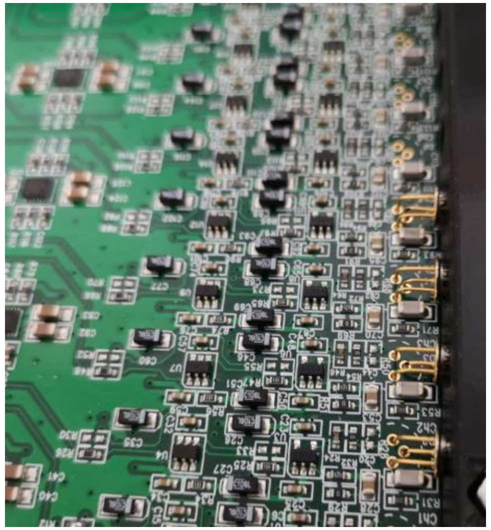

5×5×5 cm^3 25×25×5 cm^3

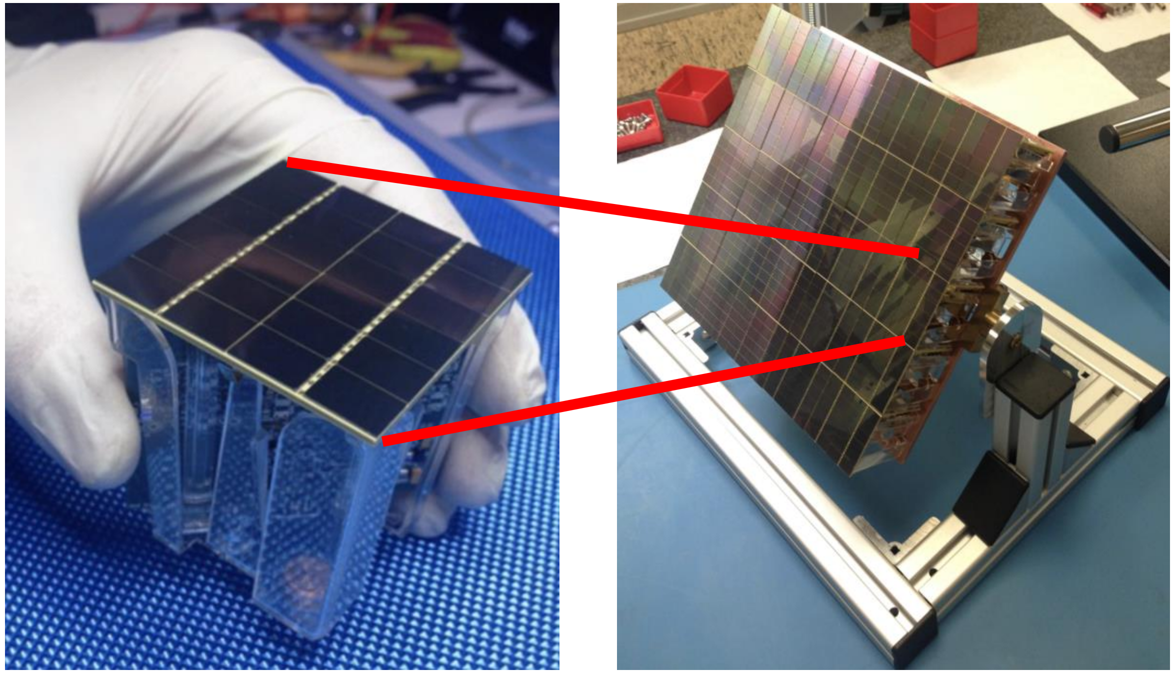

Photo Detection Module (PDM)

SiPM array +electronics

Motherboard (MB)
25x25 cm^2 PDM array + steering module + **optical transmitters**

The future of DarkSide

PDM= Photo Detector Module

38 PMTs

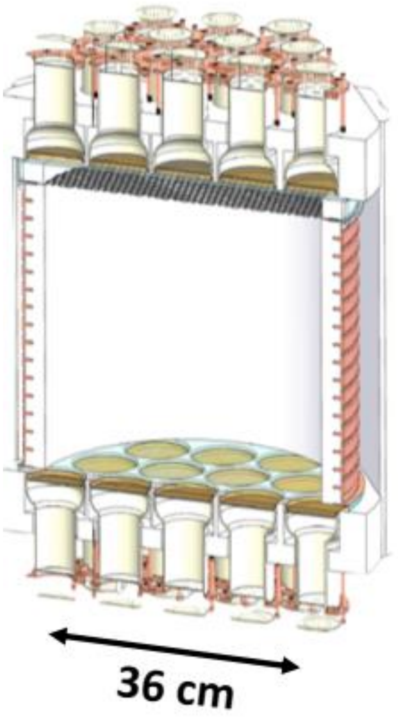

DS-50
(2014–present)
46 kg active
Conventional TPC

50 PDMs

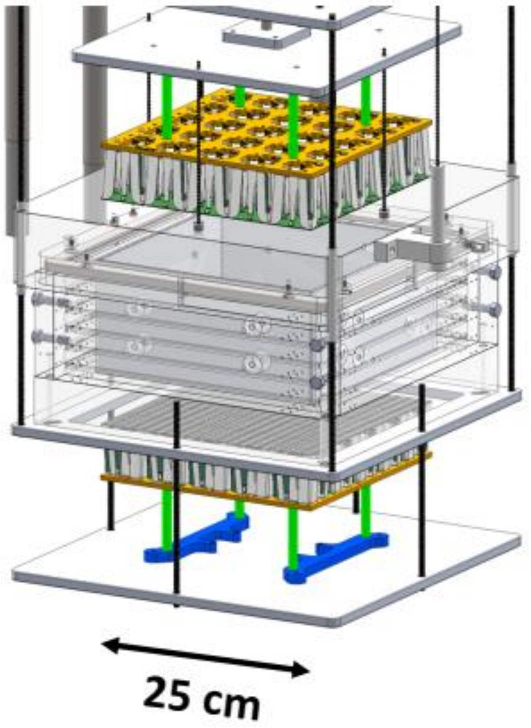

DS-Proto-0
(2019–2020)
10 kg active
Test bench

370 PDMs

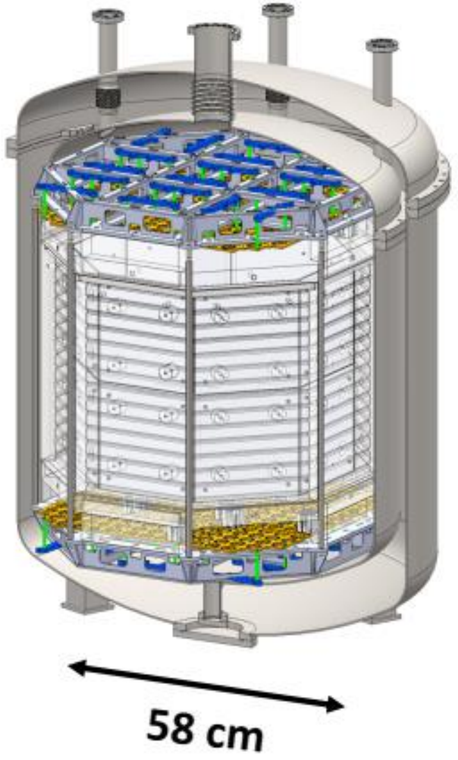

DS-Proto-1
(2020–2021)
175 kg active
Scaled-down of
DS-20k TPC

8280 PDMs

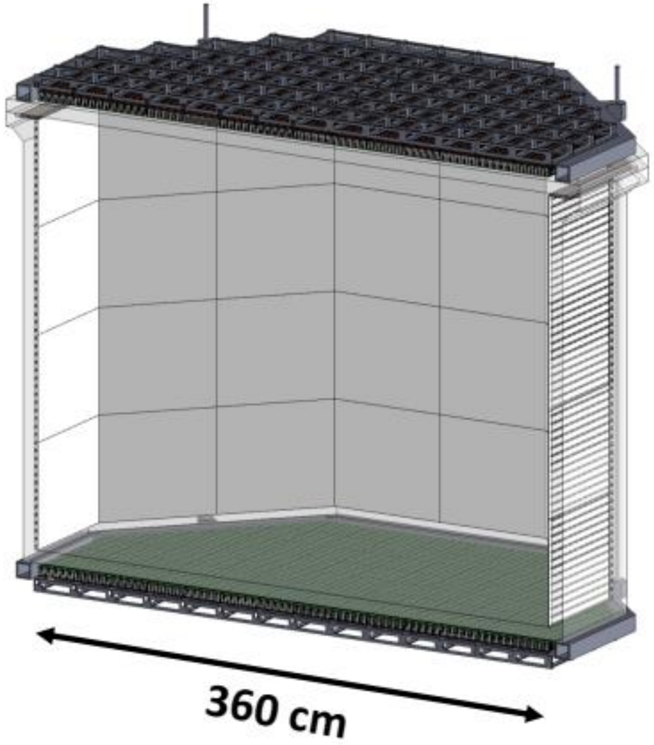

DS-20k
(2022–)
48 ton active
Novel sealed TPC

Supernova neutrinos detection in DS20K and ARGO

Tipe II supernovae are very rare events (2/3 per century on average), in which 3 x10^46 J are released in ~ 10 s, mainly via neutrinos of any flavour

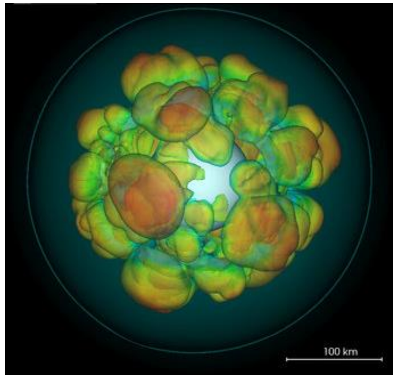

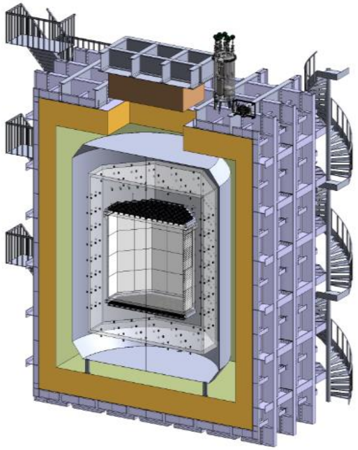

Via CevNS scattering DS20K and ARGO have shown to have a 5sigma discovery potential on an eventual galactic supernova, thanks to the extraordinary low background at energies < 10 MeV and the high (and flavour insensitive) cross section

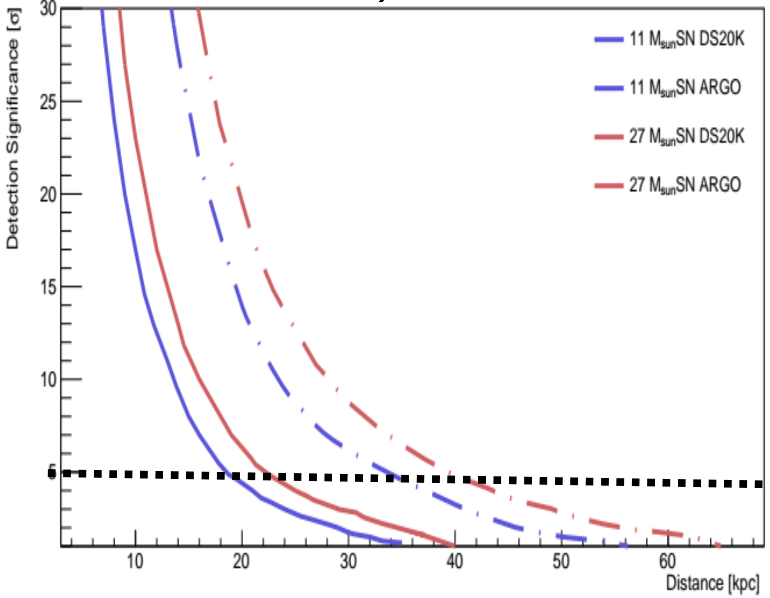

As we are going to be sensitive to all flavours, we can reconstruct the two main parameters of the global emission : the total energy released via neutrinos and the average energy of neutrinos

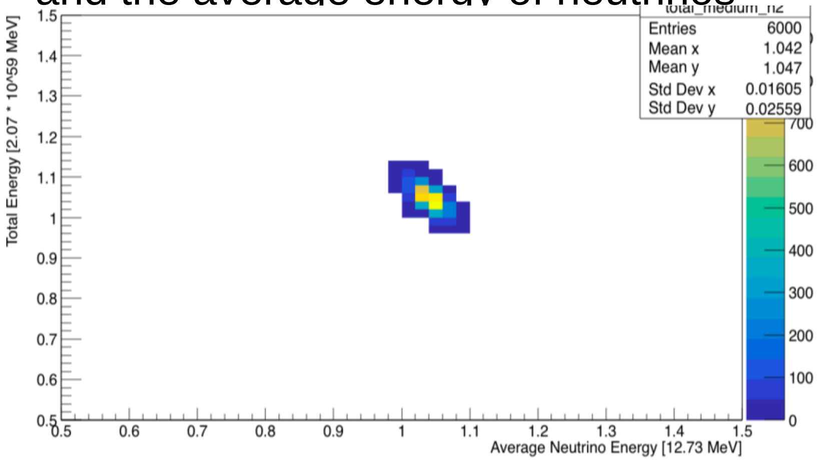

Michela Lai & Walter M. Bonivento

For all these reasons we are going to be inserted in SNEWS-2.0

Multiple interacting darks matter particels in DEAP-3600

For masses greater than 10^5 GeV and cross section above 10^-30 cm^2, dark matter particles are expected to interact more than once in the detector, giving a almost collinear track of nuclear recoils, each ~ 40 keV_{NR}

Looking at the data from the last run of DEAP-3600, a single phase TPC filled with Atmospheric argon at SNOLAB (2 km underground) we can exclude (or find? Who knows…) such “MIMPs”, multiple interacting massive particles.

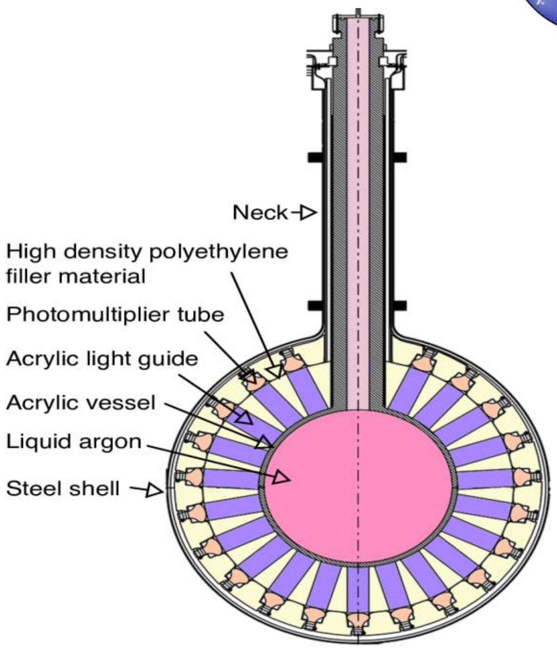

DEAP-3600 sensitivity

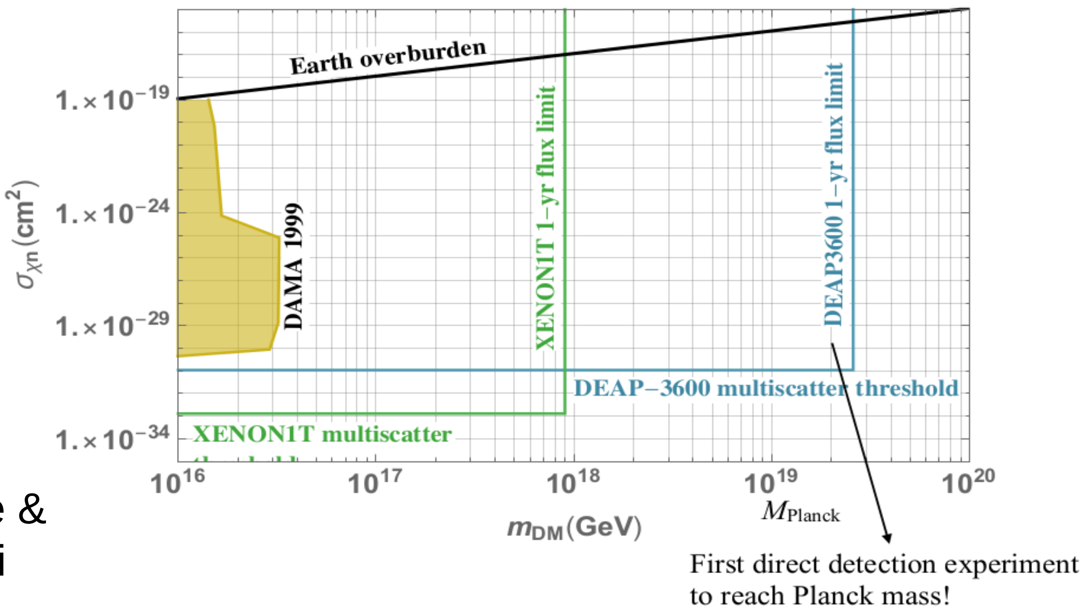

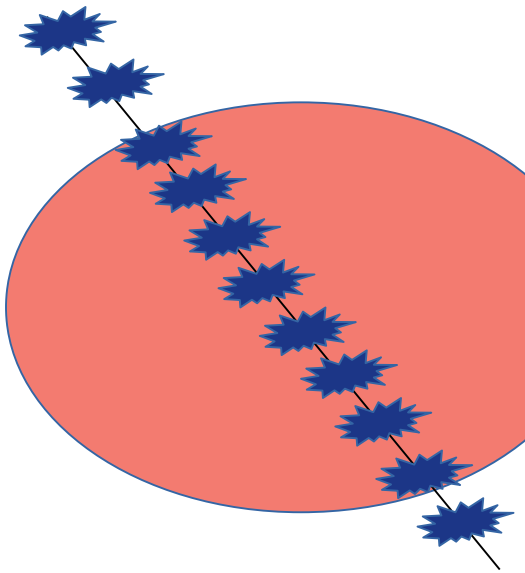

Shawn Westerdale & Michela Lai

X-Y reconstruction in DarkSide detectors

In DarkSide-50 the resolution on the x-y coordinate is ~ 1cm, determined by the S2 pattern on the top PMTs .
By working with Geant-4 simulation we can determine the resolution expected in DS20K, if we use the same method performed in DarkSide-50.

S2 light distribution on top Sipm (from G4 simulation of DS20K)

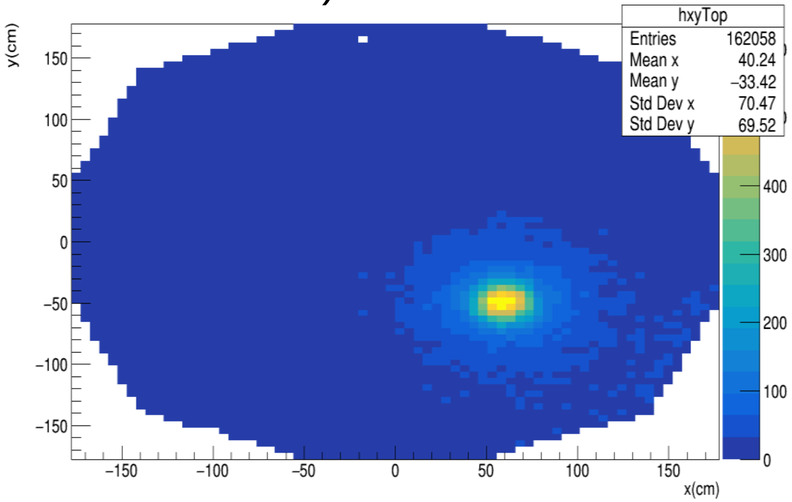

The next step will be study the eventual improvements by the application of Neural networks

First applications will be on ReD data, as they are already available and next, on spring, to Dart data.

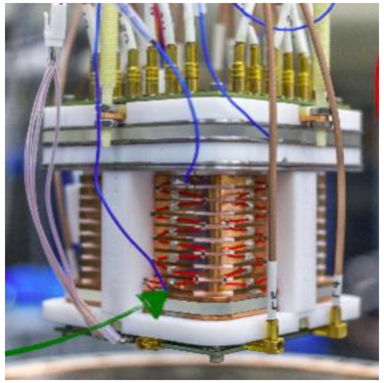

ReD TPC

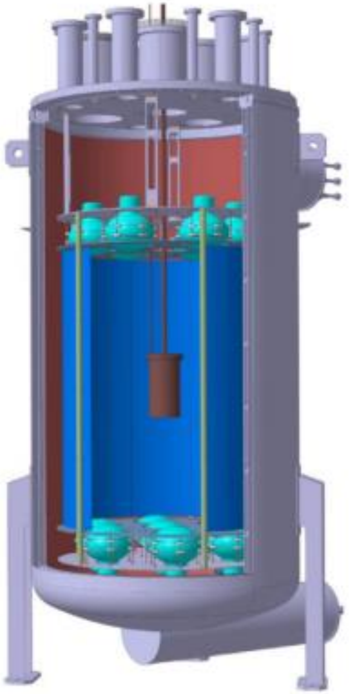

Dart TPC in the ArDM cryostat

Alessandro deFalco &
Michela Lai

Directional Dark Matter detection

- **Non rotating Wimp Halo + Barionic matter rotation**

Apparent Wimp wind

Solar System orbit at $v_0 \sim 220$ km/s around the galactic center

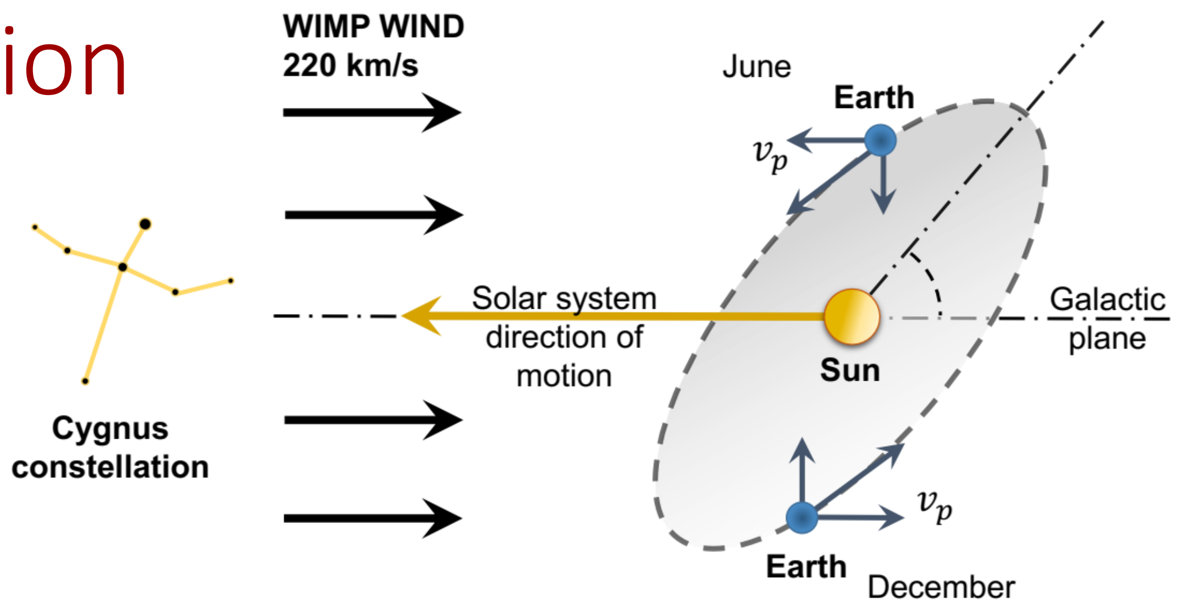

Standard technique: Annual (daily) rate modulation

-Annual modulation due to Earth revolution around the sun $v_E \cong \pm 30$ km/s: few percent effect

-Daily modulation due to Earth rotation around its own axis (~ 0.46 km/s): negligible effect!

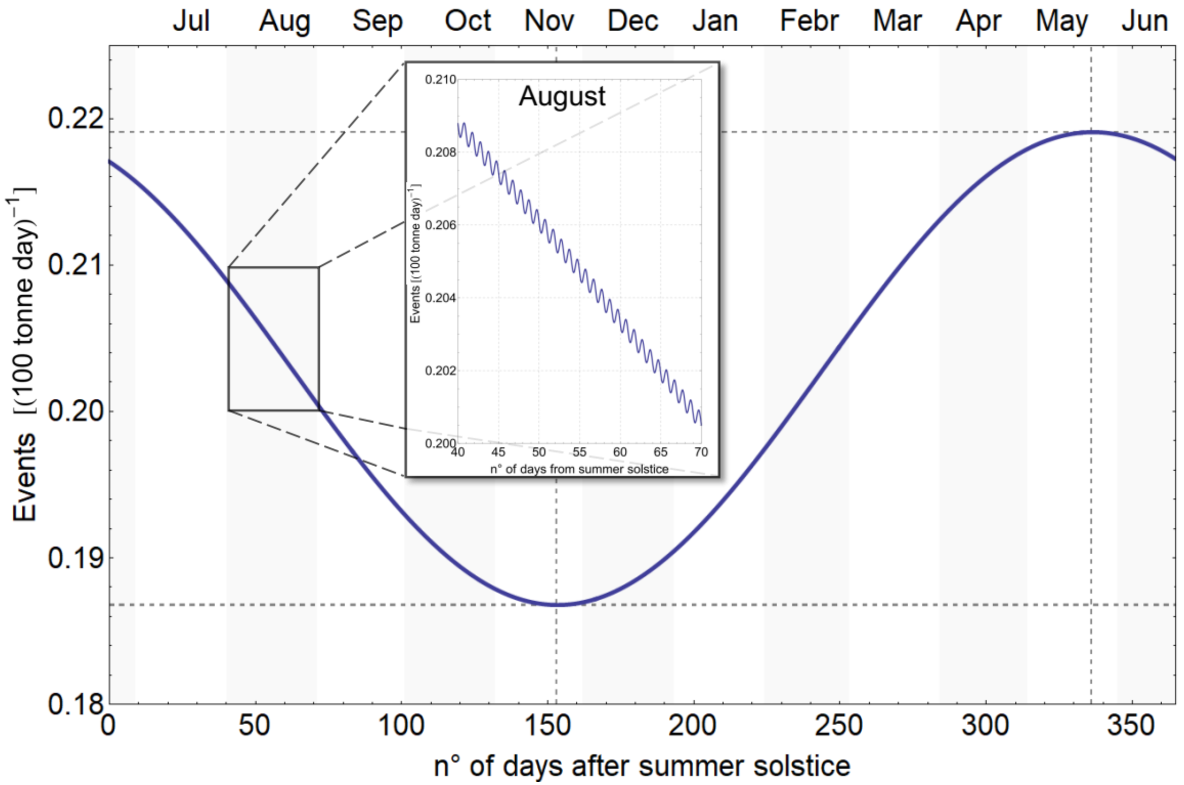

Innovative technique: sidereal direction modulation

Measuring the angle between WIMP and Earth gives a directionality signature unique to WIMPs.

Directionality may be the most robust signature of the WIMP nature of DM

Horizontal and Vertical events modulation

M. Cadeddu *et al., EPJ vol. 164, no. 07036, 2017.*
M. Cadeddu *et al., Arxiv:1704.03741 (submitted to JHEP), 2017*
G. Fiorillo and **M. Cadeddu***, PoS, vol. NOW2016, p. 091, 2017.*
M. Cadeddu*, Nuovo Cim., vol. C40, no. 1, p. 66, 2017.*
M. Cadeddu*, J. Phys. Conf. Ser., vol. 689, no. 1, p. 012015, 2016.*

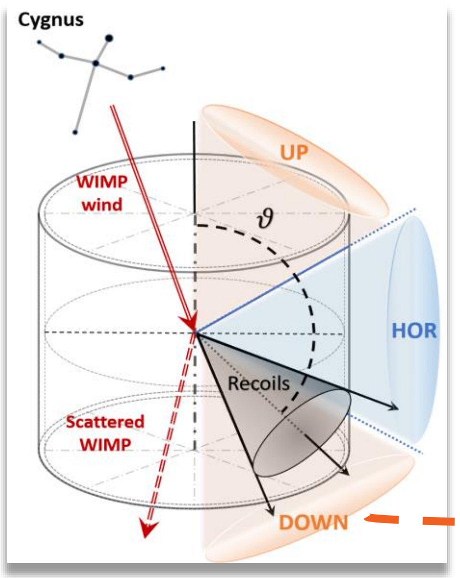

Cygnus close to the zenith: vertical events are greater than horizontal ones at the beginning of the day, until 8:00 a.m.

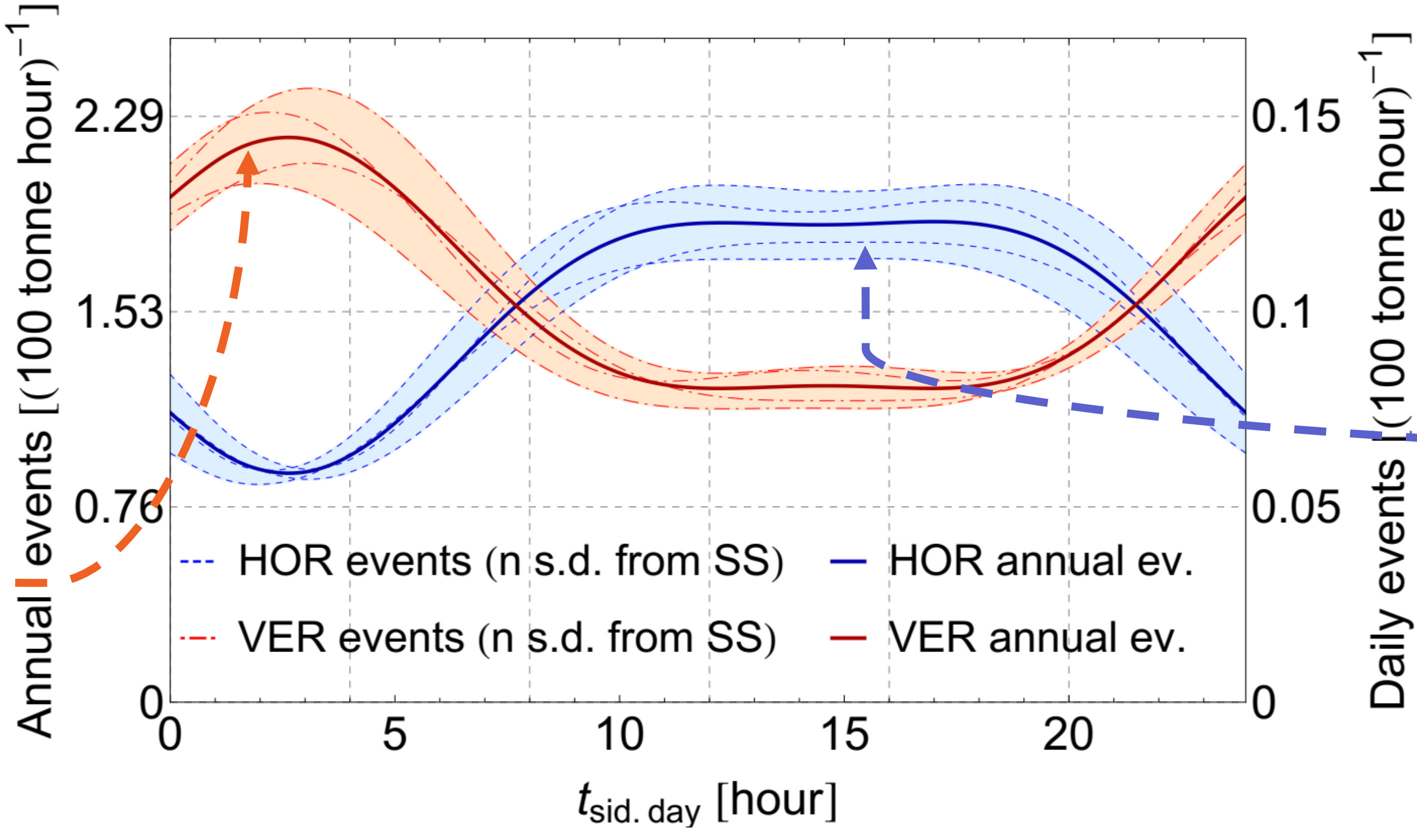

The single horizontal (vertical) component shows a huge variation within a sidereal day, a 38% (30%) effect with respect to the average.

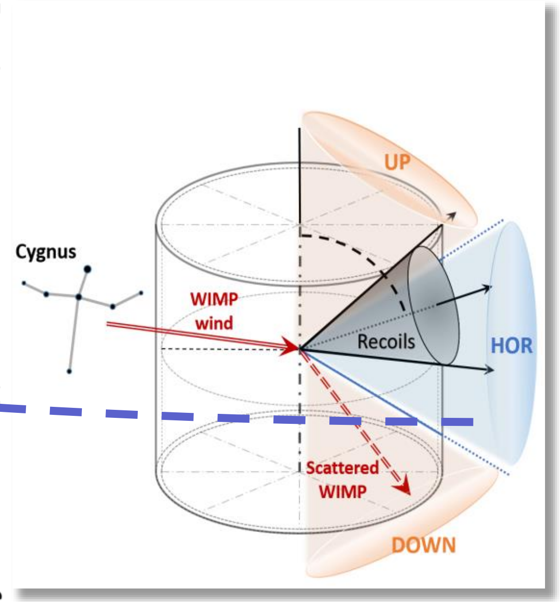

Cygnus close to the horizon: horizontal events are greater than vertical ones in the middle of the day, after 8:00 a.m.

The study of angular properties of the observed nuclear recoils can corroborate the belief that the observed signal can be attributed to genuine DM interactions

Wimp directionality in Galactic frame

$$\frac{dR}{d\cos\vartheta\, d\varphi} = \int_{50\ keV}^{200\ keV} \frac{dR}{dE_r d\cos\vartheta\, d\varphi} dE_r$$

In the Galactic coordinate system $\boldsymbol{x}$ points from the Sun towards the Galactic center, $\boldsymbol{y}$ in the direction of the Solar motion and $\boldsymbol{z}$ towards the Galactic north pole; therefore, $\boldsymbol{V} = V_{SG}\ \boldsymbol{y}$.

Unambiguous difference between WIMP and background!

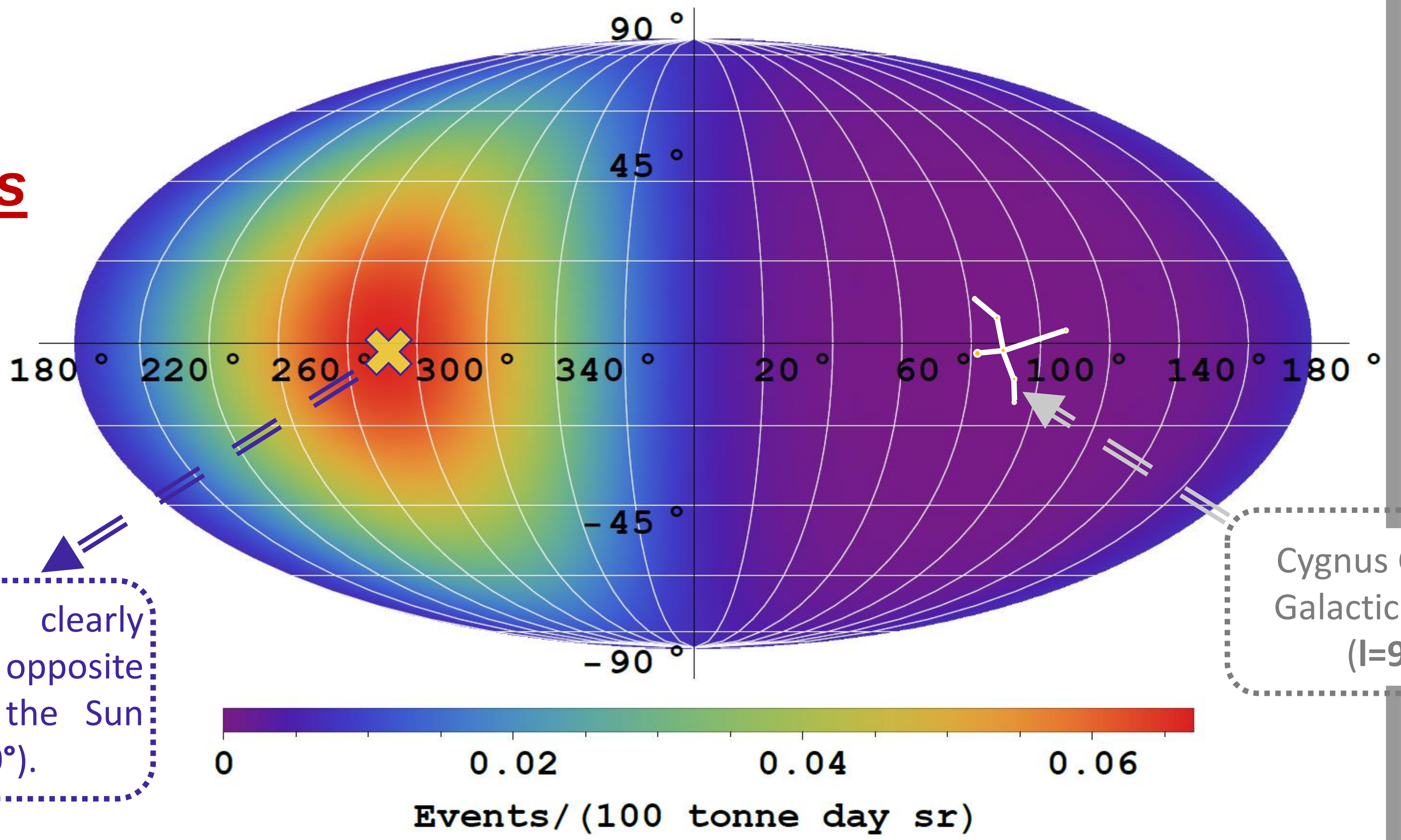

The recoil rate is clearly anisotropic and points opposite to the direction of the Sun motion (**l = 270°; b = 0°**).

Cygnus Constellation Galactic Coordinates (**l=90°,b=0°**)

Angular distribution of Argon recoils in Mollweide equal area projection maps of the celestial sphere in galactic coordinates (l, b)

Moving from theory to experiment (SCENE experiment)

Scintillation

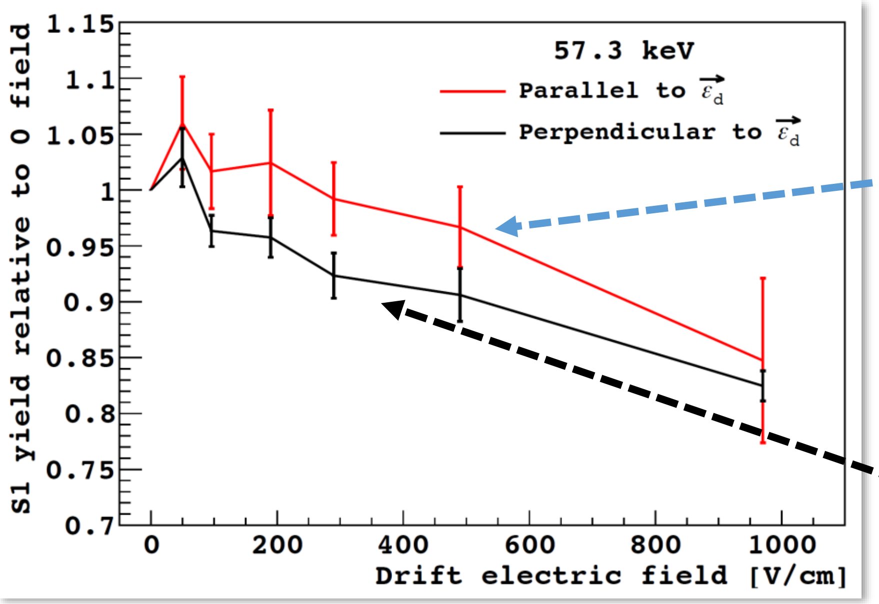

Ionization

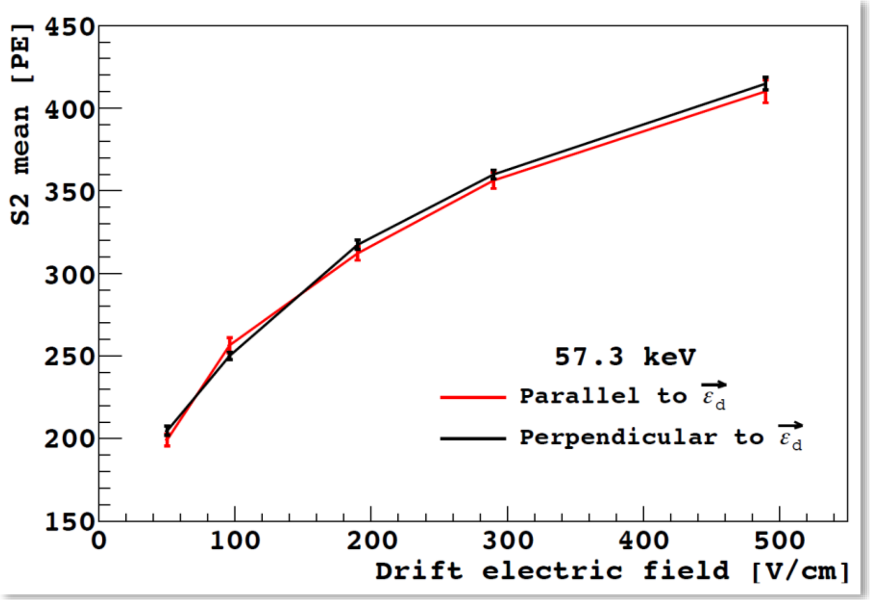

Substantial CR: **more light (S1)**, less charge (S2)

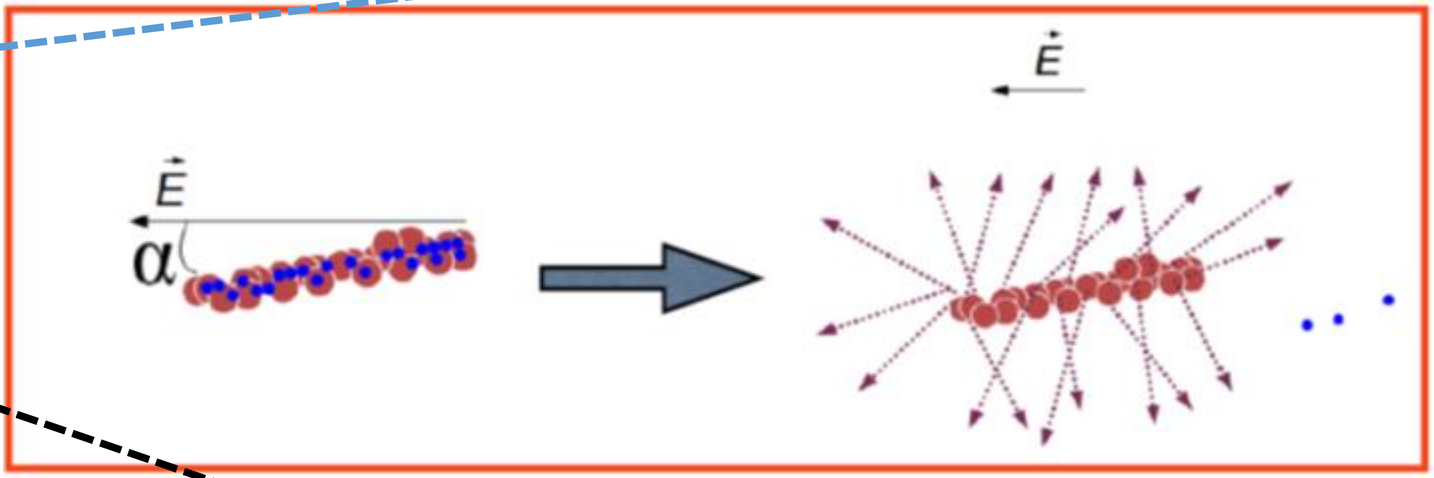

CR small: **less light (S1)**, more charge (S2)

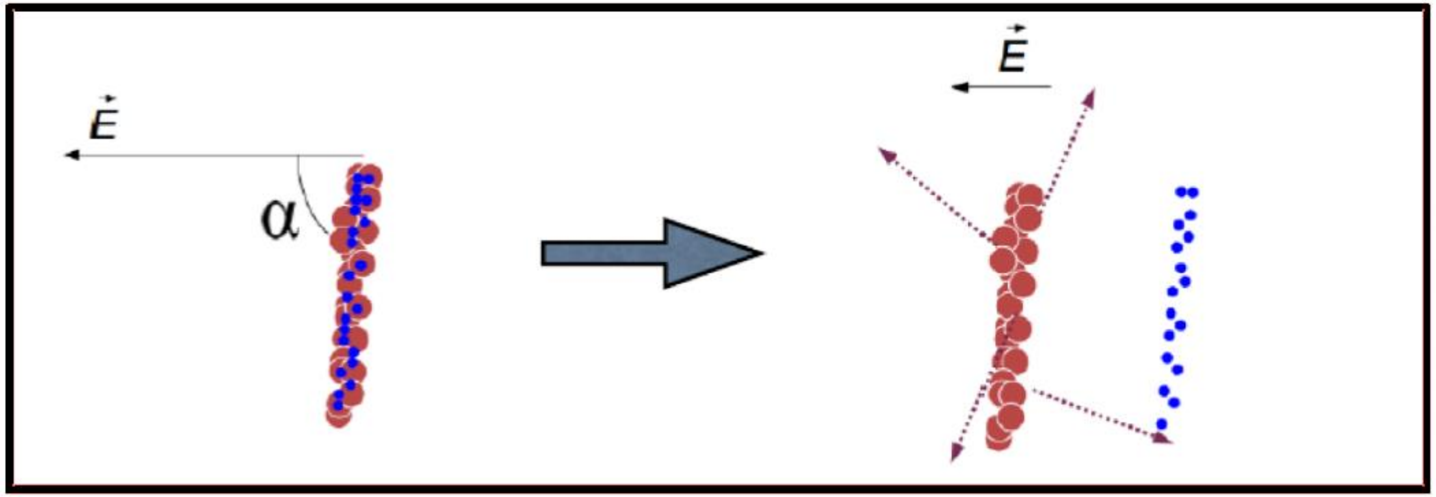

WIMP/neutrino discrimination using directional information

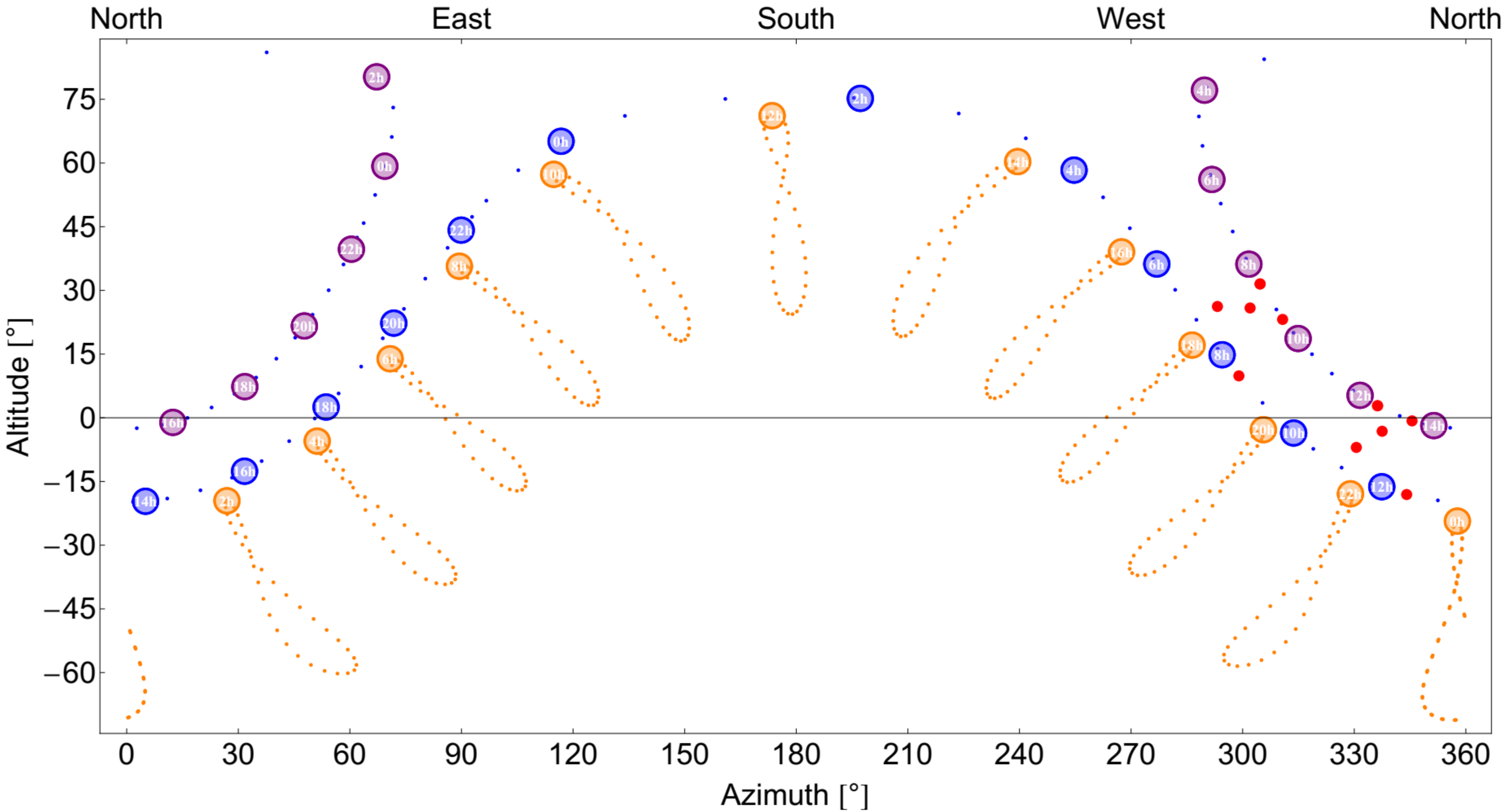

As seen in the laboratory (LNGS)

For an Earth-bound laboratory the velocity $\mathbf{V}$ can be decomposed as $\mathbf{V} = -\mathbf{V_{SG}} - \mathbf{V_{ES}}$, where $\mathbf{V_{ES}}$ is the Earth velocity relative to the Sun, $|\mathbf{V_{ES}}| \cong 29.8\ km/s$. The detector is a rotating reference frame.

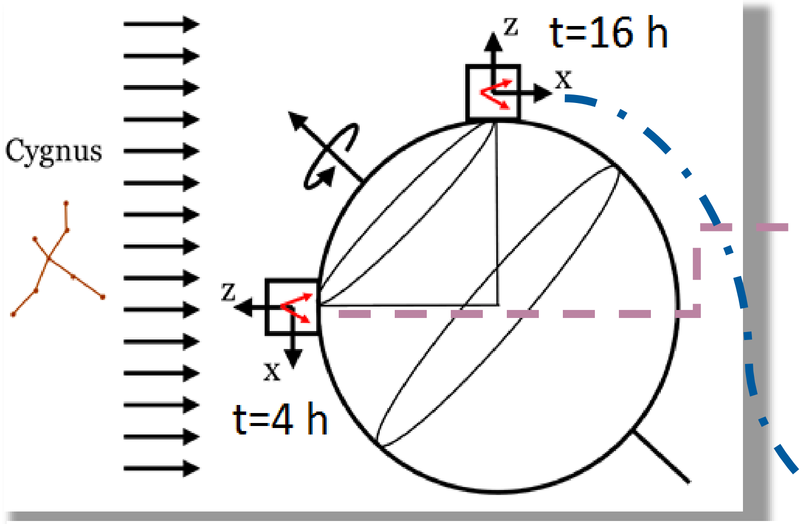

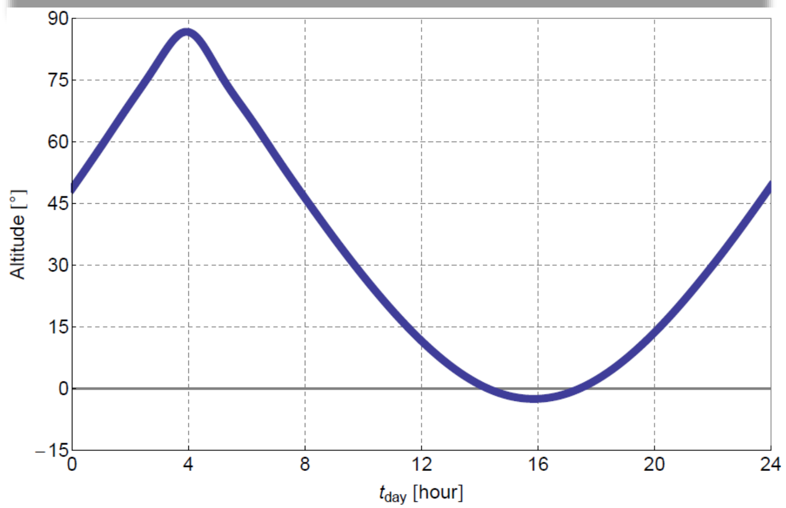

**The azimuthal ϕ angle is integrate [0, 2π]*

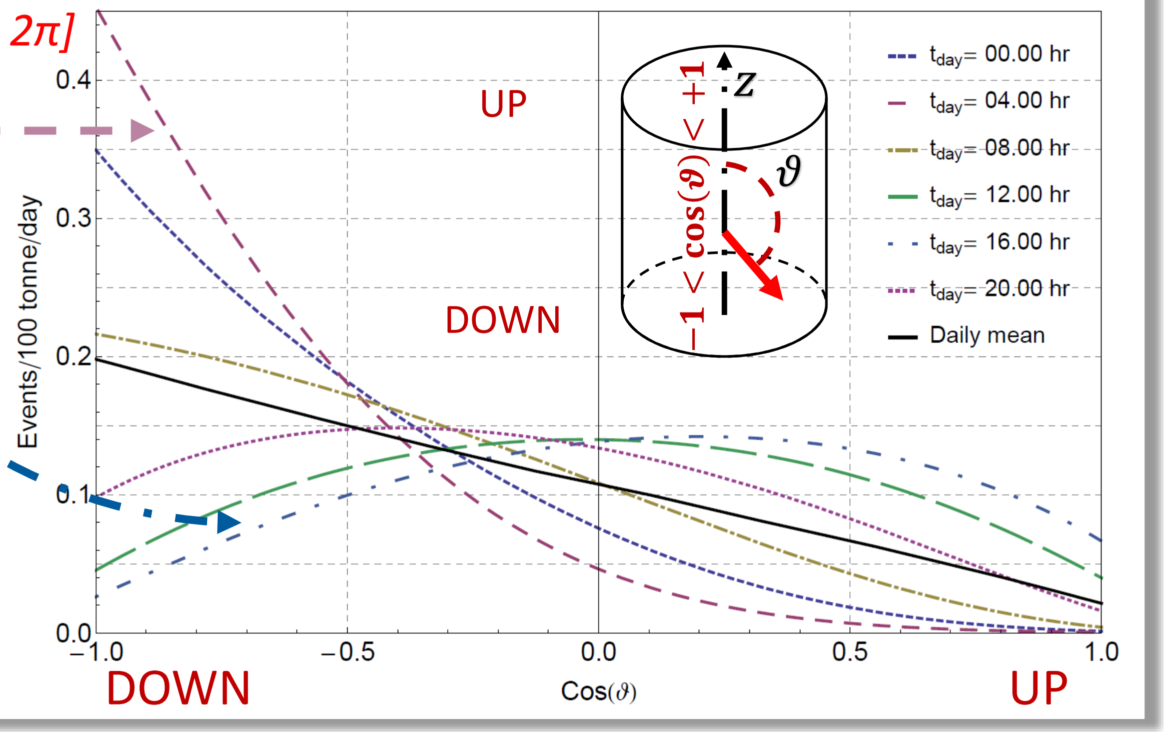

Strong angular dependence of the event rate with respect to the z-axis of the detector as a function of the time of the day.

The dependence remains also when it is mediated over the full day (see the black line: "Daily average").

Columnar recombination (CR)

The basic idea of CR:

When a nuclear recoil is parallel to the electric field, as in Case 1, there will be more electron-ion recombination since the electrons pass more ions as they drift through the chamber.

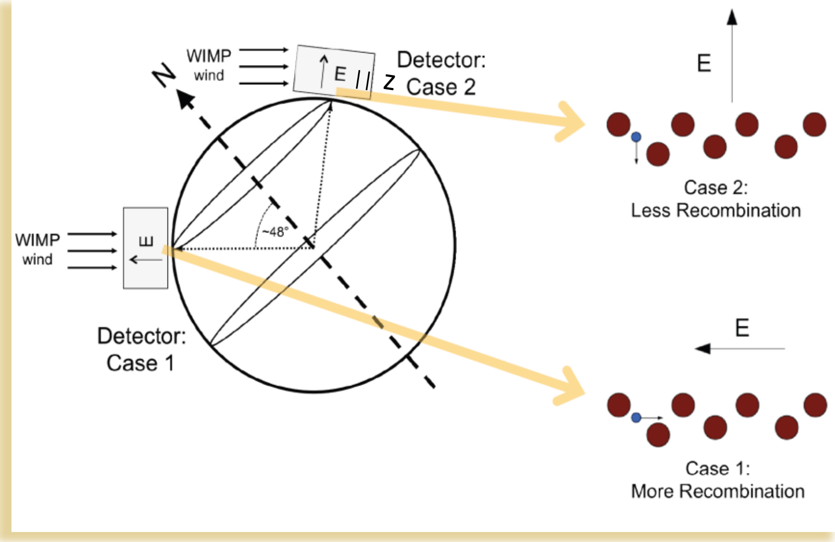

Recoils at 180° give the same signal in detectors based on CR

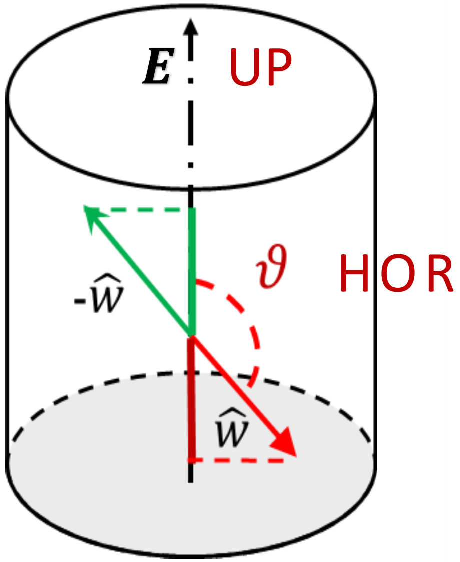

Columnar Recombination may display a sensitivity to the angle between nuclear recoil direction and drift field ***E*** in a LAr TPC.

We introduce a **"folded"** recoil rate:

$$\frac{dR_F(|\cos\vartheta|)}{d\cos\vartheta} \equiv \frac{dR(\cos\vartheta)}{d\cos\vartheta} + \frac{dR(-\cos\vartheta)}{d\cos\vartheta}$$

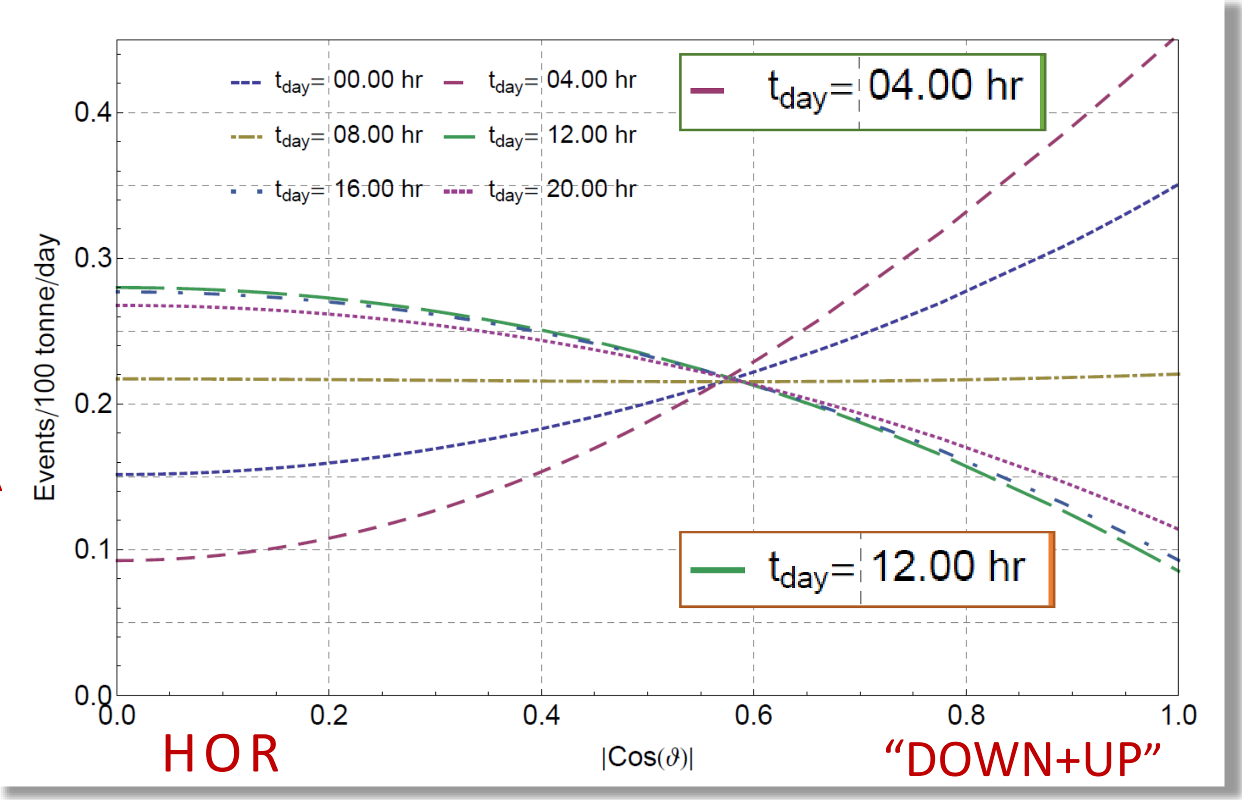

Strong angular dependence of the event rate with respect to the z-axis of the detector as a function of the time of the day

	liquid Ar	liquid Xe
Z (A)	18 (40)	54 (131)
temperature	87 K (close to nitrogen)	166 K
density	1.4 g/cm^3	3.1 g/cm^3
ionisation yield	42 e$^-$/keV	64 e$^-$/keV
scintillation yield	40 ɣ/keV	46 ɣ/keV
scintillation wavelength	128 nm	178 nm
radio-purity	^{39}Ar contamination, can be reduced	intrinsically pure
pulse-shape discrimination	yes (singlet ~7 ns, triplet ~1600 ns)	very limited (singlet ~2 ns; triplet ~27 ns)
sensitivity	better for m_{WIMP} > 100 GeV spin-independent only	also to low masses and spin-dependent

The WIMP spectrum

Standard **recoil spectrum**, i.e. differential event rate **per unit detector** mass:

$$\frac{dR}{dE_r} \propto \frac{\sigma_{SI}^{p}}{2\,\mu_{\chi p}^{2} M_\chi} \quad A^2|F(E_r)|^2 \quad \rho_0 \int_{v_{min}}^{\infty} \frac{f_1(v)}{v}\, dv$$

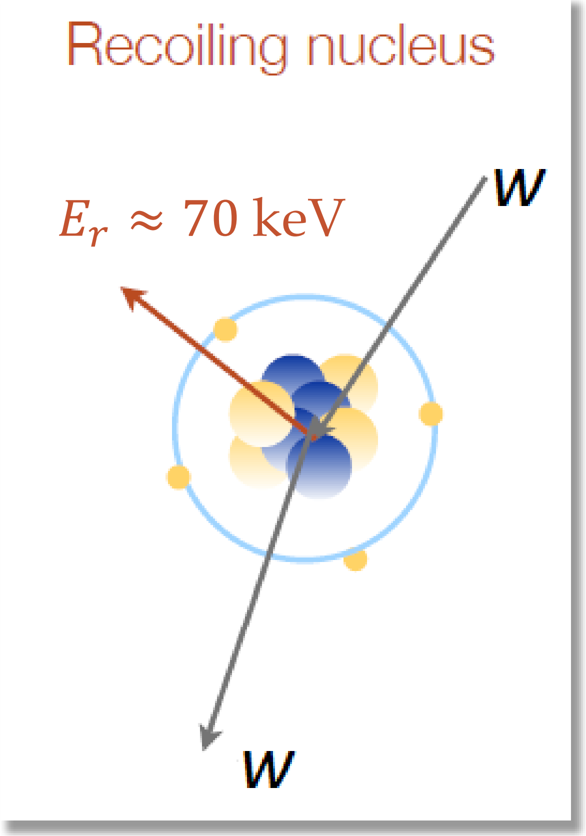

Physics

σ_{SI}^{p} → WIMP-nucleon cross section

M_χ → WIMP mass

$\mu_{\chi p}$ → WIMP-nucleon reduced mass

$\mu_{\chi N}$ → WIMP-nucleus reduced mass

Target material

A → atomic mass of target material

$F(E_r)$ → The finite size of the nucleus is implemented with a nuclear **Helm form Factor**

E_{th} → Energy threshold

Astrophysics (DM halo properties)

ρ_0 → local WIMP mass density

$f(v)$ → WIMP velocity distribution

v_{min} → minimum WIMP speed required to transfer an energy E_r to the nucleus of mass m_n in the detector.

E_r → Recoiling nucleus energy

$$v_{min} = \sqrt{m_N E_r / (2\mu_{\chi N}^2)}$$

After unblinding: Step by step…

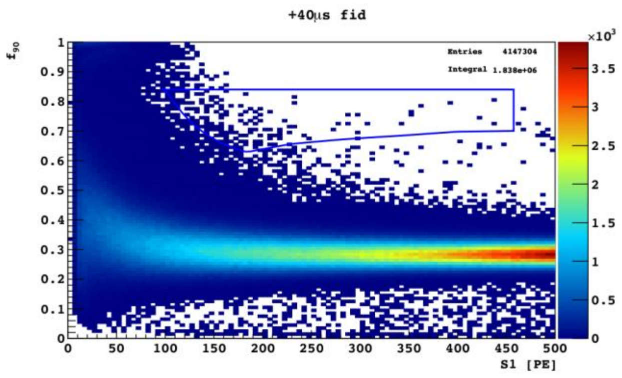

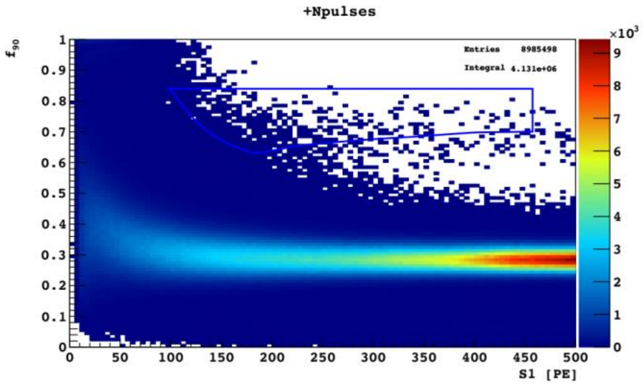

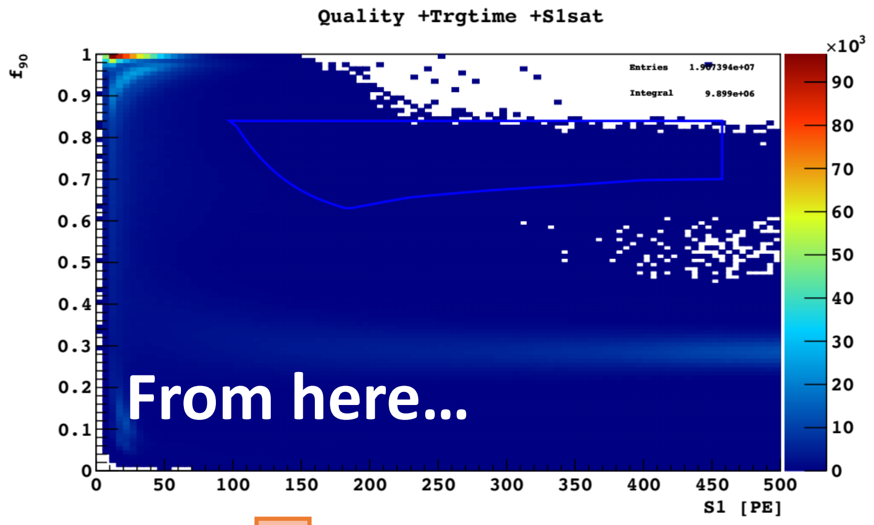

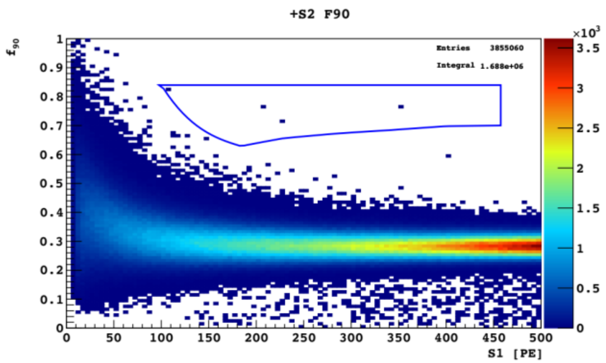

Cut over cut…

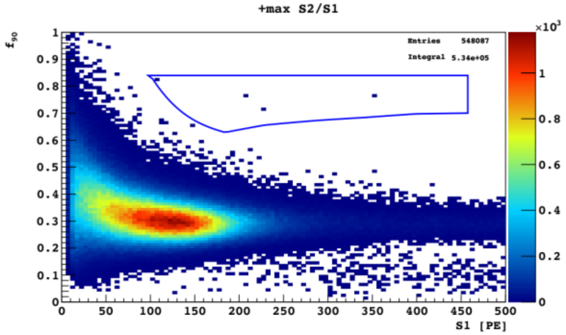

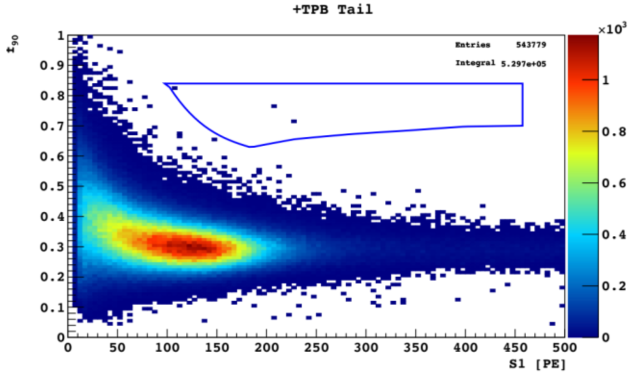

…to here: the final data set

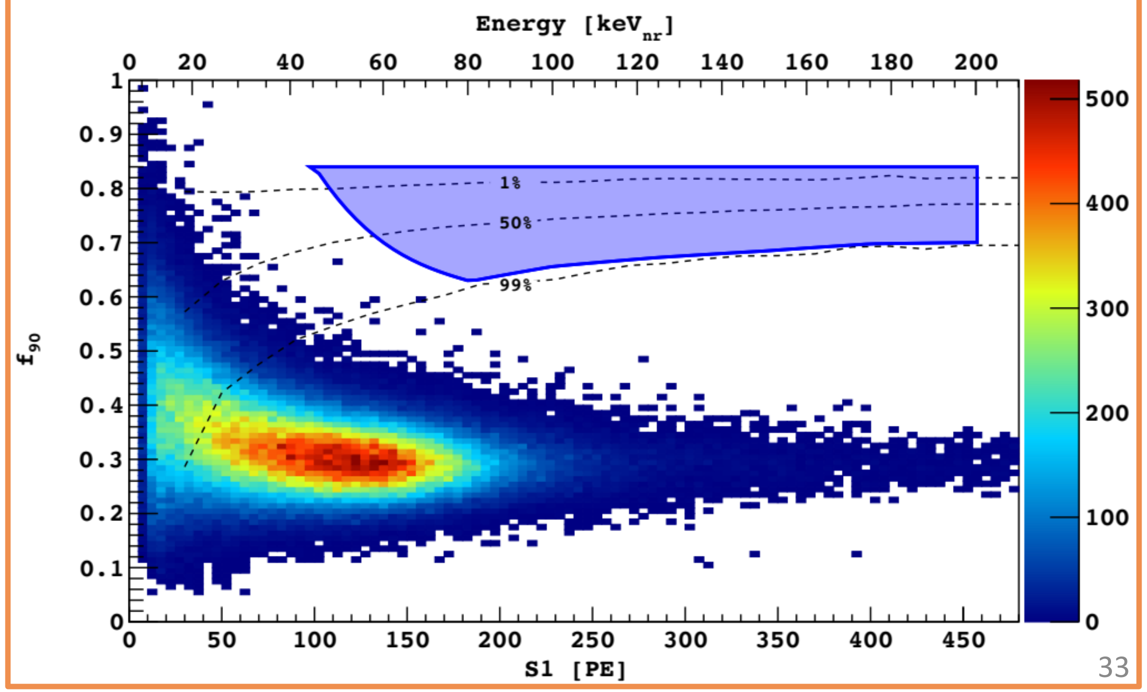

Nuclear and Electron recoil backgrounds

Surface α decays

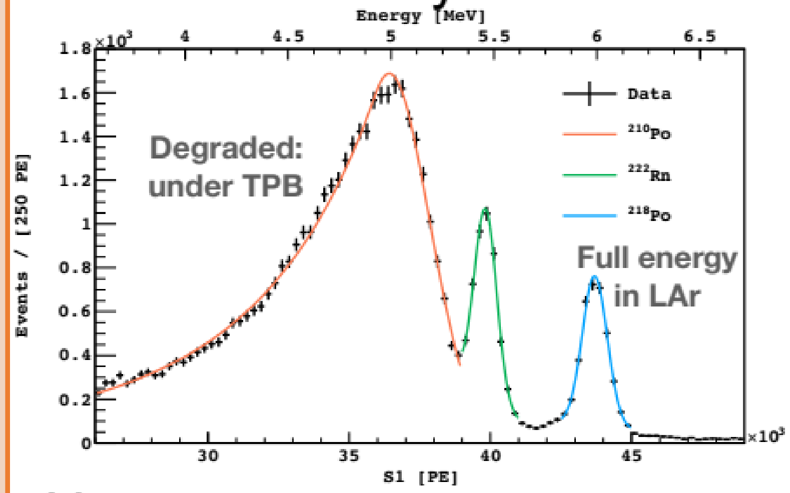

Neutrons

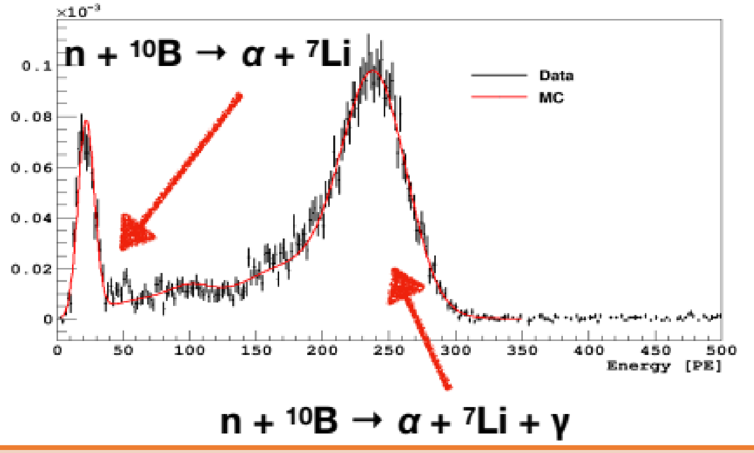

Background rejection:

- S1 < 460
- Self-vetoing in DS-50!
  - -Small or no S2
  - -Long scintillation tail from TPB

Background rejection:

- TPC: multi-scatter
- LS Veto

Measured neutron efficiency with Am-C for TPC single-NR is 0.9964±0.0004

- Cosmogenics:

Water Cherenkov Veto

Electron Recoils: S1 + Cherenkov

γ-ray multiple-Compton scatters once in LAr and again in a nearby Cherenkov radiator.

Background rejection:

- Underground argon
- S1 fraction in max PMT
- PSD: f90 = S1 fraction in first 90 ns

(*) Design cut to reduce ER to <0.08 event of background

Summary of NR and ER backgrounds

Background	Est. Survive
Surface a decays	0.001
Cosmogenic n	<0.0003
Radiogenic n	<0.005
ER S1+Cherenkov	0.08*
Total	**0.09±0.04**

Goal achieved: open the box!

Low-mass WIMP search with ionization only data

ArXiv:1802.06994 *Low-mass Dark Matter Search with the DarkSide-50 Experiment*

$$E_R = \frac{q^2}{2m_N} \leq \frac{2\mu_{\chi N}^2 v^2}{m_N} \simeq 50\ keV \left(\frac{m_\chi}{100\ GeV}\right)^2 \left(\frac{100\ GeV}{m_N}\right)$$

$m_N^{Ar} \sim 37$ GeV

For $m_\chi = 10$ GeV ➡ $E_R \sim 1.4$ KeV

Below threshold for S1 production ($\sim 6\ keV_{nr}$) but S2 has threshold $\sim 0.4\ keV_{nr}$

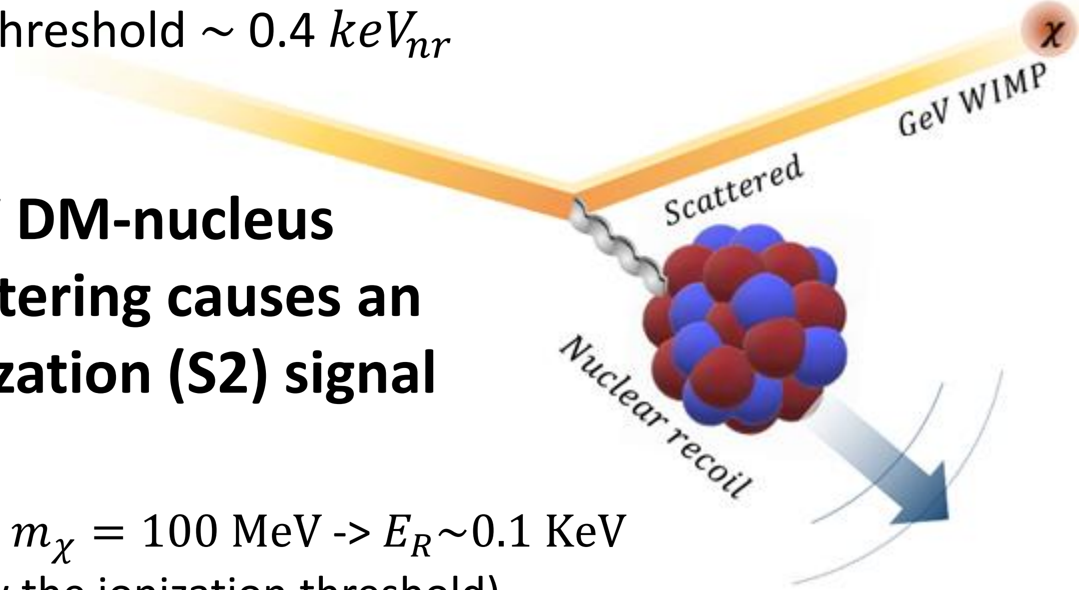

GeV DM-nucleus scattering causes an ionization (S2) signal

*(For $m_\chi = 100$ MeV -> $E_R \sim 0.1$ KeV below the ionization threshold)

ArXiv:1802.06998 *Constraints on Sub-GeV Dark Matter-Electron Scattering from the DarkSide-50 Experiment*

$$E_R = \vec{q} \cdot \vec{v} - \frac{q^2}{2\mu_{\chi N}} \sim \frac{1}{2}\ eV \times \left(\frac{m_\chi}{MeV}\right)$$

For $m_\chi = 100$ MeV ➡ $E_R \sim 50$ eV

Comparable with electron binding energies in argon (~16-34 eV)!

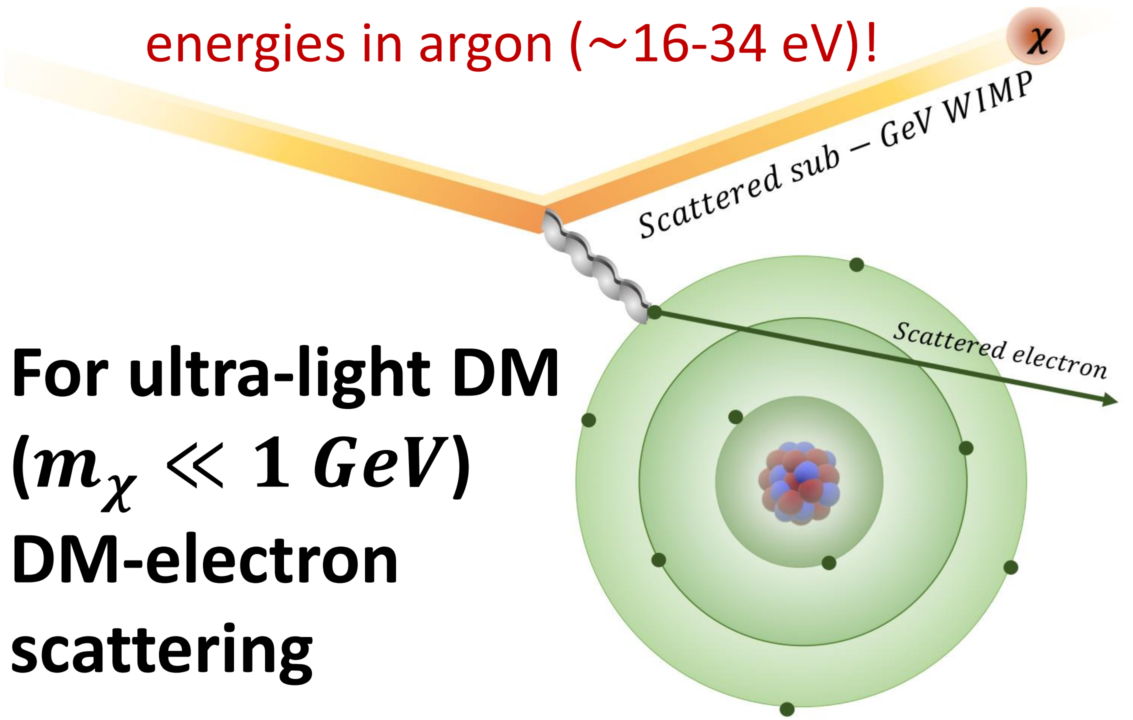

For ultra-light DM ($m_\chi \ll 1\ GeV$) DM-electron scattering

Ionization measurement

Scintillation signal (S1): threshold at $\sim 2\ keV_{ee}$ / $6keV_{nr}$ weak sensitivity to low mass WIMPs.

In DS-50, we easily detect single ionization electrons

Ionization signal (S2): threshold > $\sim 0.1\ keV_{ee}$ / $0.4keV_{nr}$
Sensitive to low mass WIMPs!!

We use Ionization (S2) only

Detection efficiency: estimated from Data + MC

Fiducialization: use volume under 7 central PMTs

In DS-50, we can detect down to **single electron:**

One ionization electron ($N_e = 1$) under the center PMT creates 23 ±1 PE

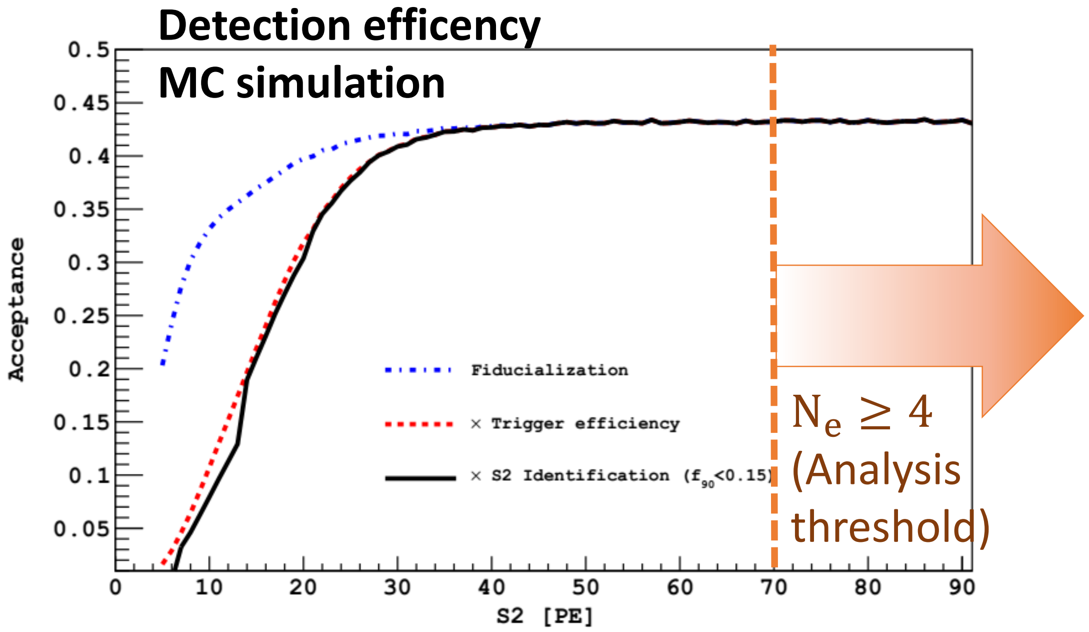

The efficiency is flat above the analysis threshold of number of electrons >4

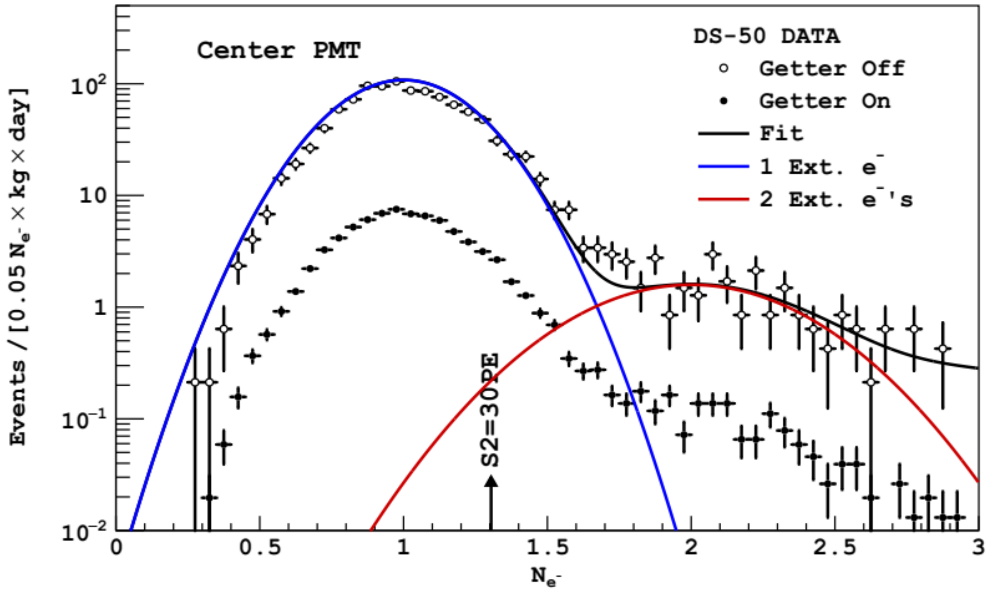

Energy scale for ER and NR

- ^{37}Ar provides two x-rays, 2.82 keV and 0.27 keV.
- ^{37}Ar Decayed out with 35 day half-life and not remain in the last 500-days data set.
- Good agreement of BR with measured value.

- AmBe and AmC neutron sources are used to extract ionization yield at ROI
- The difference between other measured points is take as systematics

NR ionization yield is obtained by fitting AmBe and AmC neutron calibration data

Electron recoil energy scale

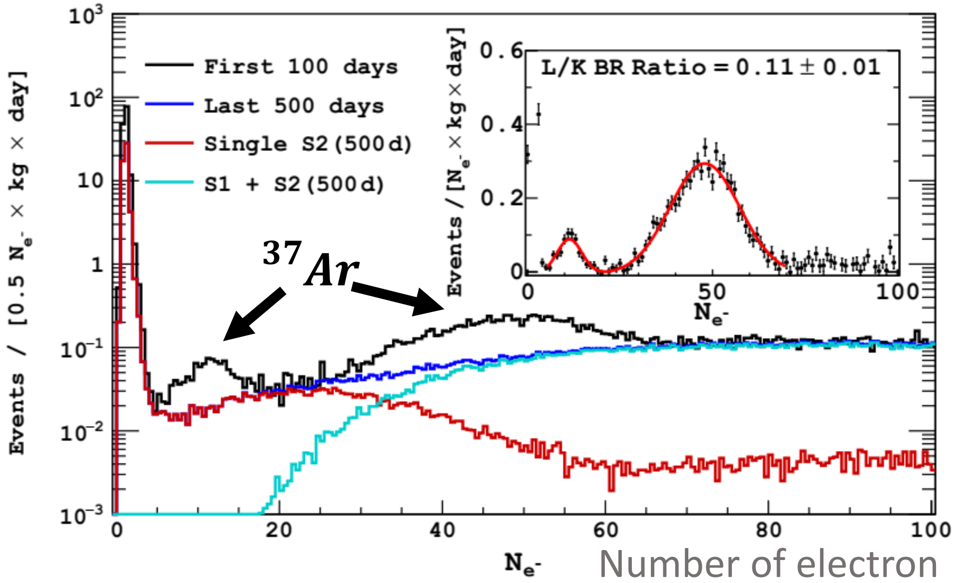

Nuclear recoil energy scale

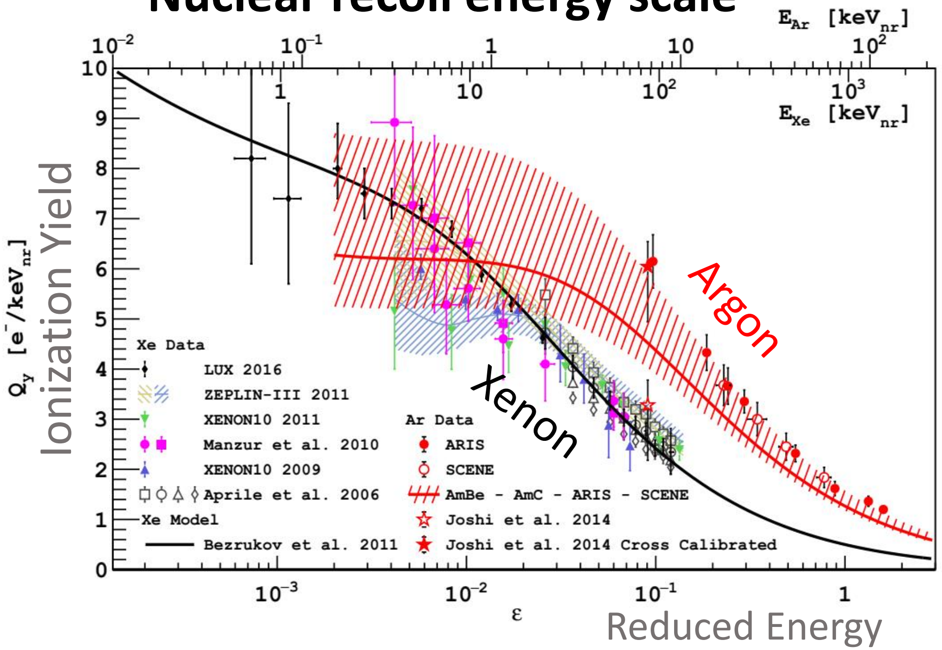

Interpretation for DM-electron scattering

DM-electron differential scattering rate

$$\frac{dR}{d\ln E_{\rm er}} = N_T \frac{\rho_\chi}{m_\chi} \frac{\overline{\sigma}_e}{8\,\mu_{\chi e}^2} \times \sum_{nl} \int dq\, q \left|f_{\rm ion}^{nl}(k',q)\right|^2 \left|F_{\rm DM}(q)\right|^2 \eta(v_{\rm min})$$

$$v_{\rm min} = \frac{|E_b^{nl}| + E_{\rm er}}{q} + \frac{q}{2m_\chi}.$$

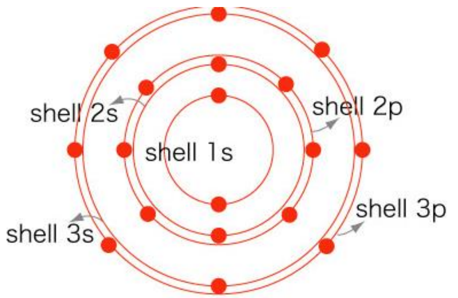

$E_b^{3p} \sim 16.08$ eV , $E_b^{3s} \sim 34.76$ eV,

$E_b^{2p} \sim 260.45$ eV, $E_b^{2s} \sim 335.30$ eV, $E_b^{1s} \sim 3227.51$ eV

Ionization form factor: DM-e rate depends on the initial and final-state wavefunction of the electron. The outgoing wavefunction is obtained by solving the Schroedinger equation with a hydrogenic potential of some effective screened charge Zeff.

$$|F_{\rm DM}(q)|^2 = \begin{cases} 1, & m_{\rm med} \gg \alpha m_e \\ (\alpha m_e/q)^4, & m_{\rm med} \ll \alpha m_e, \end{cases}$$

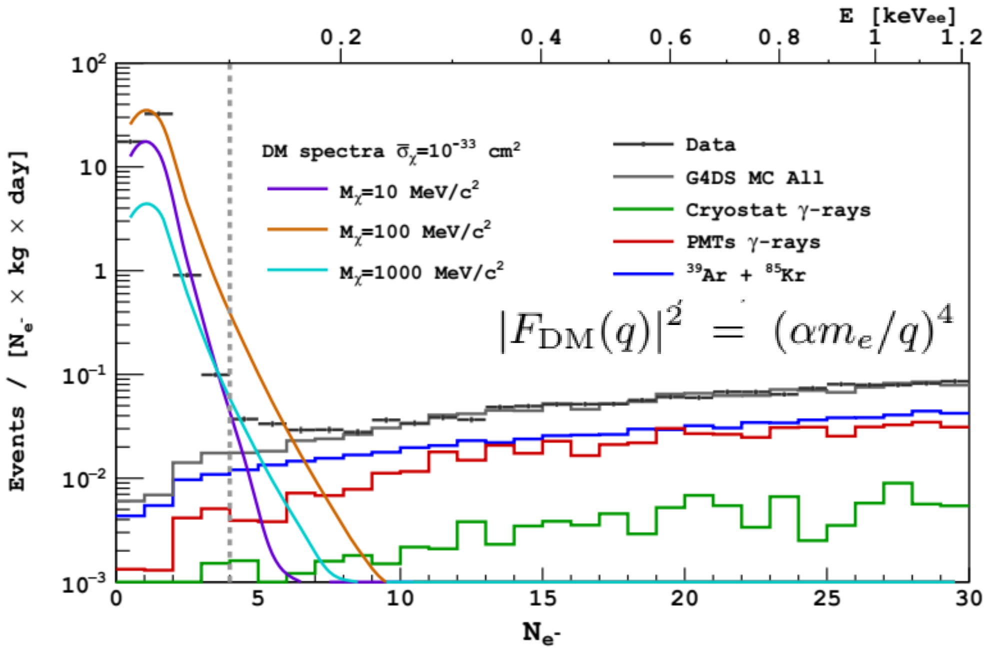

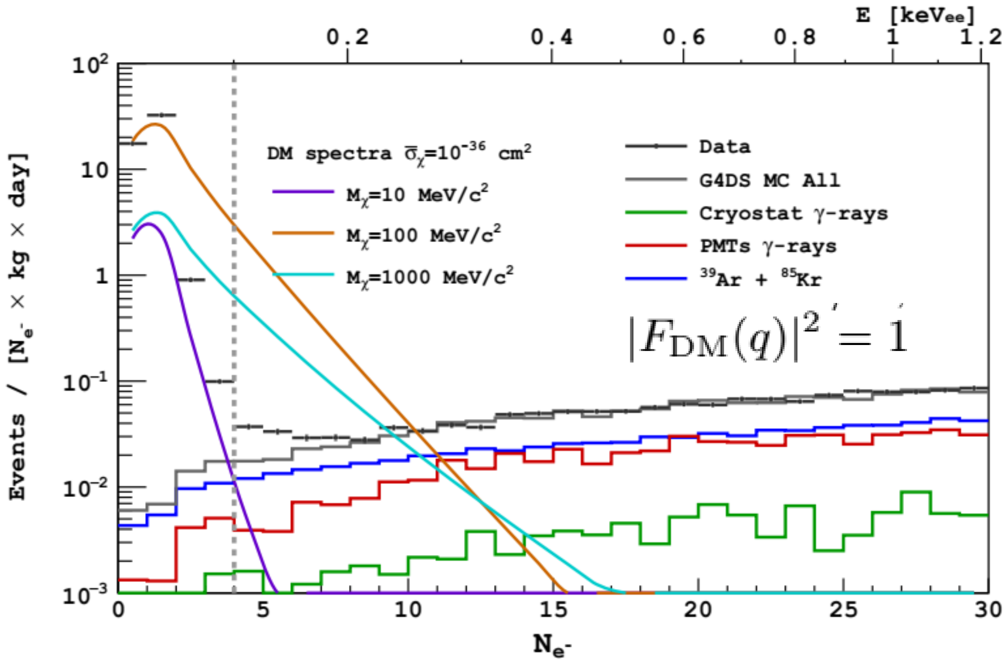

Coherent elastic neutrino nucleus scattering

CEnNS will induce nuclear recoils almost indistinguishable from those potentially induced by WIMPs.

$$\frac{d\sigma}{dE_r} = \frac{G_F^2}{4\pi} Q_w^2 m_N \left(1 - \frac{m_N E_r}{2E_\nu^2}\right) |F(E_r)|^2$$

$$\frac{dR_\nu(E_r)}{dE_r} = \eta \times \int_{E_{\nu_{min}}} \frac{dN}{dE_\nu} \times \frac{d\sigma(E_\nu, E_r)}{dE_r} dE_\nu$$

Neutrino fluxes @Earth

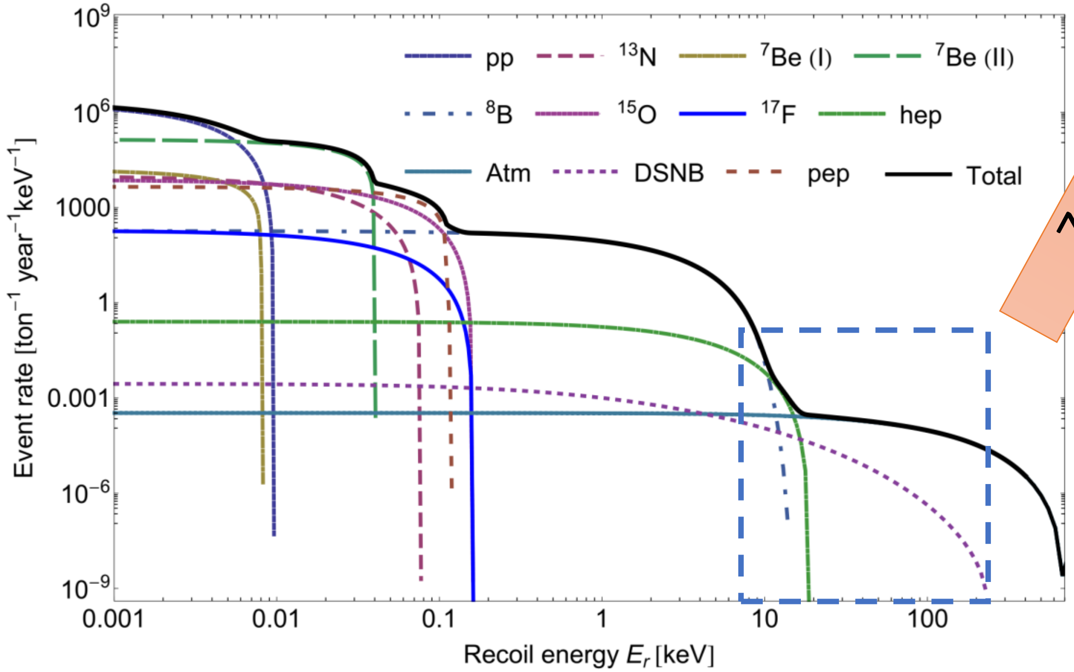

Zoom

Region of interest 1 keV$\lesssim E_r \lesssim$ 200 keV

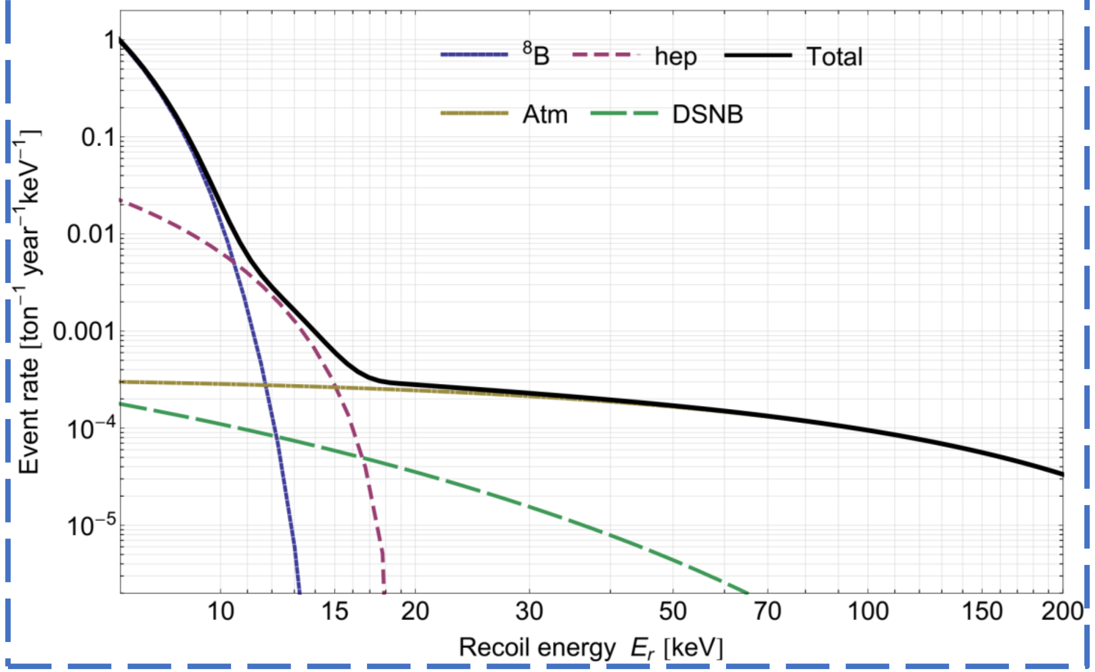

Atmospheric neutrinos are the dominant component for DarkSide-20k in the high-mass search region!

Current experimental results

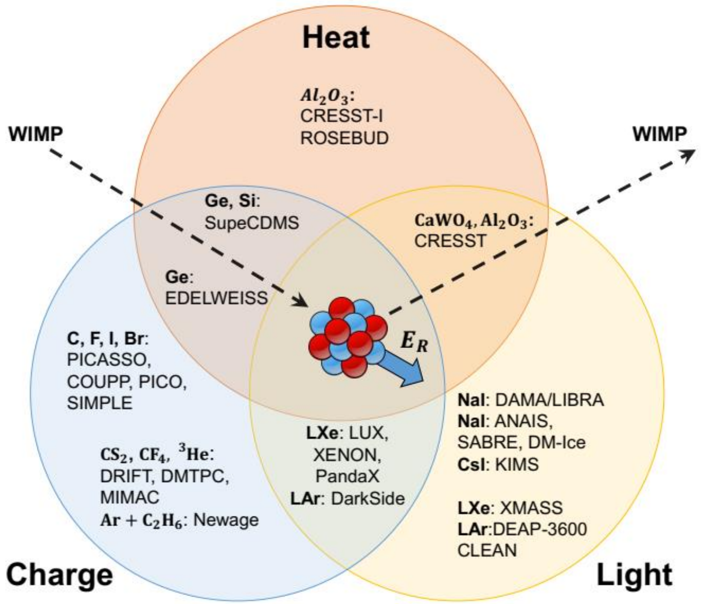

Scatterings of DM particles off nuclei can be detected via subsequently produced

- **light** (scintillation photons from excitation and later de-excitation of nuclei)
- **charge** (ionization of atoms in a target material)
- **heat** (phonons in crystal detectors)

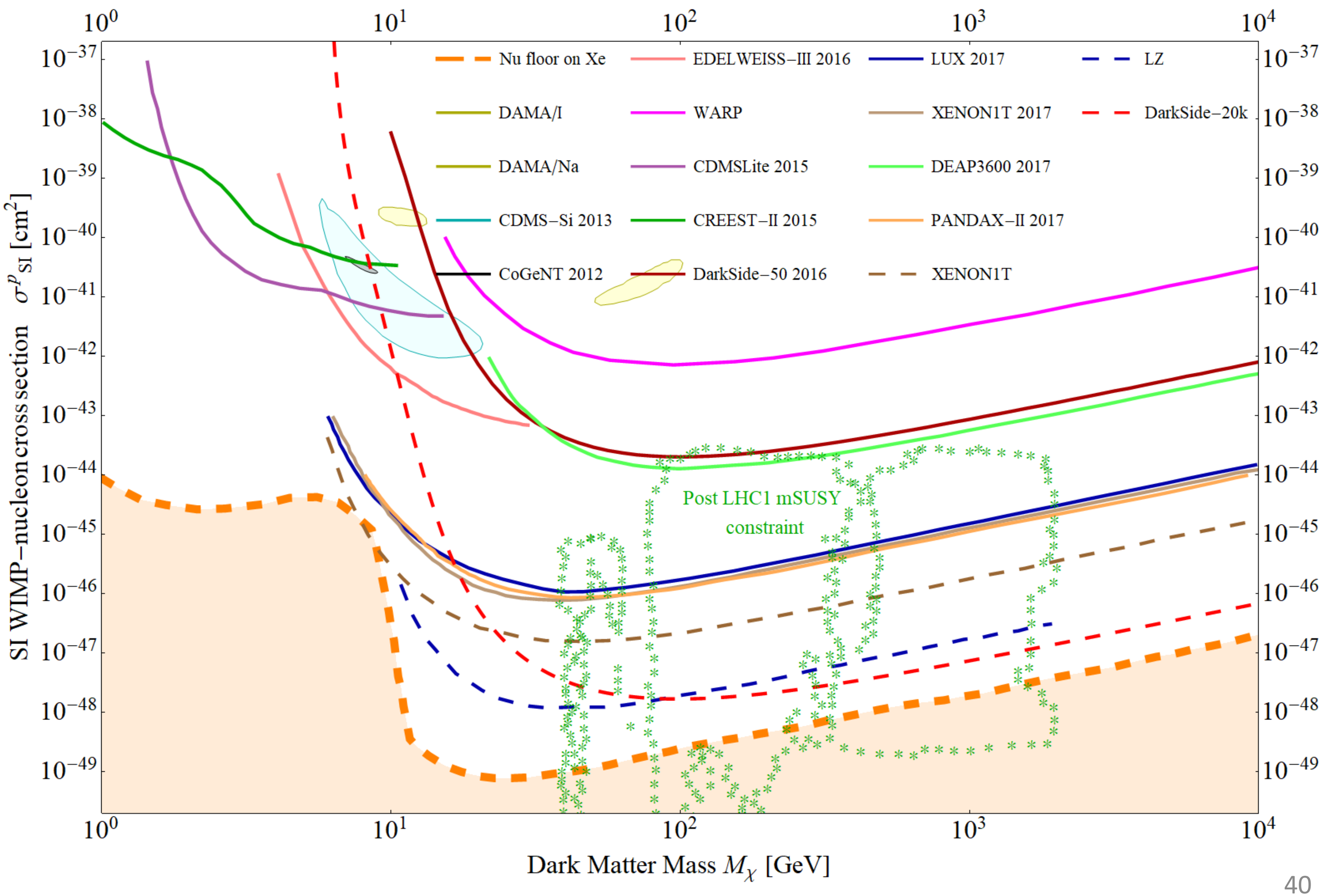

Suppression: AAr Vs UAr

Suppression: AAr Vs Uar

- Underground argon (UAr): 150 kg successfully extracted from a CO_2 well in Colorado

- **^{39}Ar depletion factor >1400**

PRD, 93 (2016): 081101(R)

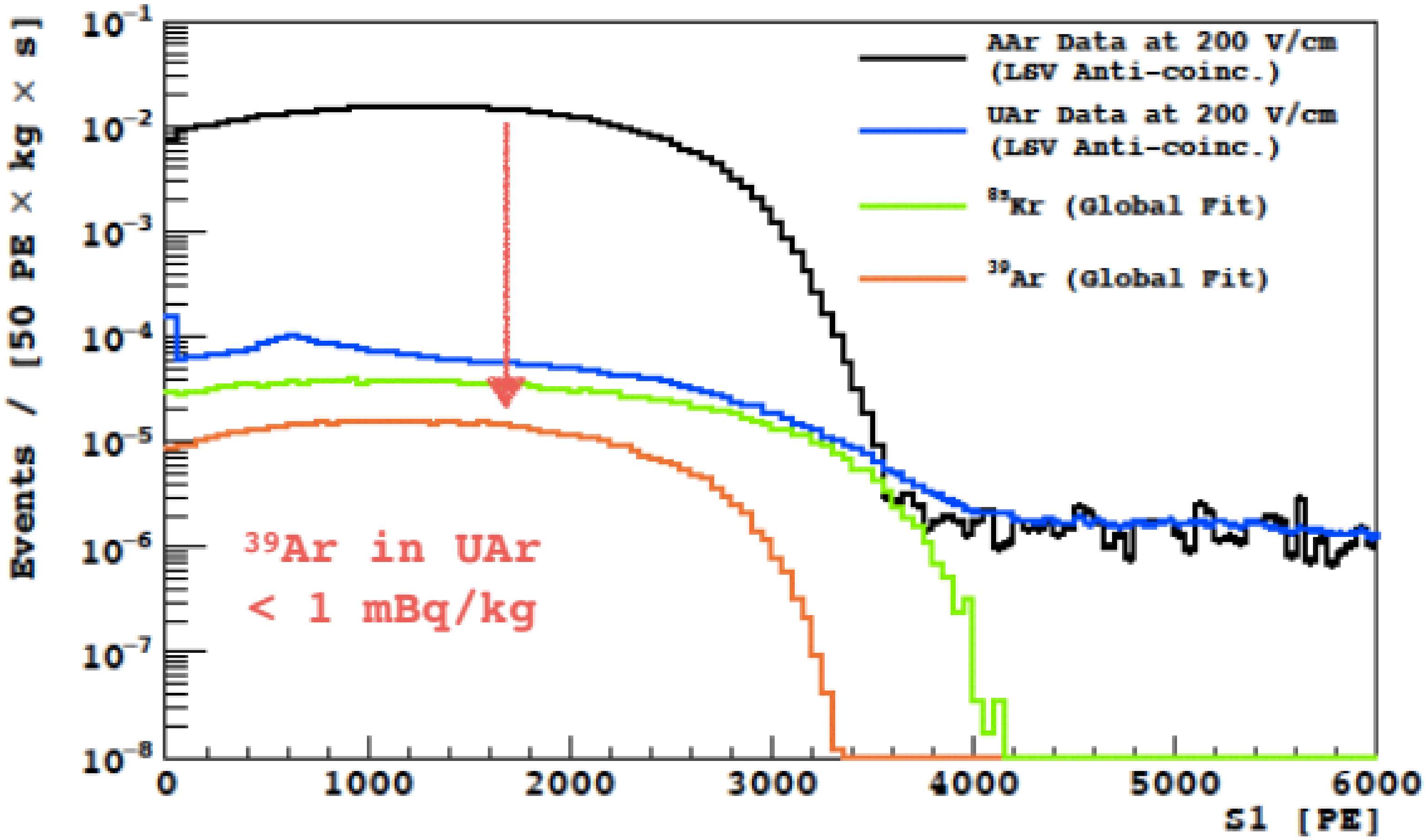

Backgrounds and nuclear recoil acceptance

Being dark matter interactions very rare it is of utmost importance to contain the number of **instrumental background interactions to <0.1 events**, so that a positive claim can be made with few events as possible

PSD incorporated in the f_{200} parameter (the fraction of S1 detected in the first 200 ns of the pulse)

NR acceptance region defined by requiring < 0.005 ER events/(5-PE bin) (< 0.1 events in the WIMP search region) .

The resulting ER reduction factor is $> 3 \times 10^9$

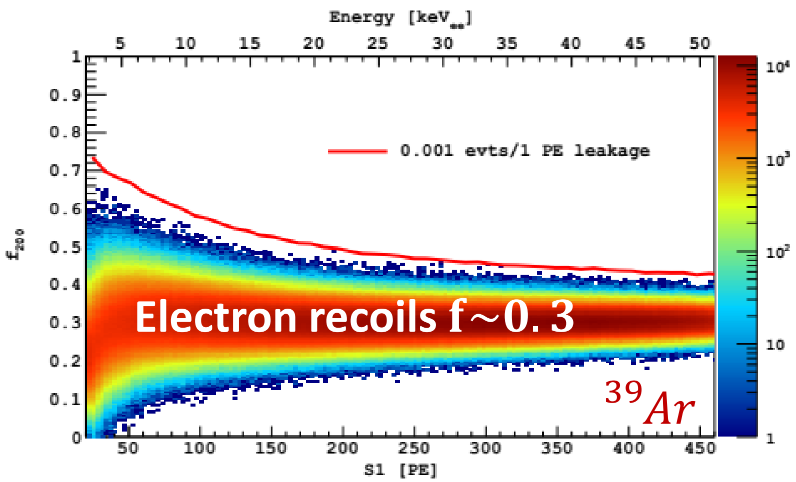

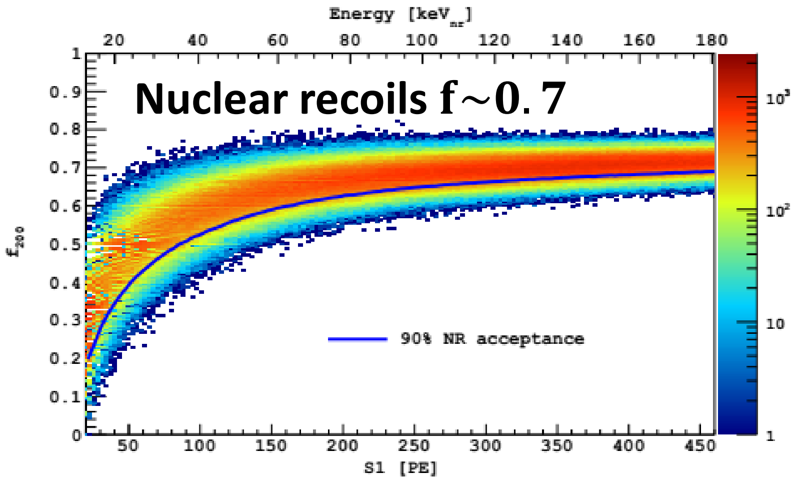

Background	Events in ROI $[100\,t\,yr]^{-1}$	Background $[100\,t\,yr]^{-1}$
Internal β/γ's	1.8×10^8	0.06
Internal NRs	negligible	negligible
e^--ν_{pp} scatters	2.0×10^4	negligible
External β/γ's	10^7	<0.05
External NRs	<81	<0.15
Cosmogenic β/γ's	3×10^5	$\ll$0.01
Cosmogenic NRs	–	<0.1
ν-Induced NR	1.33±0.26	1.33±0.26

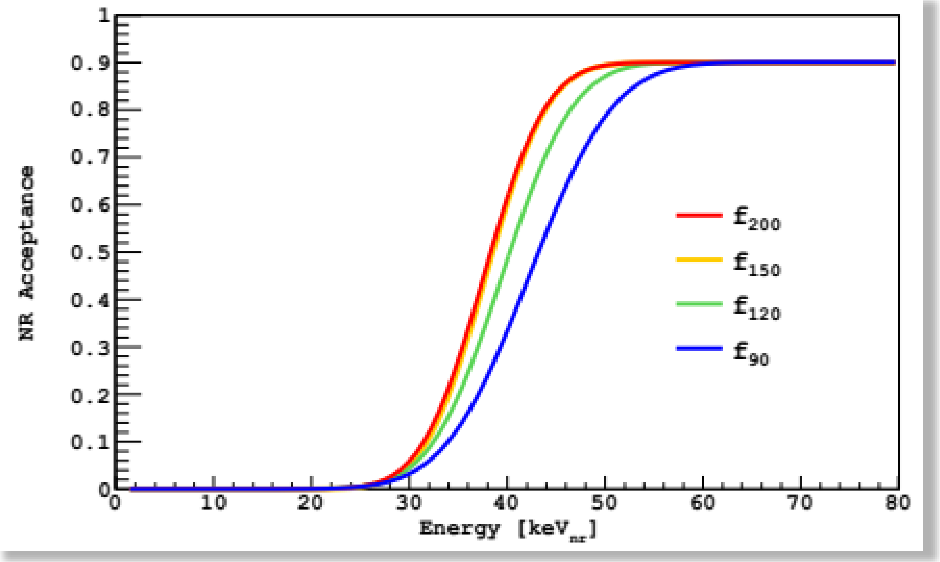

DarkSide-20k (GADMC) sensitivity

C. E. Aalseth et al., "DarkSide-20k: A 20 Tonne Two-Phase LAr TPC for Direct Dark Matter Detection at LNGS," Arxiv:1707.08145

(2021-) DarkSide-20k approved by INFN and LNGS in April 2017 and by NSF in October 2017 Officially supported by LNGS, LSC, and SNOLab.

(2027-) The argon community (ArDM, DarkSide, DEAP, MiniCLEAN) has coalesced into a Global Argon Dark Matter Collaboration (**GADMC**), to construct a **300 tonne** argon detector allowing a kilotonne-year exposure which will follow the DarkSide-20k experiment at LNGS.

90% CL WIMP-nucleon cross section in cm^2 sensitivity

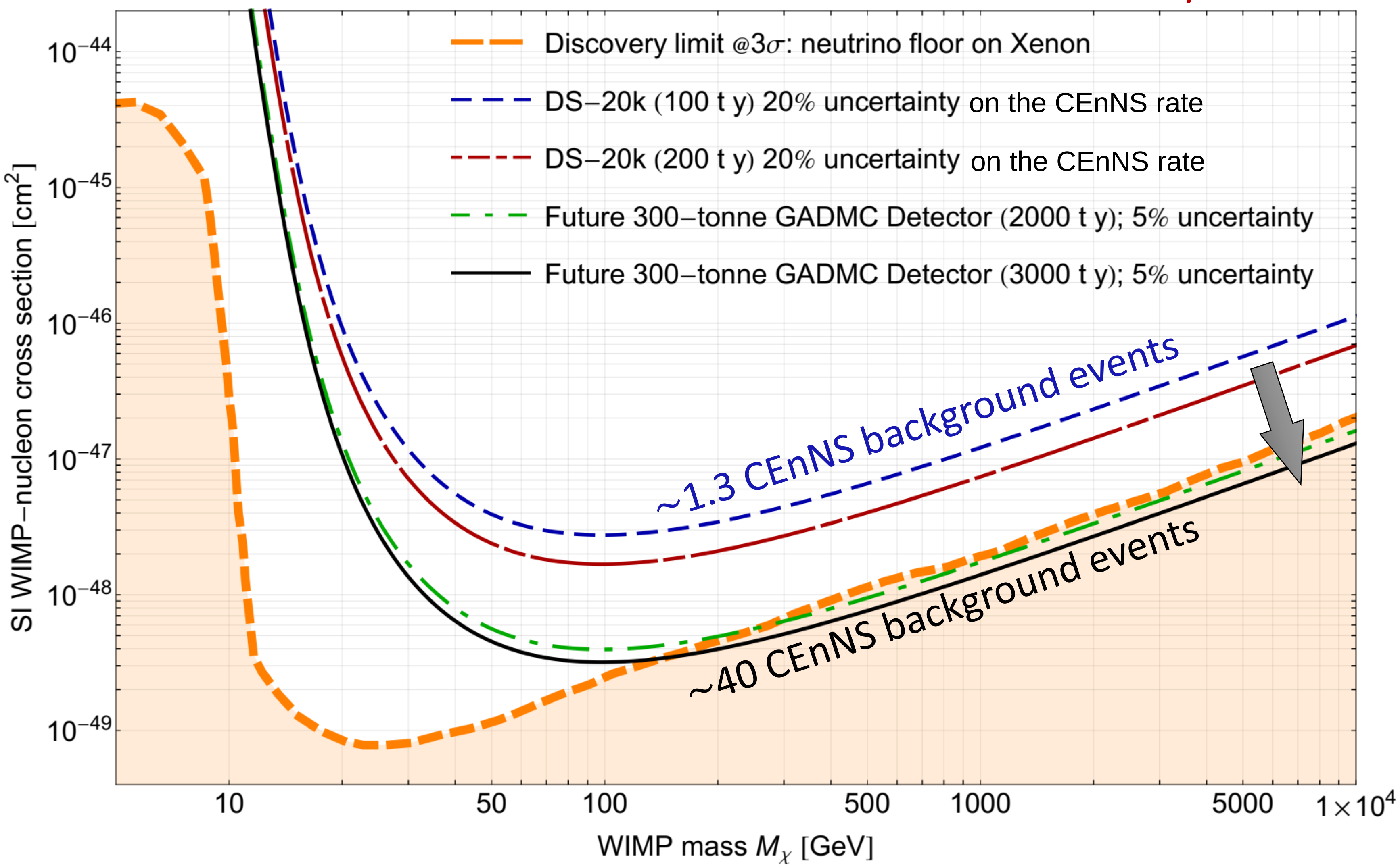

DS-20k (100 ty) will be able to exclude cross sections down to $2.8 \times 10^{-48}\ cm^2$ @100 GeV. For the same WIMP mass GADMC (3000 ty) $\sigma_{\chi p} = 3 \times 10^{-49}\ cm^2$

The Helm Nuclear Form factor

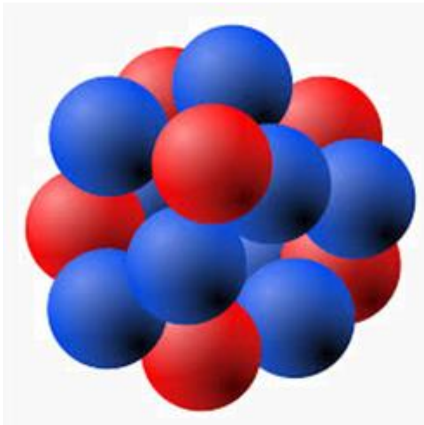

- The nuclear form factor, F(q), is taken to be the **Fourier transform** of a spherically symmetric ground state **mass distribution** normalized so that F(0) = 1:

$$F(q) = \frac{1}{M}\int \rho_{\text{mass}}(r) e^{-i\mathbf{q}\cdot\mathbf{r}} d^3r = \frac{1}{M}\int_0^\infty \rho_{\text{mass}}(r)\,\frac{\sin qr}{qr}\,4\pi r^2 dr.$$

Since the mass distribution in the nucleus is difficult to probe, it is generally assumed that mass and charge densities are proportional so that charge densities, determined through **elastic electron scattering**, can be utilized instead.

$$\rho_{\text{mass}}(r) = \frac{m_N}{Ze}\rho_{\text{charge}}(r)$$

It is convenient to have an analytic expression. This expression has been provided by the **Helm form factor**, given by

$$|F^{SI}(q)|^2 = \left(\frac{3j_1(qR_1)}{qR_1}\right)^2 e^{-q^2s^2}$$

Where j_1 is the spherical Bessel function of the first kind and R_1 is an effective nuclear radius and s is the nuclear skin thickness, parameters that need to be fit separately for each nucleus

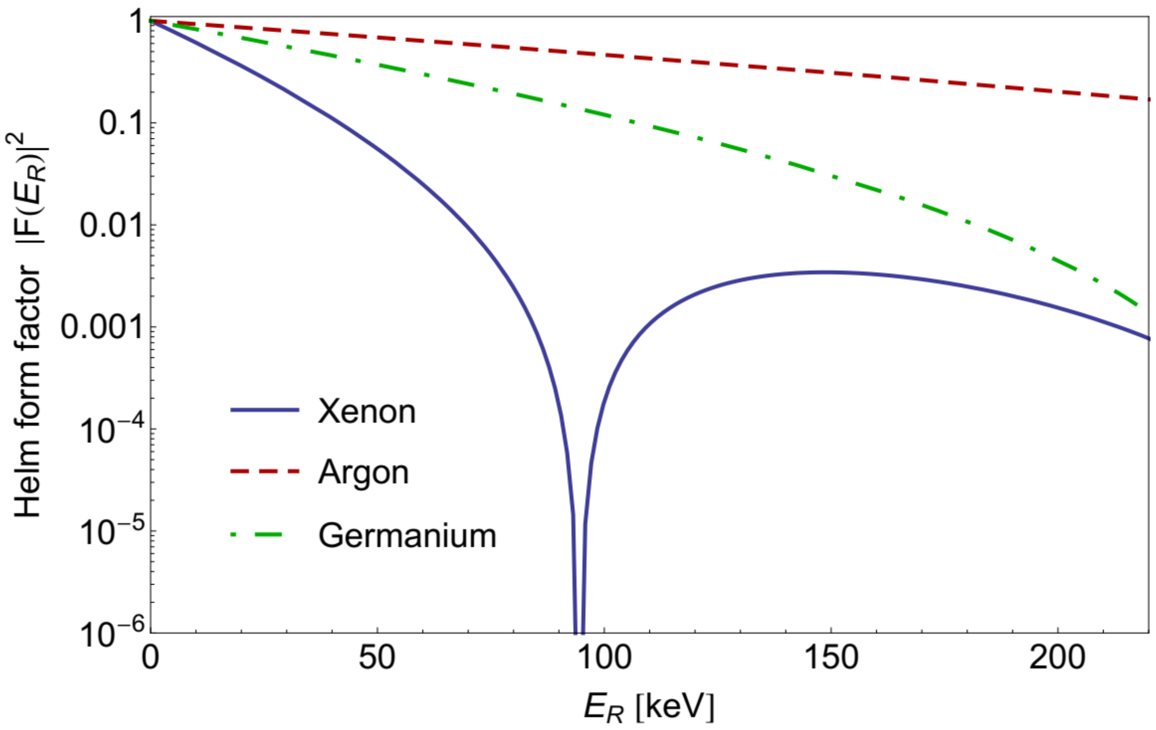

Final WIMP spectra

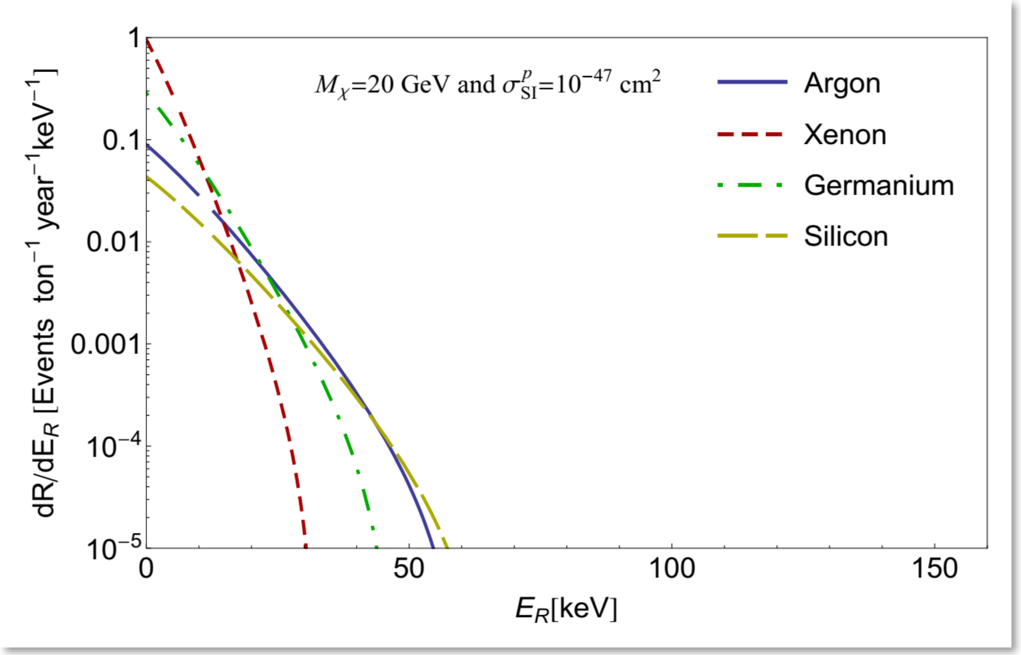

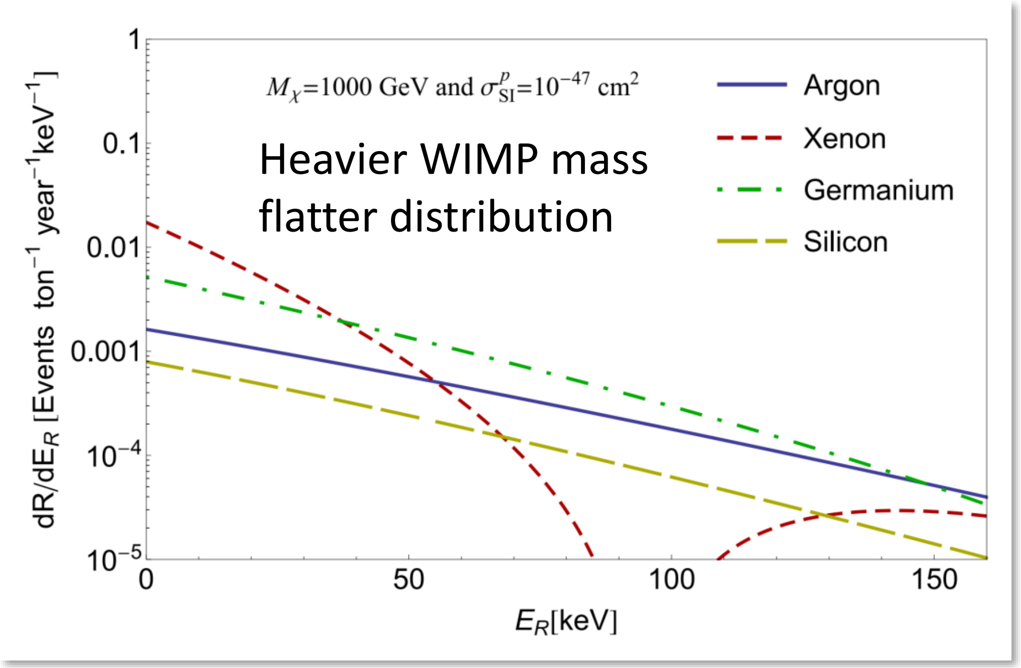

In a real experiment there will be also a **nuclear recoil acceptance function**, $A(E_R)$, which takes into account all the backgrounds cuts, the WIMP signal selection efficiency and the experimental resolution.

The total number of WIMP events is then given by

$$N_\chi = M\,T \int_{E_{\rm th}}^{E_{\rm up}} A(E_R) \frac{\mathrm{d}R}{\mathrm{d}E_R}\, \mathrm{d}E_R$$

Experiment exposure [tonne x year]

Best WIMP sensitivity in the presence of CEnNS (Neutrino floor)

1000 background-free exclusion limits, isovalues of WIMP events (2.3 at 90% C.L.), as a function of the WIMP mass, with varying thresholds (E_{th}) from **0.001 to 200 keV** and adjusted each curve's exposure (MT) such that each experiment expects a neutrino background of one event.

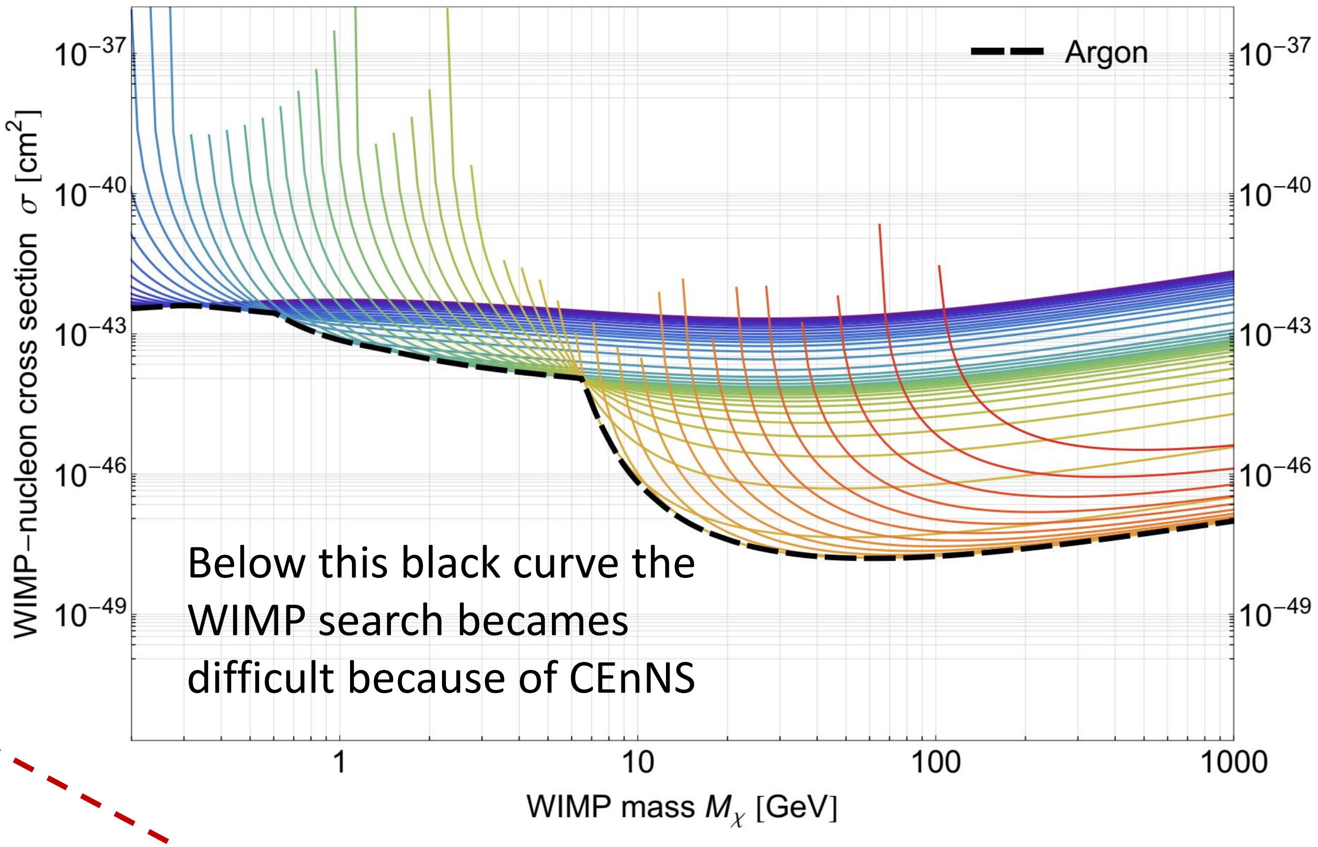

$$\hat{\sigma}_{90\%}(E_{th}, M_\chi) = \frac{2.3}{(MT)_{1\,neutr} \times \int_{E_{th}}^{E_{up}} \frac{dR_\chi}{dE_r} dE_r}$$

Coherent elastic neutrino nucleus background

$$\frac{dR_\nu(E_r)}{dE_r} = \eta \times \int_{E_{\nu_{min}}} \frac{dN}{dE_\nu} \times \frac{d\sigma^{CNS}(E_\nu, E_r)}{dE_r} dE_\nu$$

$$(MT)_{1\,neutr} = \frac{1\ \nu\ events}{\int_{E_{th}}^{E_{up}} \frac{dR_\nu}{dE_r} dE_r\ \ [\nu\ events\ ton^{-1} year^{-1}]}$$

WIMP-nucleus recoil spectrum

$$\frac{dR_\chi}{dE_r} = \frac{\sigma_{w-n}}{2M_w\,\mu_n^2} A^2 F^2(E_r)\,\rho_0 \int \frac{f_1(v)}{v} dv$$

Comparison between argon and xenon isoevents curve

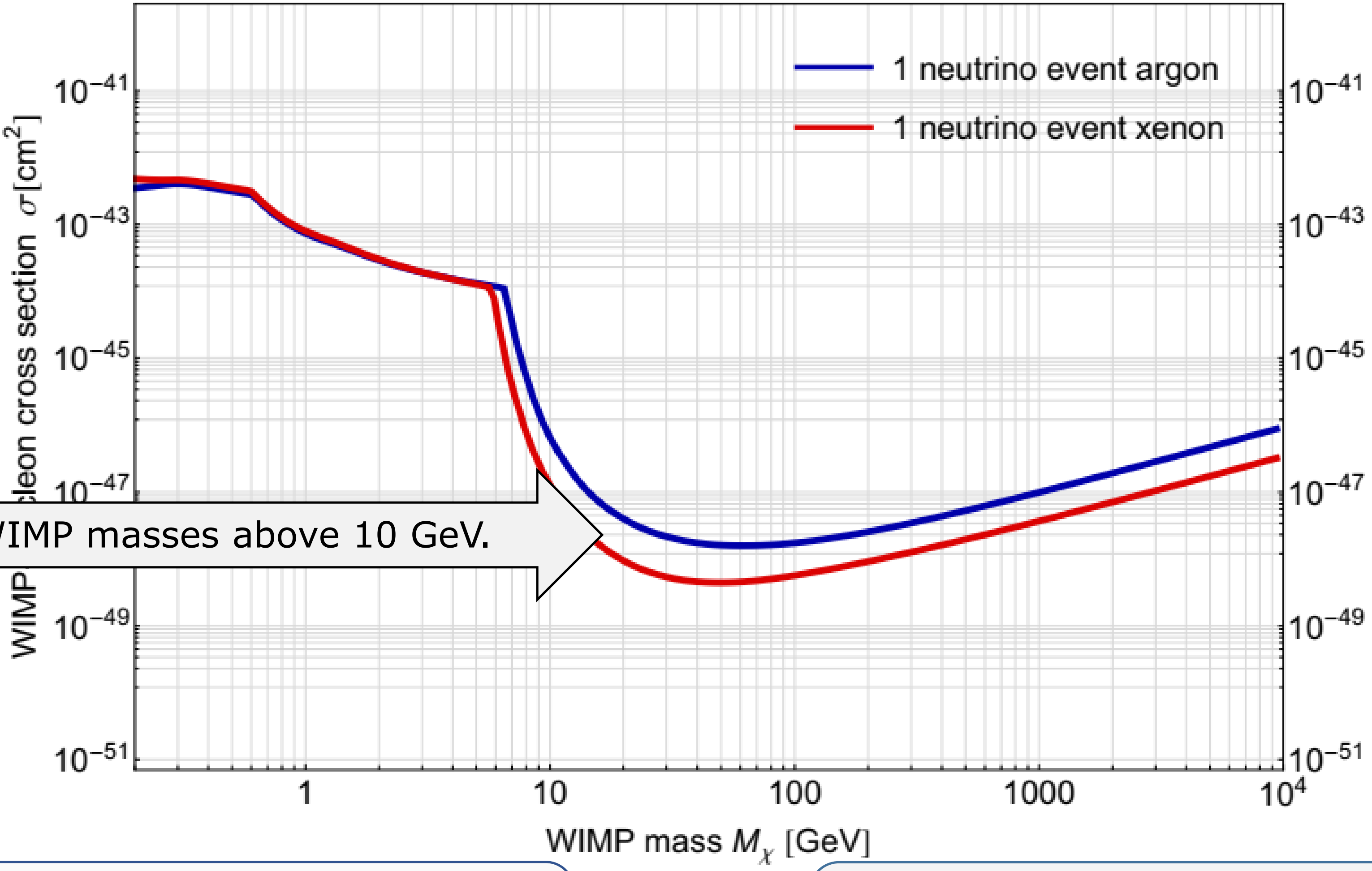

Differences for WIMP masses above 10 GeV.

Xenon

$\sigma_{\chi-n}(M_\chi = 100\ \text{GeV}) = 5.6 \cdot 10^{-49}\ \text{cm}^2$

Argon

$\sigma_{\chi-n}(M_\chi = 100\ \text{GeV}) = 1.7 \cdot 10^{-48}\ \text{cm}^2$

DarkSide Proto-1ton

- A scaled down version with full DS-20k TPC features, ~1 ton LAr in total
- 370 PDM channels
- Acrylic bonding is under development at University of Alberta
- Scheduled to operate at CERN in 2021

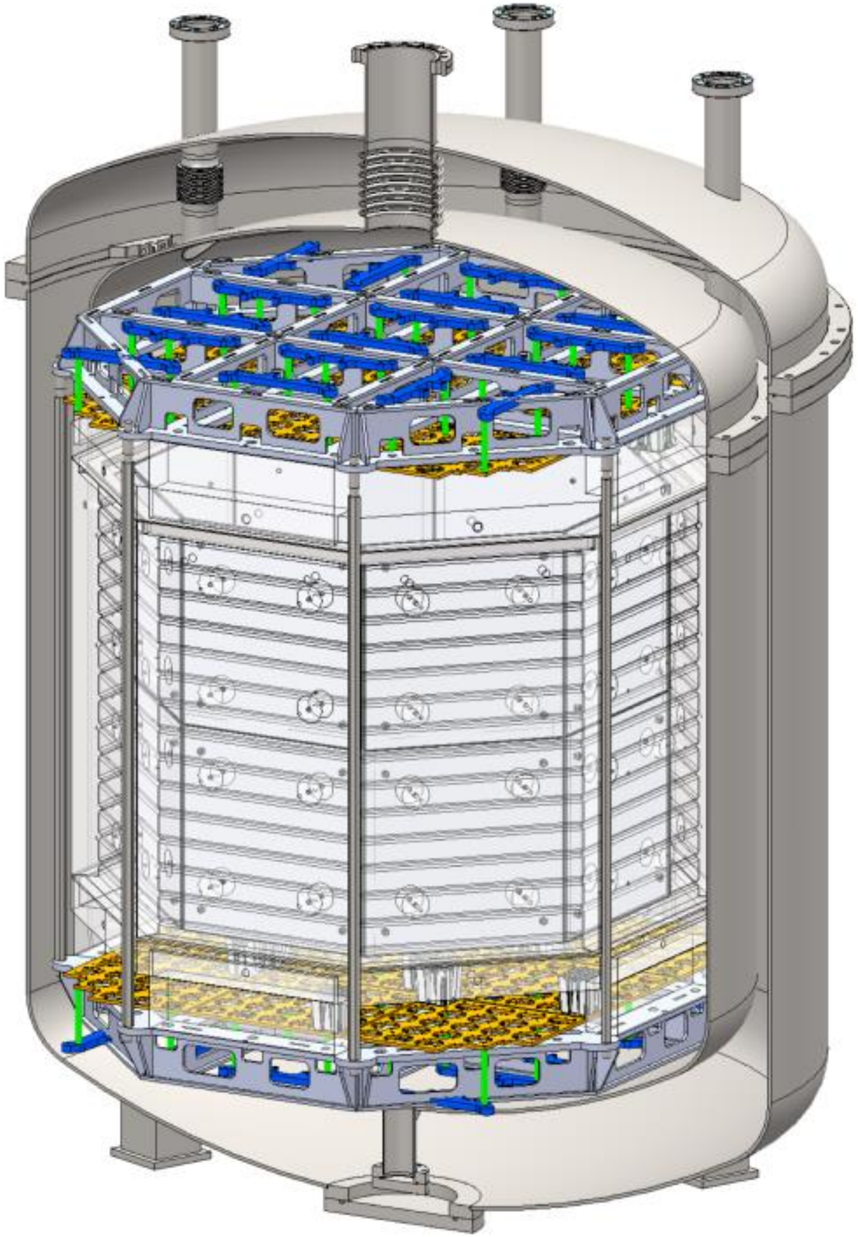

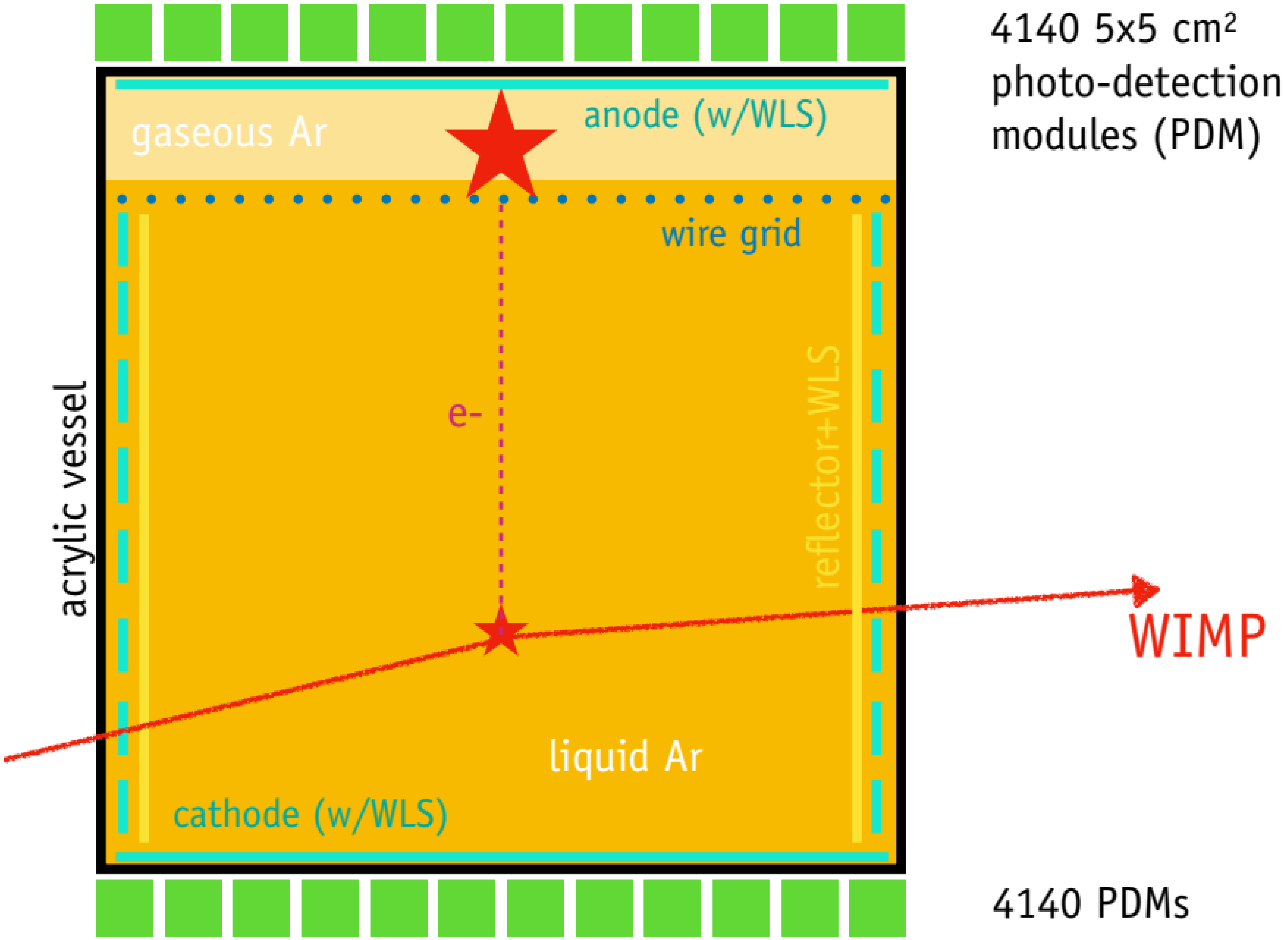

4140 5x5 cm²
photo-detection
modules (PDM)
gaseous Ar
anode (w/WLS)
wire grid
acrylic vessel
e-
reflector+WLS
WIMP
liquid Ar
cathode (w/WLS)
4140 PDMs

DarkSide Proto-0 @CERN

25 cm x 25 cm x 12 cm TPC, as test bench for:

- DS-20k TPC design: Clevios, ESR, wire grid, resistor chain…
- S2 study: S2 pulse shape, X-Y position reconstruction…
- Online adjustable gas pocket to optimize configuration
- Motherboard full-chain readout
- Full DAQ scheme

First phase with one motherboard on top will start to operate in the end of Oct. 2019

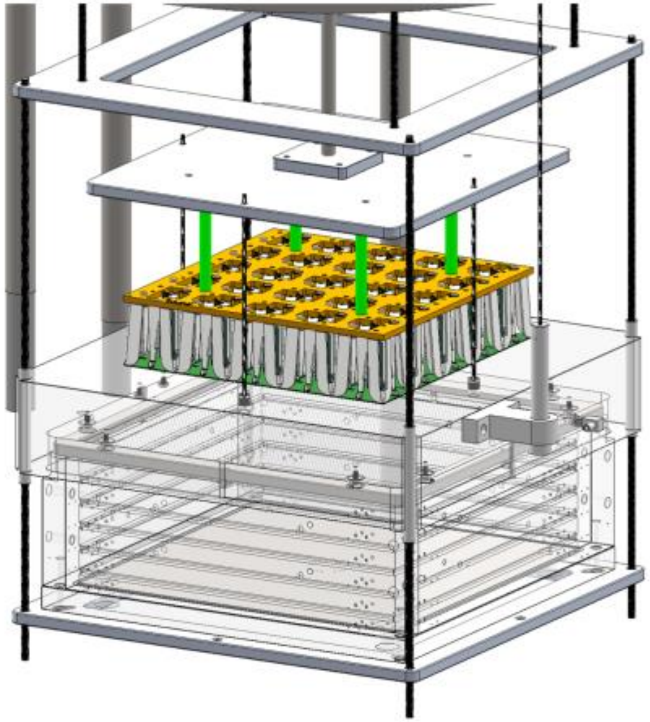

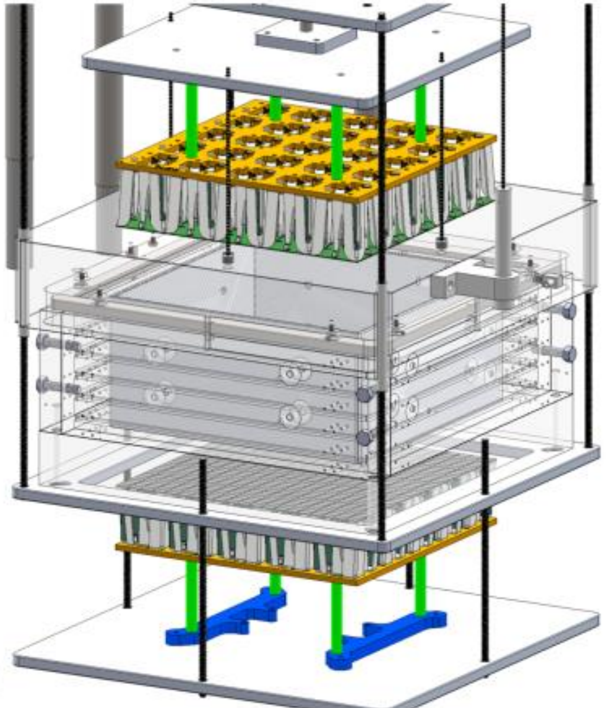

DarkSide-20k Design

- Sealed acrylic TPC containing 50 t of UAr
- Membrane cryostat containing ~700 t of AAr
- 2% Gd-doped acrylic panels + AAr buffer as neutron veto
- SiPMs as photosensors: 8280 channels for TPC; ~3000 channels for Veto

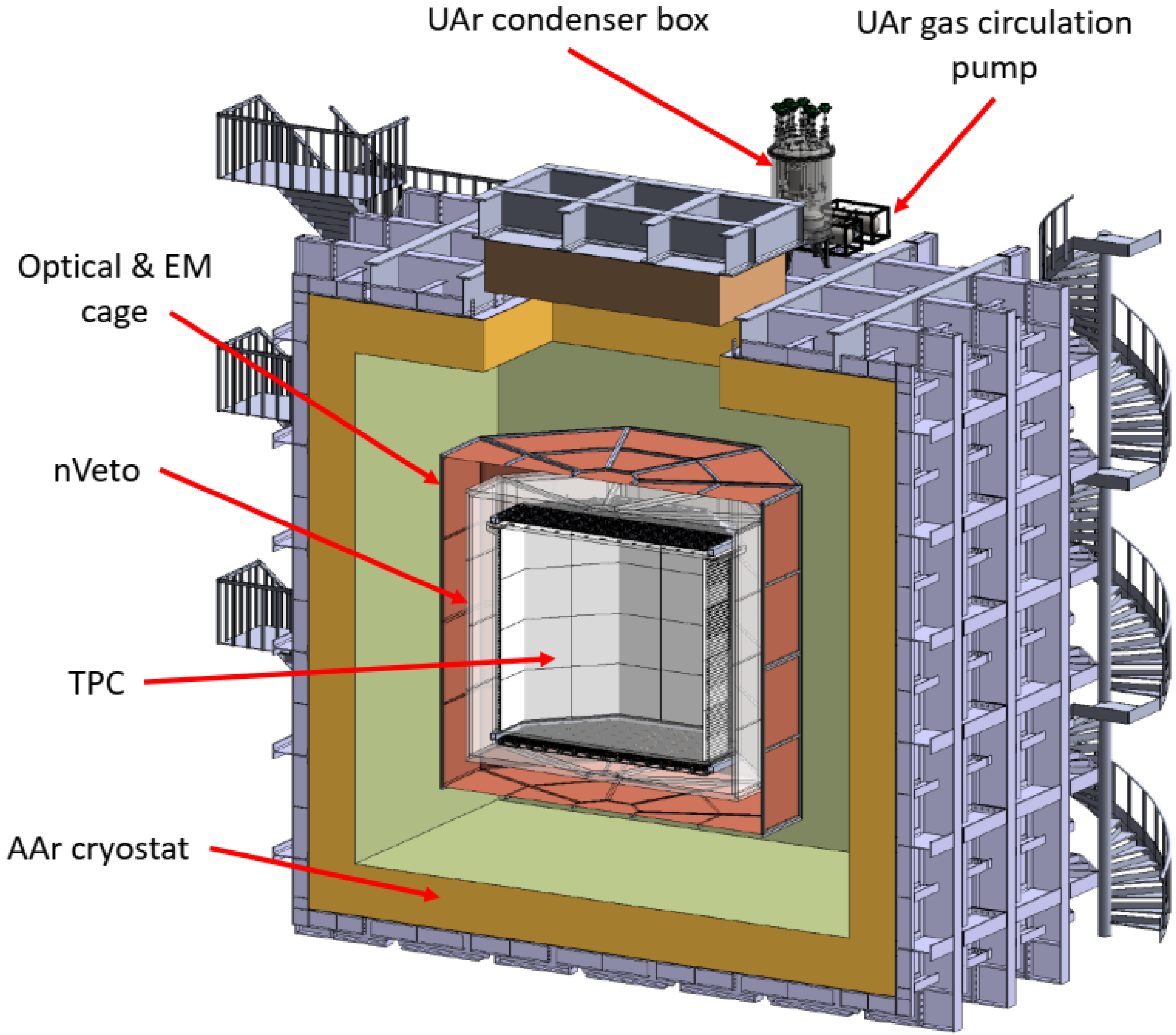

(Conceptual drawing, mechanical structure not shown)

Sealed Acrylic TPC

- Sealed (bonded) acrylic vessel itself serving as part of TPC, to minimize inactive volume and make full use of UAr
- No extra UAr vessel needed, to reduce background
- SiPM arrays, electronics and cables moved out of TPC, much less outgassing
- Clevios layer as anode, cathode, bottom ground and field shaping rings
- ESR foil as reflectors
- All internal surface coated with TPB as wavelength shifter

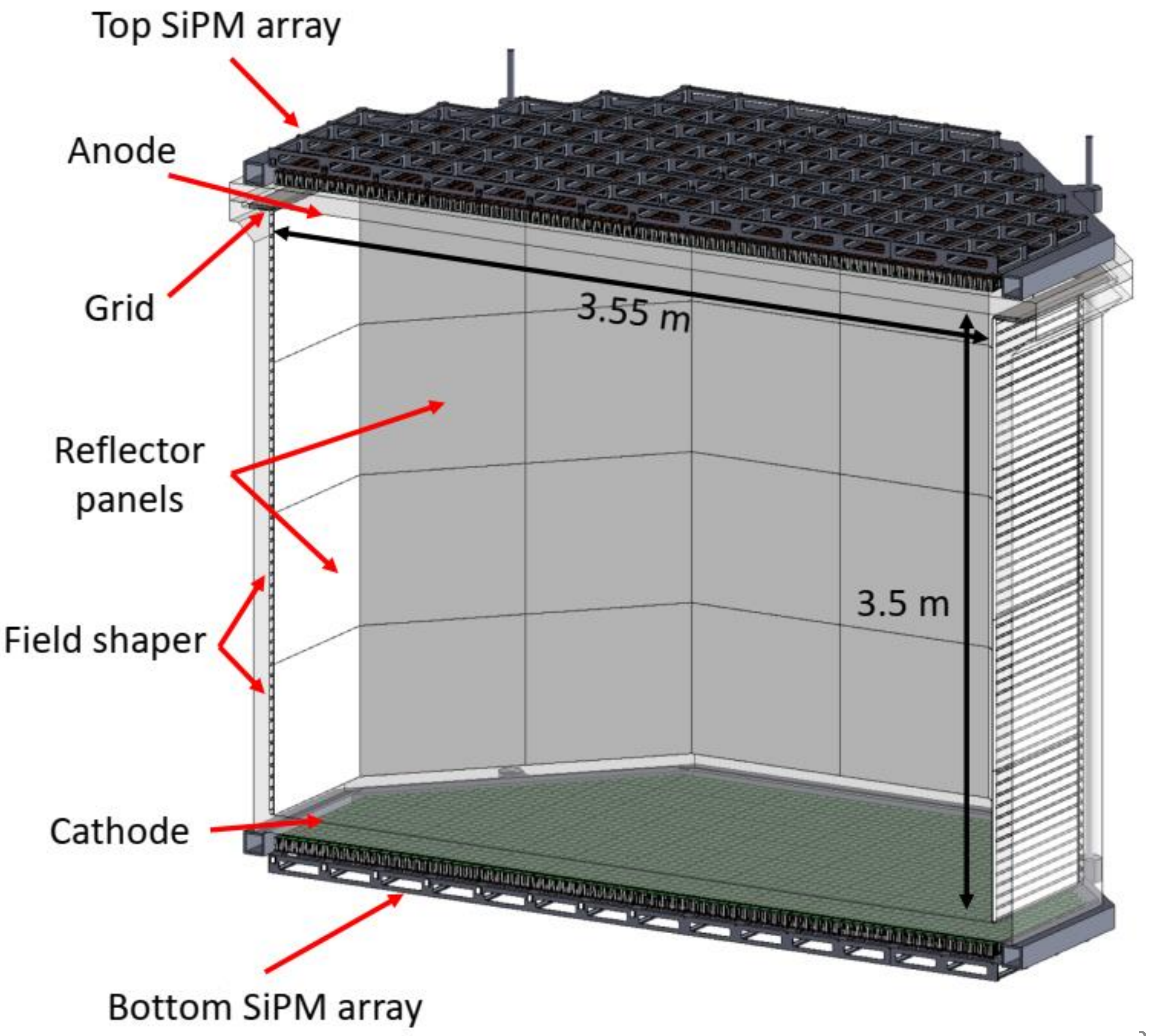

Neutron Veto

- 10 cm thick passive 2% Gd-doped acrylic panels
- 40 cm thick inner and outer active liquid AAr volumes
- Neutrons moderated and captured by Gd (H or Ar), emitted gammas then detected by active liquid AAr
- ~3000 SiPMs readout channel
- Vertical segmentations to reduce ^{39}Ar pile-up rate
- ESR foil as reflector
- TPB or PEN as wavelength shifter
- Faraday cage for electrical and optical isolation
- Goal: 0.1 n/(200 t y) after all cut

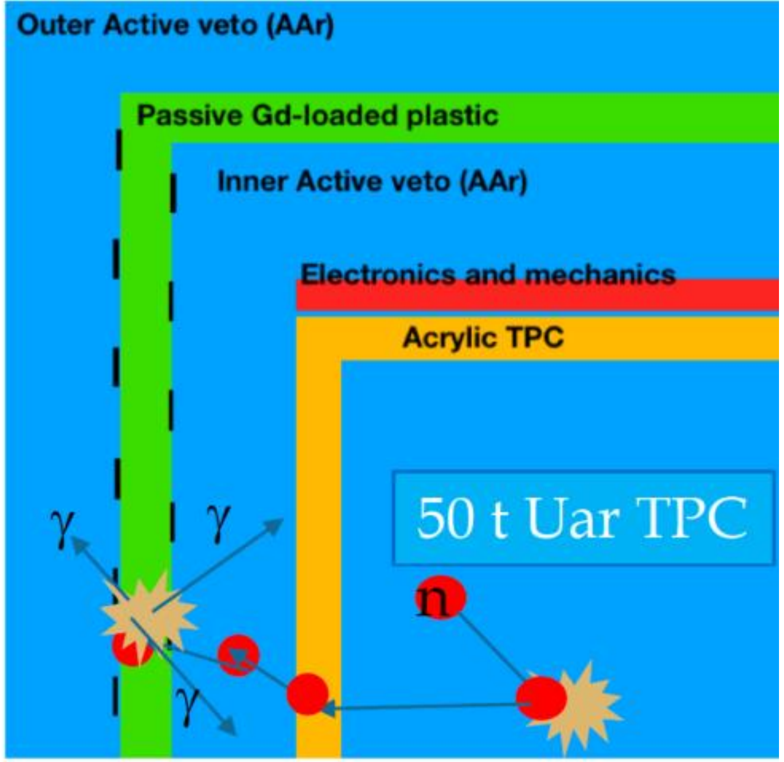

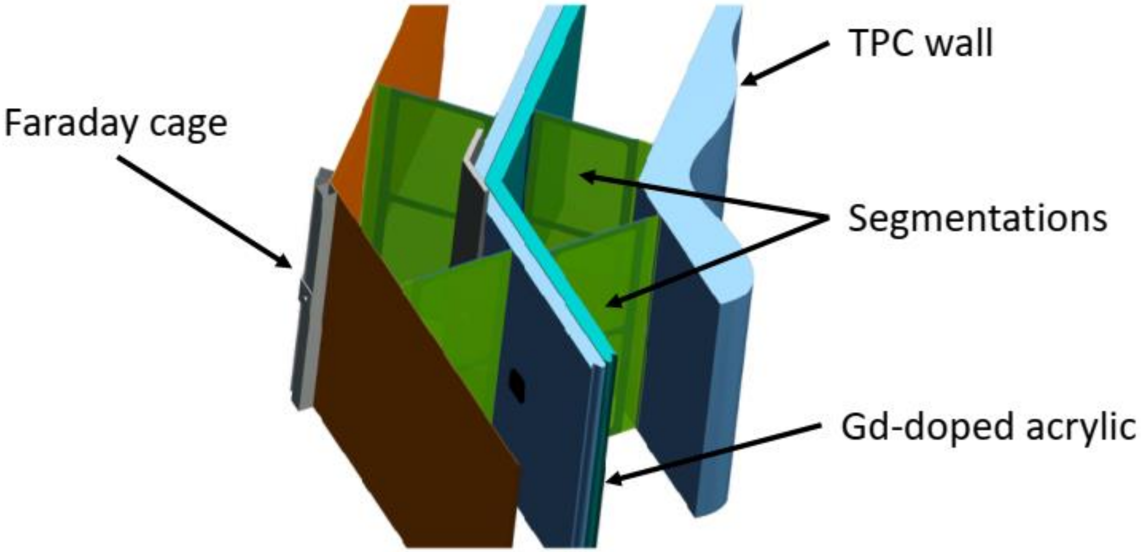

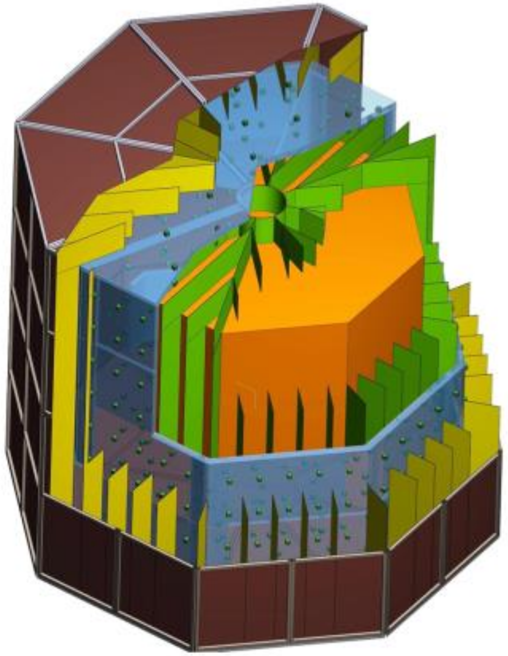

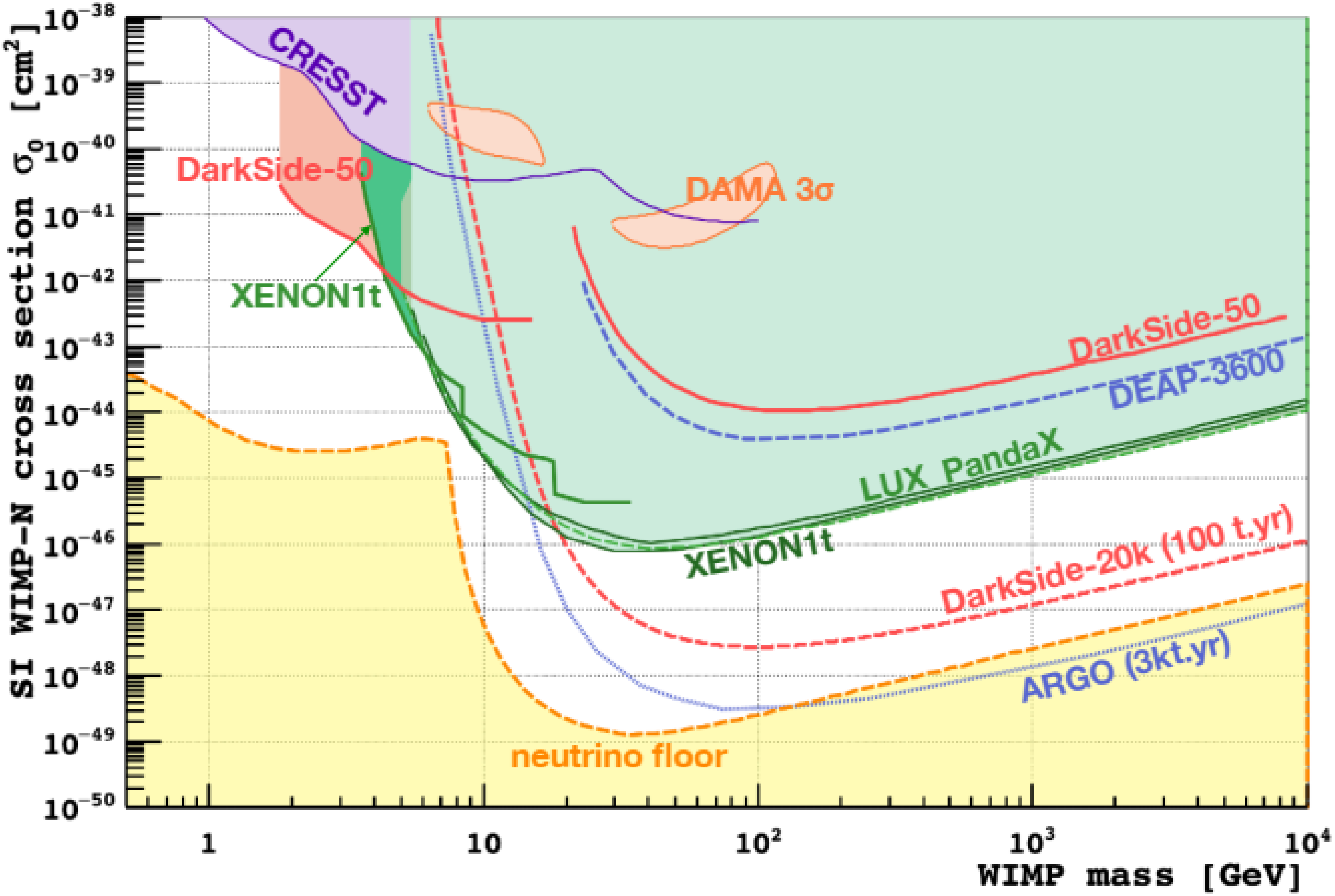

SI WIMP-N cross section σ_0 [cm^2]
10^{-38}
10^{-39}
10^{-40}
10^{-41}
10^{-42}
10^{-43}
10^{-44}
10^{-45}
10^{-46}
10^{-47}
10^{-48}
10^{-49}
10^{-50}
CRESST
DarkSide-50
DAMA 3σ
XENON1t
DarkSide-50
DEAP-3600
LUX PandaX
XENON1t
DarkSide-20k (100 t.yr)
ARGO (3kt.yr)
neutrino floor
1
10
10^2
10^3
10^4
WIMP mass [GeV]

Experimental status

- ✓ Theory prediction very precise: the width of the blue curve exceeds the theory uncertainty
- Complementarity of high and low energy measurements to constraint new physics

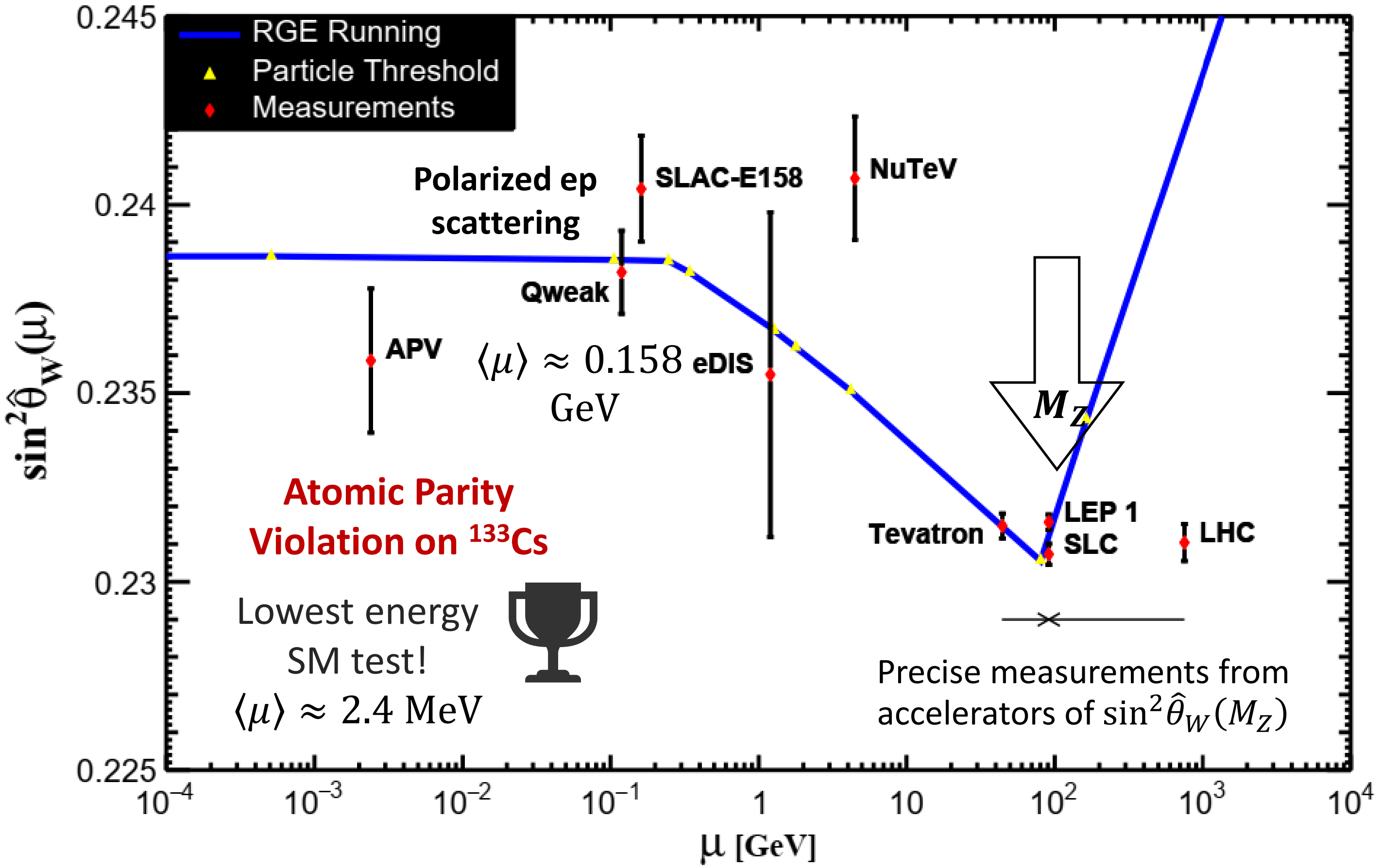

Lowest energy determination of $\sin^2\hat{\theta}_W$ from **APV (Atomic Parity Violation)** obtained measuring weak charge of ^{133}Cs

$$Q_W^{SM} \approx -N + Z\left(1 - 4\sin^2\theta_W^{\mathrm{APV}}\right) \Rightarrow Q_W^{SM}(\mathrm{Cs}) = -73.23(1)$$

- Latest measurement by Q_{weak} Collaboration

"Precision measurement of the weak charge of the proton, Nature 557, 207–211 (2018)"

$$Q_W^p = 1 - 4\sin^2\theta_W \Rightarrow \sin^2\theta_W$$

Q_W^p can be extracted from the **parity-violation asymmetry** A_{ep} (interference between electromagnetic and weak scattering amplitudes) that can be measured with a longitudinally polarized electron beam incident on an unpolarized-proton target:

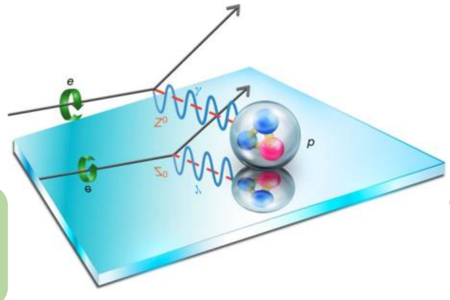

$$A_{ep} = \frac{\sigma_+ - \sigma_-}{\sigma_+ + \sigma_-}$$

$\sigma_\pm$ cross-section of helicity-dependent elastic scattering of polarized electrons on protons

$$\sin^2\hat{\theta}_W(0) = 0.2383 \pm 0.0011$$

WMA USING COHERENT DATA

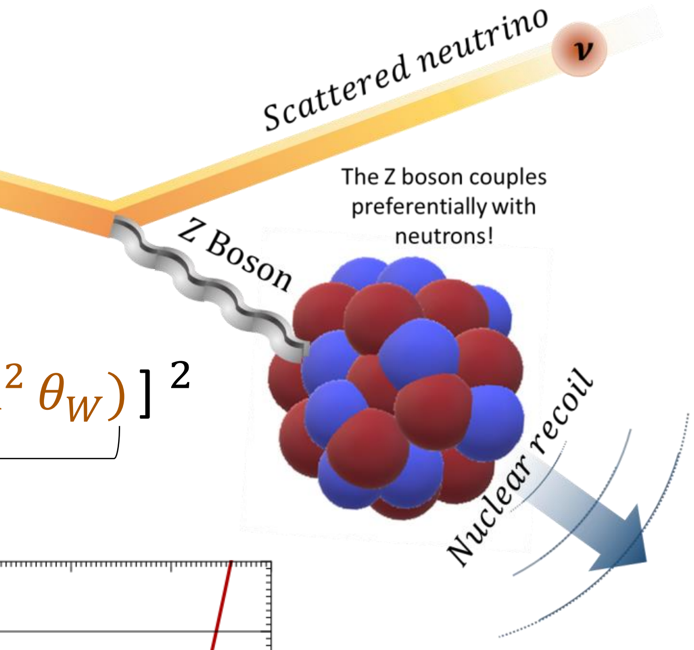

CEvNS cross section depends on $\sin^2\theta_W$

Neutron & proton form factors and radii

$$\frac{d\sigma}{dT} = \frac{G_F^2 M}{4\pi}\left(1-\frac{MT}{2E_\nu^2}\right)\Big[\underbrace{N\, F_N(T,R_n)}_{\text{NOT suppressed}} - \underbrace{F_Z(T,R_p)\, Z(1-4\sin^2\theta_W)}_{\text{Very suppressed}}\Big]^2$$

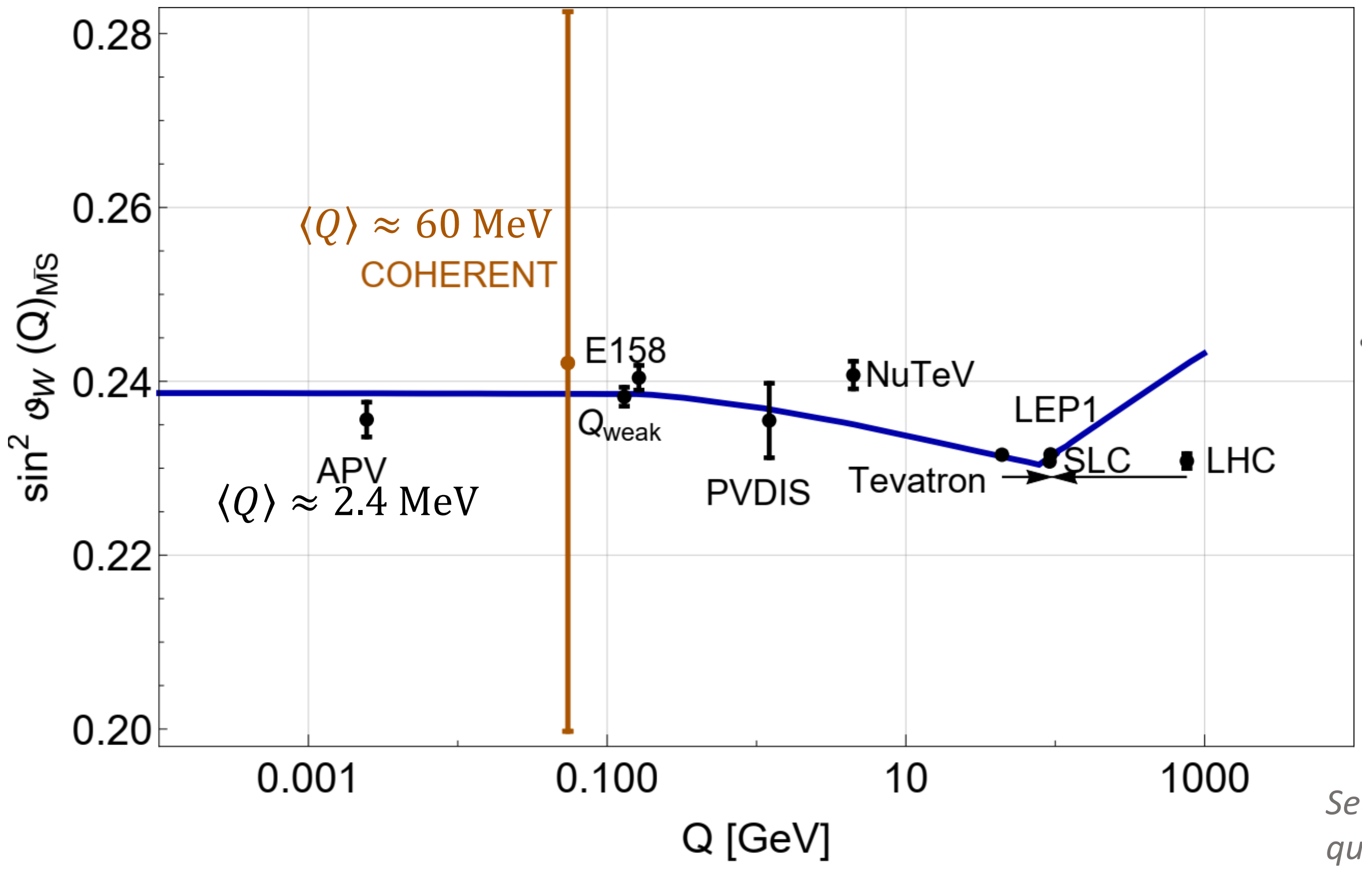

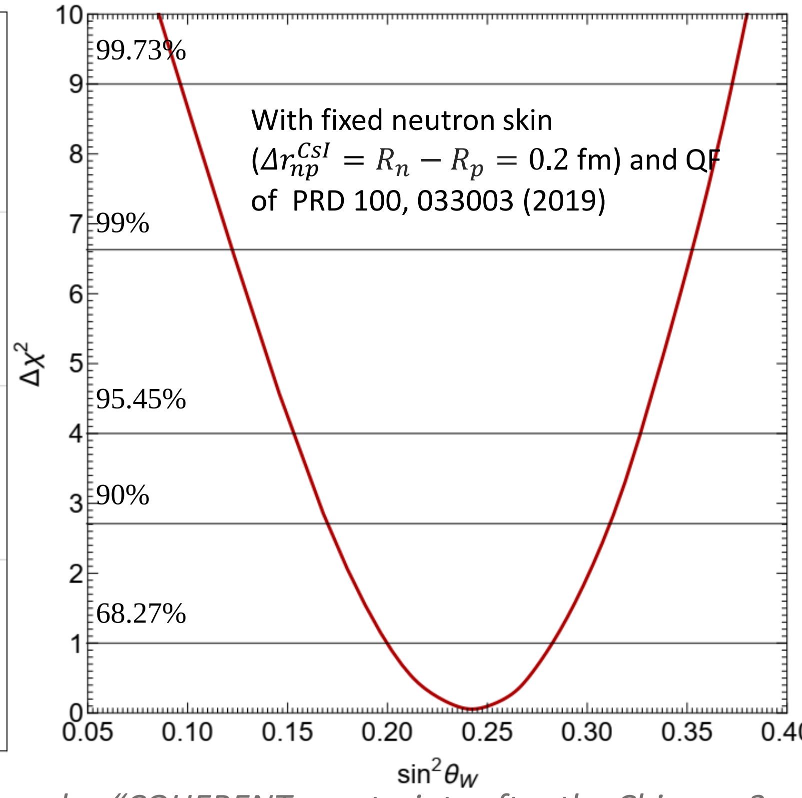

Quite big uncertainty due to the suppression of the proton contribution!

See also "COHERENT constraints after the Chicago-3 quenching factor measurement" Papoulias D. , ArXiv:1907.11644

…BUT IT COULD HELP IN ANOTHER WAY

CEvNS cross section depends also on R_n

$$\frac{d\sigma}{dT} = \frac{G_F^2 M}{4\pi}\left(1 - \frac{MT}{2E_\nu^2}\right)\Big[\underbrace{N\,F_N(T, R_n)}_{\text{NOT suppressed}} - \underbrace{(1 - 4\sin^2\theta_W)\,Z\,F_Z(T, R_p)}_{\text{Very suppressed}}\Big]^2$$

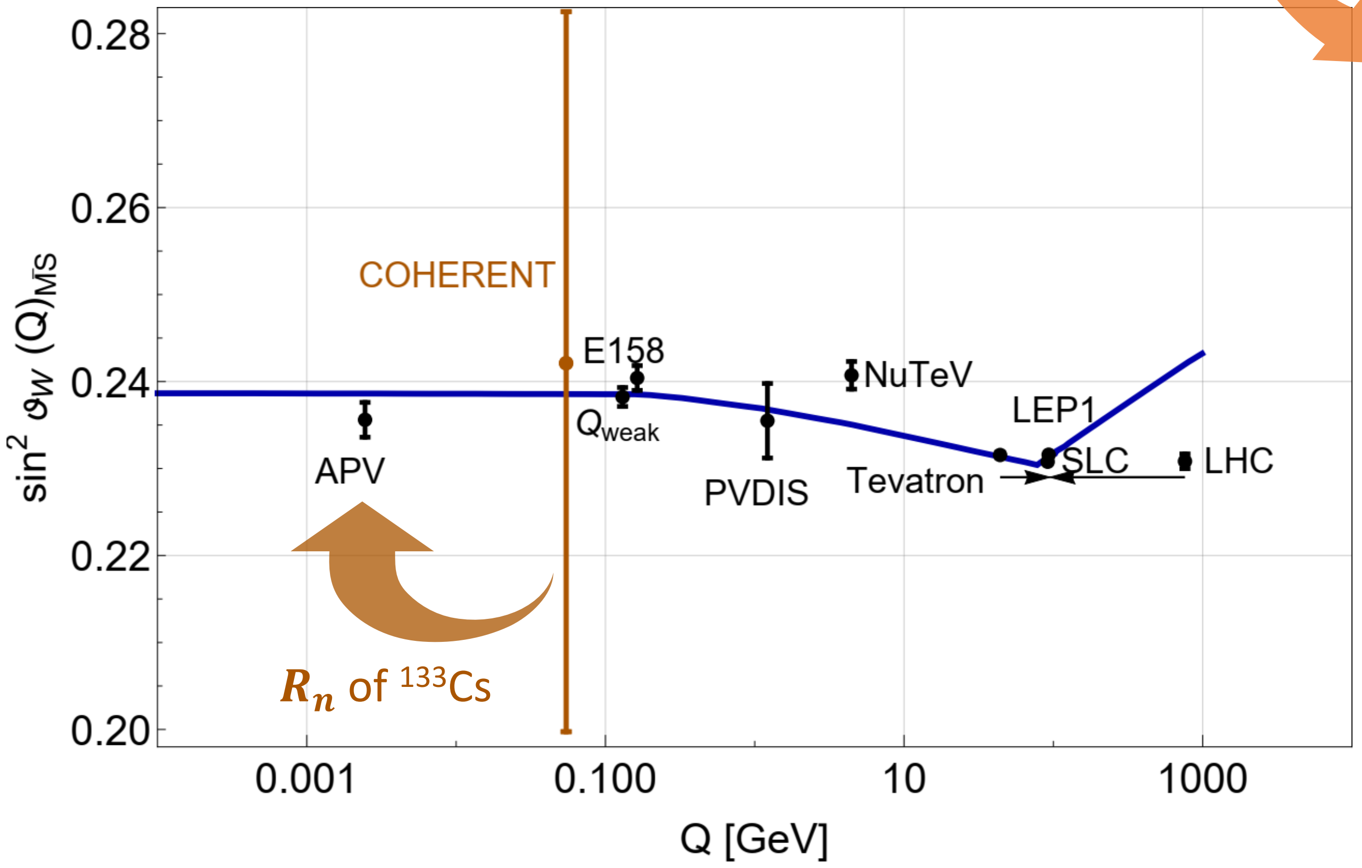

COHERENT is sensitive to the neutron radius, R_n , of ^{133}Cs, and simultaneously APV measurement depends crucially on it (or on the neutron skin)

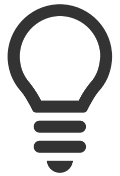

$$R_n^{CsI} = 5.5^{+0.9}_{-1.1}\ \text{fm}$$

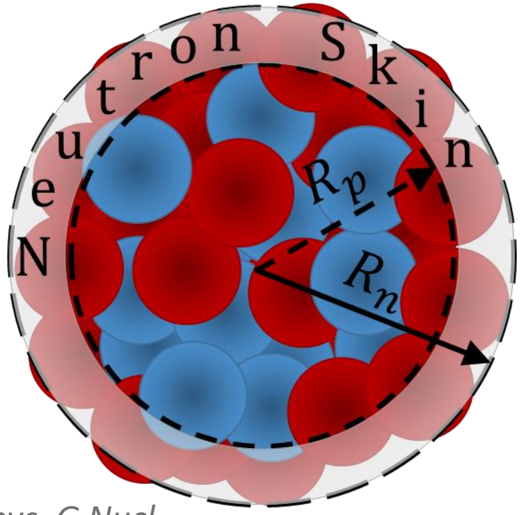

[C.M., Giunti C., Y.F. Li, Y.Y. Zhang, **Average CsI neutron density distribution from COHERENT data**, PRL 120 (2018) 072501, arXiv:1710.02730]

[P. S. Amanik and G. C. McLaughlin *J. Phys. G Nucl. Part. Phys.* 36 015105 (2009), K. Patton et al., PRC 86 024612 (2012)]

Atomic parity violation* on Cs

*also known as PNC (Parity nonconservation)

- In the absence of electric fields and weak neutral currents, **an electric dipole** (E1) transition between two atomic states with same parity (6*S* and 7*S* in Cs) is forbidden by the parity selection rule.
- However an electric dipole transition amplitude can be induced by a Z boson exchange between atomic electrons and nucleons → Atomic Parity Violation (APV)

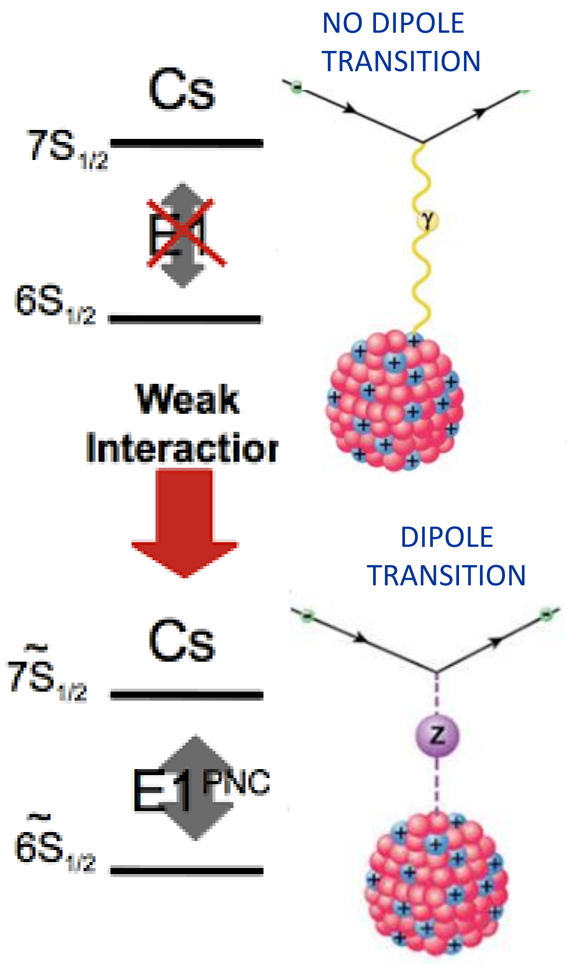

➢ The weak NC interaction violates parity and mixes a small amount of the *P* state into the 6*S* and 7*S* states ($\sim 10^{-11}$), characterized by the quantity $\mathbf{Im}(\boldsymbol{E1_{PNC}})$, giving rise to a 7S → 6S transition.

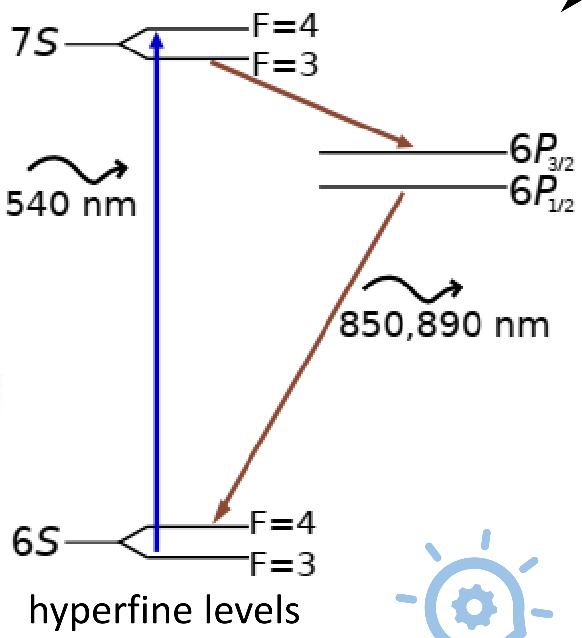

➢ To obtain an observable that is at first order in this amplitude, an electric field **E** (that also mixes S & P) is applied. **E** gives rise to a "**Stark induced**" E1 transition amplitude, $\mathbf{A_E}$ that is typically 10^5 times larger than $\mathbf{A_{PNC}}$ and can **interfere** with it.

$$R_{7S\to 6S} = |A_E \pm A_{PNC}|^2 =$$
$$= \boldsymbol{E1_\beta}^2 \pm 2\boldsymbol{E1_\beta}\boldsymbol{E1_{PNC}} + E_{PNC}{}^2$$

Because the interference term is linear in $\boldsymbol{E1_{PNC}}$ it can be large enough to be measured, but it must be distinguished from the large background contribution ($E1_\beta{}^2$).

The experimental technique

For there to be a nonzero interference term, **the experiment must have a "handedness",** and if the handedness is reversed, the interference term will change sign, and can thereby be distinguished as a modulation in the transition rate

$$R_{7S\to 6S} = |A_E \pm A_{PNC}|^2 \simeq E1_\beta{}^2 \pm 2\boldsymbol{E1_\beta E1_{PNC}}$$

- **Stark-interference technique**: cesium atoms pass through a region of perpendicular electric, magnetic, and laser fields. The "handedness" of the experiment is changed by reversing the direction of all fields.

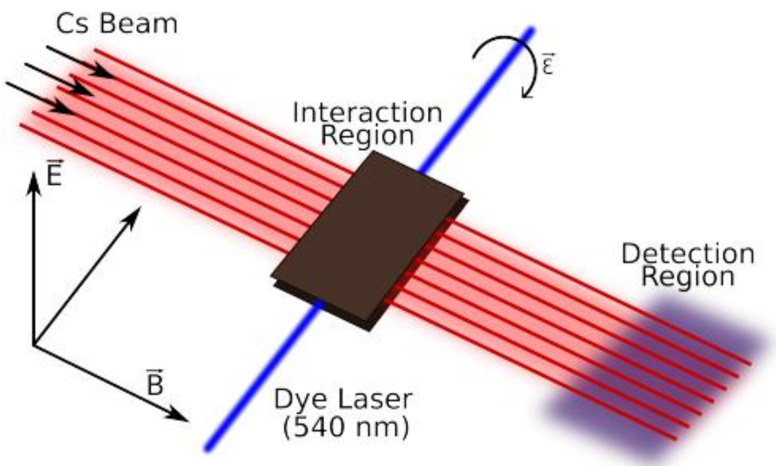

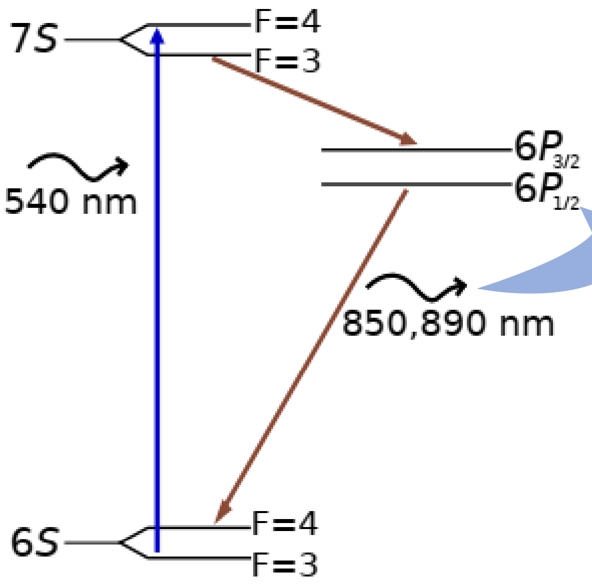

The transition rate is obtained by measuring the amount of 850- and 890-nm light emitted in the 6*P*-6*S* step of the 7*S*-6*S* decay sequence.

✓ The measurements culminated in 1997 when the Boulder group performed a measurement of A_{PNC}/A_E with an uncertainty of just 0.35%.

$$\mathrm{Im}\left(\frac{E_{PNC}}{\beta}\right) = -1.5935(56)\ \frac{\mathrm{mV}}{\mathrm{cm}}$$

[C. S. Wood et al., Science **275**, 1759 (1997)]

The PV amplitude is in units of the equivalent electric field required to give the same mixing of S and Pstates as the PV interaction

[Roberts et al., Annu. Rev. Nucl. Part. Sci. 65, 63 (2015)]

Extracting the weak charge

$$Q_W = N \left(\frac{\mathrm{Im}\, E_{\mathrm{PNC}}}{\beta}\right)_{\mathrm{exp.}} \left(\frac{Q_W}{N\, \mathrm{Im}\, E_{\mathrm{PNC}}}\right)_{\mathrm{th.}} \beta_{\mathrm{exp.+th.}}$$

Experimental value of electric dipole transition amplitude between 6S and 7S states in Cs

$$-\mathrm{Im}\left(\frac{\mathbf{E_{PNC}}}{\boldsymbol{\beta}}\right) = 1.5935(56)\ \mathrm{mV/cm}$$

[C. S. Wood et al, Science **275**, 1759 (1997)]

Theoretical PNC amplitude of the 6S-7S electric dipole transition

$$E_{\mathrm{PNC}} = \sum_n \left[\frac{\langle 6s|H_{\mathrm{PNC}}|np_{1/2}\rangle\langle np_{1/2}|\boldsymbol{d}|7s\rangle}{E_{6s} - E_{np_{1/2}}} + \frac{\langle 6s|\boldsymbol{d}|np_{1/2}\rangle\langle np_{1/2}|H_{\mathrm{PNC}}|7s\rangle}{E_{7s} - E_{np_{1/2}}} \right],$$

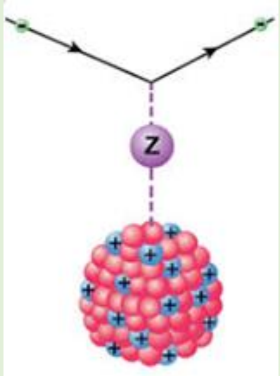

where ***d*** is the electric dipole operator, and

$$H_{\mathrm{PNC}} = -\frac{G_F}{2\sqrt{2}} Q_W \gamma_5 \rho(\boldsymbol{r})$$

is the nuclear spin independent Hamiltonian describing the **electron-nucleus weak interaction**

$\rho(\boldsymbol{r}) = \rho_p(\boldsymbol{r}) = \rho_n(\boldsymbol{r}) \rightarrow$ *neutron skin correction* needed

***β*: tensor transition polarizability**

It characterizes the size of the Stark mixing induced electric dipole amplitude (external electric field)

[Bennet and Wieman,PRL 82, 2484 (1999)]
[A. Dzuba and V. Flambaum., PRA 62, 052101 (2000)]

$$\beta = 26.957(51)\ a_B^3$$

State of the art of E_{pnC} and weak charge

[Dzuba V.A. et al. PRL 109, 203003 (2012)]

TABLE IV. All significant contributions to the E_{PNC} [in $10^{-11} i(-Q_W/N)$ a.u.] for Cs.

Contribution	Value	Source
Core ($n < 6$)	0.0018 (8)	This work
Main ($n = 6$–9)	0.8823 (17)	Ref. [10]
Tail ($n > 9$)	0.0238 (35)	This work
Subtotal	0.9079 (40)	This work
Breit	−0.0055 (1)	Refs. [5,6]
QED	−0.0029 (3)	Ref. [7]
Neutron skin	−0.0018 (5)	Ref. [5]
Total	0.8977 (40)	This work

$$E_{PNC} = 0.8977(40) \times 10^{-11} i(-Q_W/N)$$

$$Q_W^{exp.}(^{133}_{55}Cs) = -72.58(29)_{expt}(32)_{theory}$$

$$\mathbf{\sin^2 \theta_W^{APV} = 0.2356(20)}$$

✓ Weak charge in the SM including radiative corrections

$$Q_W^{SM+r.c.} \equiv -2[Z(g_{AV}^{ep} + 0.00005) + N(g_{AV}^{en} + 0.00006)]\left(1 - \frac{\alpha}{2\pi}\right)$$

$$\approx Z(1 - 4\sin^2\theta_W^{SM}) - N \Rightarrow Q_W^{SM+r.c.}(^{133}_{55}Cs) = -73.23(1)$$

SM prediction: $\sin^2\hat{\theta}_W(0) = 0.23857(5)$

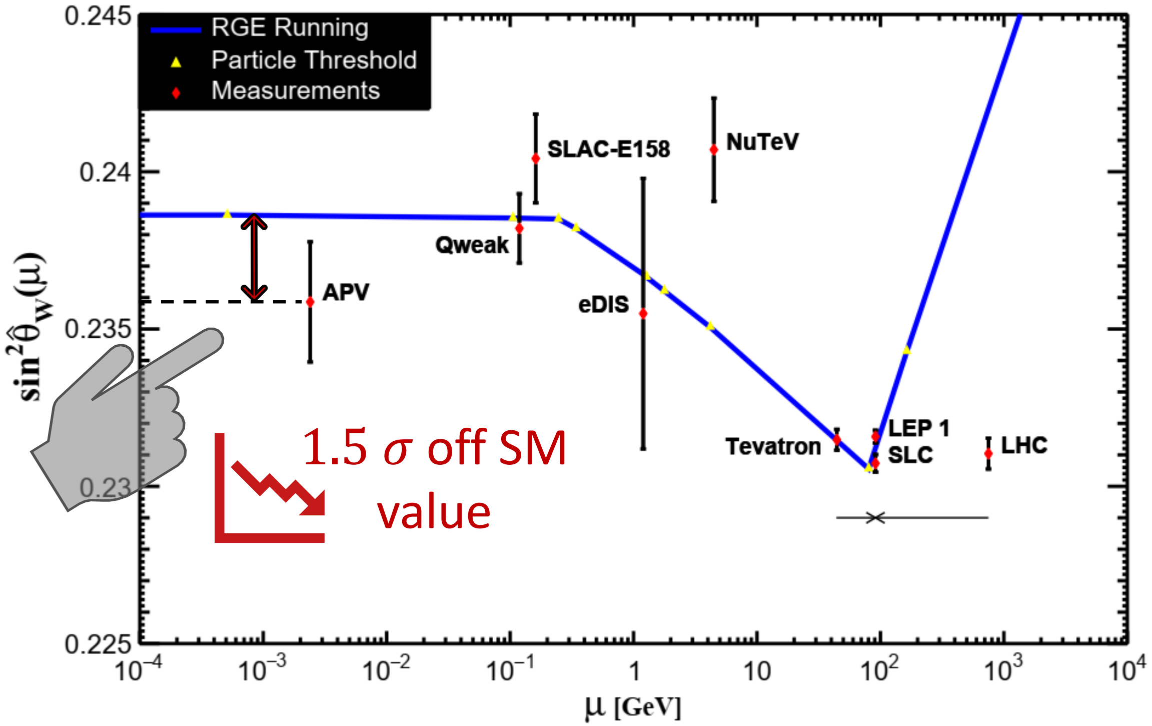

1.5 σ off SM value

EXTRAPOLATED VALUE Δr_{np}^{Cs}

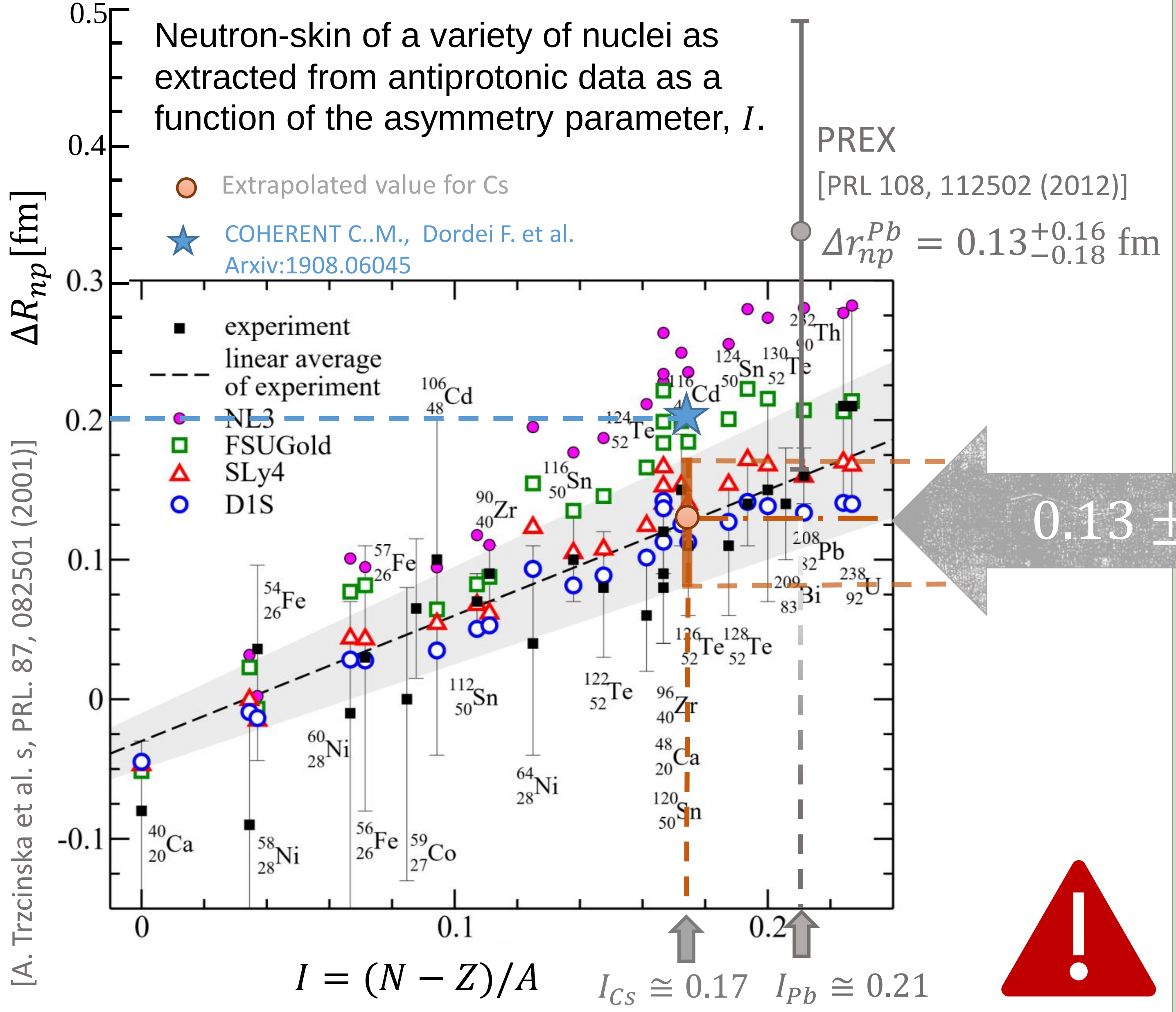

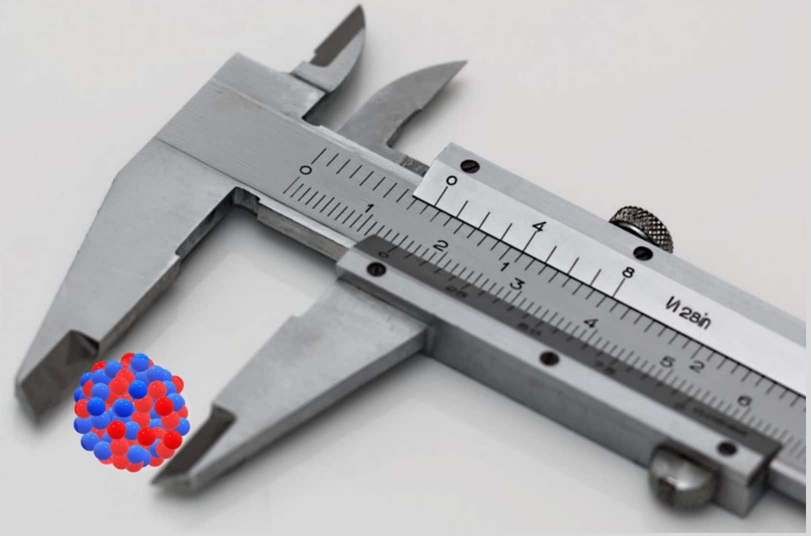

$$0.13 \pm 0.04 \text{ fm} \equiv \Delta R_{np}^{Cs}$$

Extrapolated (not measured) value for Cesium!

- The red triangles represent a semi-empirical formula derived using the nuclear droplet model:

$$\Delta R_{np}[\text{fm}] = -(0.04 \pm 0.03) + (1.01 \pm 0.15)\frac{N-Z}{A}$$

Antiprotonic data: radiochemical and the other based on x-ray data constraining the neutron distribution at the nuclear periphery

[Thiel M. et al., Journal of Physics G, 46, 9 (2019), arXiv:1904.12269v1]

"[...] Thus, we must conclude that processes involving hadronic probes tend to grossly underestimate the many sources of theoretical uncertainties."

Reinterpreting APV in view of COHERENT

1. Remove the *neutron skin* correction from the total value of the theoretical amplitude

$$(\mathrm{Im}\, E_{\mathrm{PNC}})^{\mathrm{w.n.s.}}_{\mathrm{th.}} = (0.8995 \pm 0.0040) \times 10^{-11} |e| a_B \frac{Q_W}{N}$$

2. Re-evaluate it as a function of the neutron radius

$$\delta E^{\mathrm{n.s.}}_{\mathrm{PNC}}(R_n) = \left[\frac{\mathrm{N}}{Q_W^{\mathrm{SM+rad.corr.}}} \left(1 - \frac{q_n(R_n)}{q_p}\right) \cdot E^{\mathrm{w.n.s.}}_{\mathrm{PNC}} \right] \quad \begin{cases} q_p \approx 1 - (Z\alpha)^2 (0.26) \\ q_n(R_n) \approx 1 - (Z\alpha)^2 \left(0.26 + 0.221 \left(\frac{R_n^2}{R_p^2} - 1\right)\right) \end{cases}$$

[Viatkina A. V. et al., PRC 100, 034318 (2019), see also Derevianko A., PRA 65 012106 (2001)]

[S. Pollock, E. N. Fortson, and L. Wilets, PRC 46, 2587 (1992), S. Pollock and M. Welliver, PLB 464, 177182 (1999), C. J. Horowitz, et al. PRC 63 025501 and man others]

3. Derive the new experimental value of $Q_W^{\mathrm{exp.}}({}^{133}_{55}Cs)$ using R_n^{Cs} found fitting COHERENT data

$$Q_W^{\mathrm{n.s.}}(R_n) = N \left(\frac{\mathrm{Im}\, E_{\mathrm{PNC}}}{\beta}\right)_{\mathrm{exp.}} \left(\frac{Q_W}{N\, \mathrm{Im}\left(E^{\mathrm{w.n.s.}}_{\mathrm{PNC}} + \delta E^{\mathrm{n.s.}}_{\mathrm{PNC}}(R_n)\right)}\right)_{\mathrm{th.}} \beta_{\mathrm{exp.+th.}}$$

$$Q_W^{\mathrm{exp.,n.s}}\left({}^{133}_{55}Cs, R_n^{Cs} = 5.5^{+0.9}_{-1.1}\ \mathrm{fm}\right) = -73.3^{+1.3}_{-1.6}$$

[C. M. and Dordei F. PRD 99, 033010 (2019)]

$$\sin^2 \theta_W^{\text{APV+COHERENT}} = 0.239^{+0.006}_{-0.007}$$

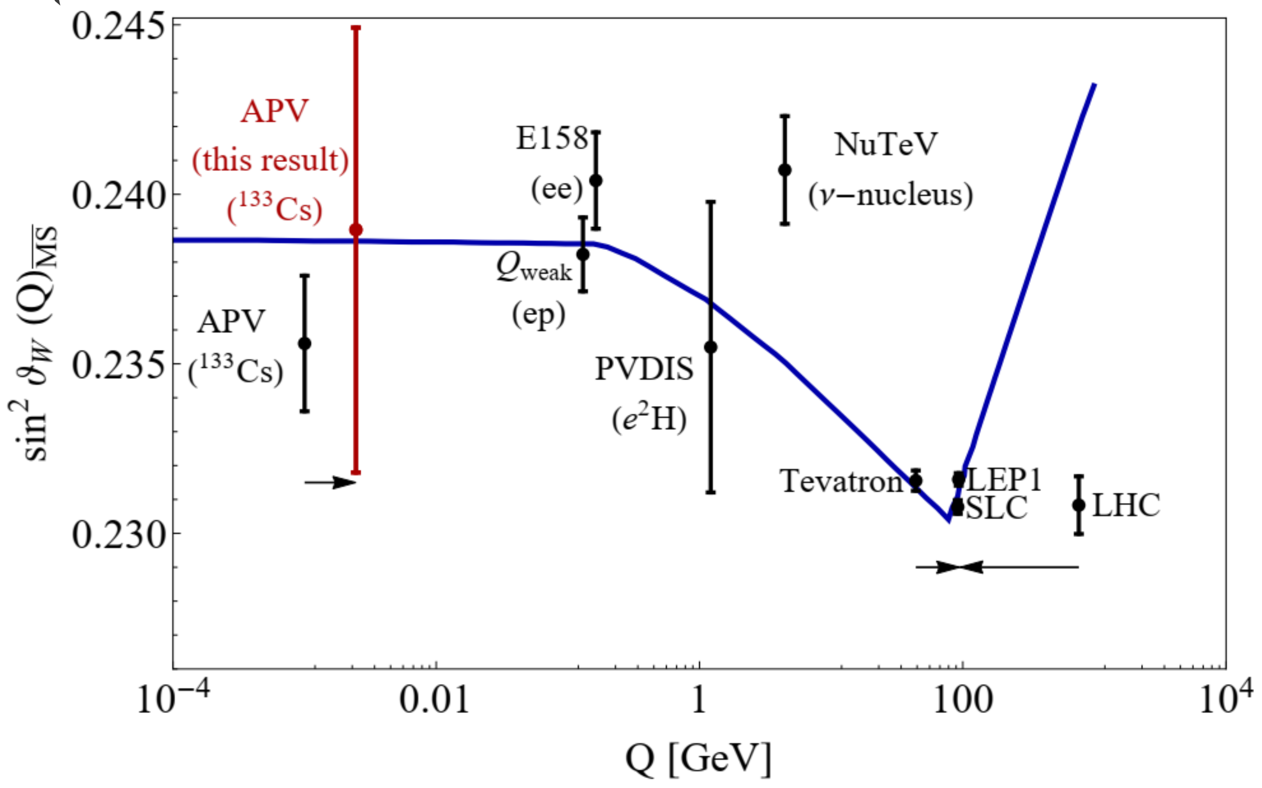

SM prediction: $\sin^2\hat{\theta}_W(0) = 0.23857(5)$

REINTERPRETING APV IN VIEW OF COHERENT

[Cadeddu M. and Dordei F. PRD 99, 033010 (2019)]

New ingredients… Quenching Factor and β

[Akimov et al. **Science** 357 (2017) 6356]

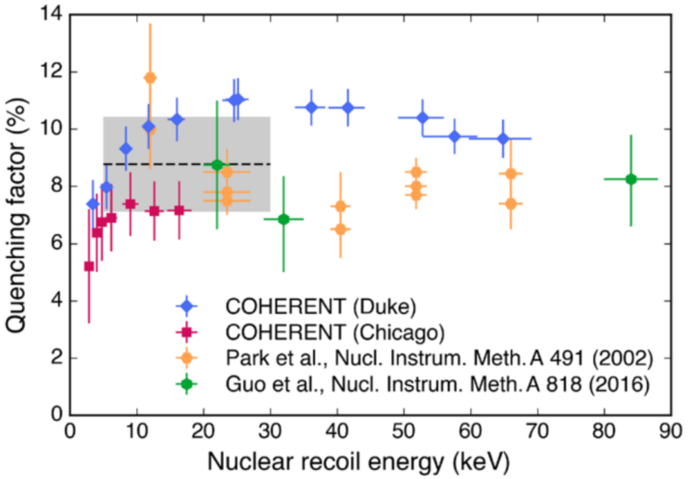

Quenching factor for CsI

[Collar et al. PRD 100, 033003 (2019)]

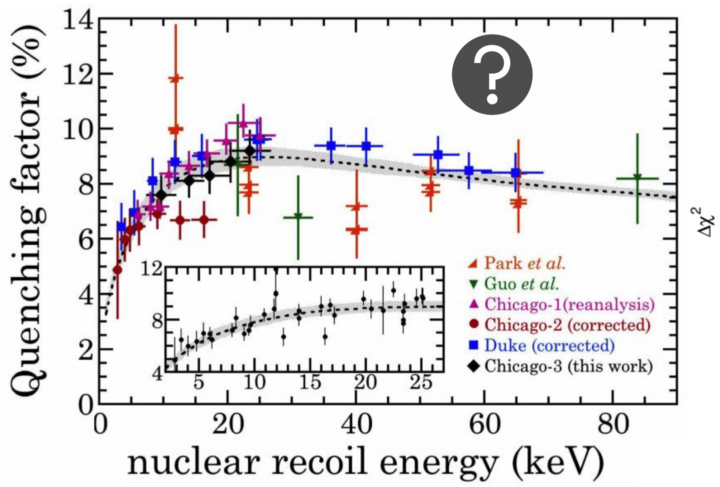

Determination of the Scalar and Vector Polarizabilities of the Cesium $6s\,^2S_{1/2} \rightarrow 7s\,^2S_{1/2}$ Transition and Implications for Atomic Parity Nonconservation

George Toh, Amy Damitz, Carol E. Tanner, W. R. Johnson, and D. S. Elliott

Phys. Rev. Lett. **123**, 073002 – Published 16 August 2019

ABSTRACT

Using recent high-precision measurements of electric dipole matrix elements of atomic cesium, we make an improved determination of the scalar (α) and vector (β) polarizabilities of the cesium $6s\,^2S_{1/2} \rightarrow 7s\,^2S_{1/2}$ transition calculated through a sum-over-states method. We report values of $\alpha = -268.82(30)a_0^3$ and $\beta = 27.139(42)a_0^3$ with the highest precision to date. We find a discrepancy between our value of β and the past preferred value, resulting in a significant shift in the value of the weak charge Q_w of the cesium nucleus. Future work to resolve the differences in the polarizability will be critical for interpretation of parity nonconservation measurements in cesium, which have implications for physics beyond the standard model.

New β Old β

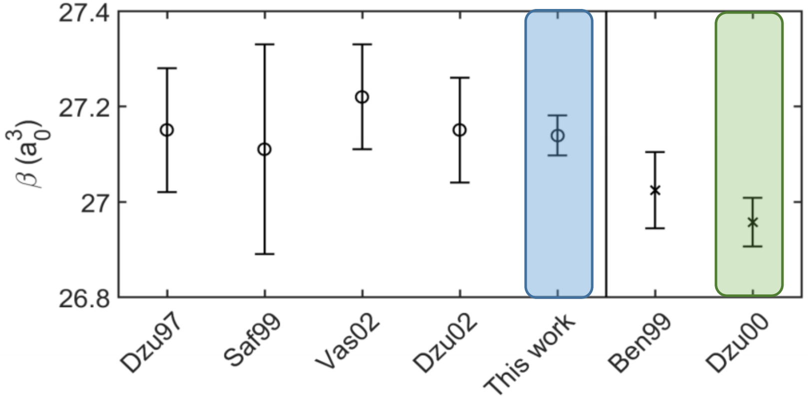

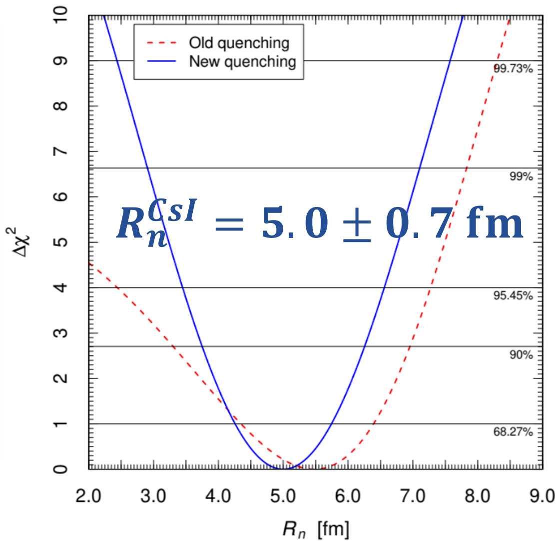

$R_n^{CsI} = 5.0 \pm 0.7$ fm

Year	Authors	Remarks	β (a_0^3)
2019	**This work**	**Sum over states (α)**	**27.139 (42)**
2002	Dzu02 [27]	Sum over states (α)	27.15 (11)
2002	Vas02 [34]	Sum over states (α)	27.22 (11)
2000	**Dzu00** [31]	**$M1_{hf}$ calculation**	**26.957 (51)**
1999	Ben99 [32]	$M1_{hf}/\beta$ expt	27.024 (80)
1999	Saf99 [33]	Sum over states (α)	27.11 (22)
1999	Saf99 [33]	Sum over states (β)	27.16
1997	Dzu97 [56]	Sum over states (α)	27.15 (13)
1992	Blu92 [22]	Sum over states (β)	27.0 (2)

$\sin^2\theta_W^{\mathrm{APV+COHERENT}} = 0.239 \pm 0.005$

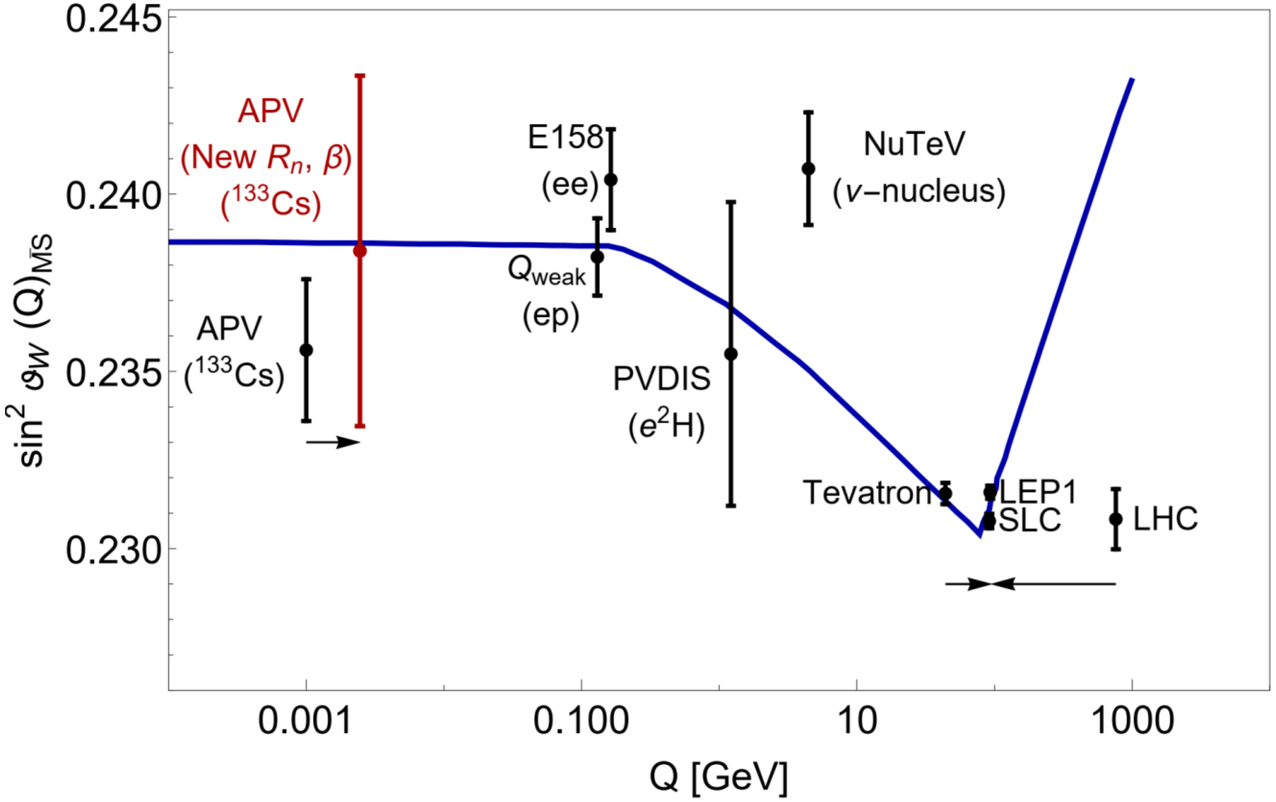

SM prediction: $\sin^2\hat{\theta}_W(0) = 0.23857(5)$

REINTERPRETING APV IN VIEW OF COHERENT (NEW QUENCHING FACTOR AND NEW β)

[C. M., Dordei F., Giunti C., Li Y.F., Zhang Y.Y., ArXiv:1908.06045]

Simultaneous fit of COHERENT dATA and APV*

* Since the APV depends so crucially on ΔR_{np}^{Cs}, the first can be used in combination with COHERENT to determine R_n^{Cs}. Assuming that the SM is correct, and so assuming the SM weak mixing angle $Q^2 = 0$, the combined APV and COHERENT least-squares function can be built

$$\chi^2 = \chi^2_{\rm C} + \left(\frac{(Q_W^{\rm Cs\,n.s.}(R_n)) - Q_W^{\rm SM+rad.corr.}}{\sigma_{APV}} \right)^2$$

DATA SET	COHERENT	COHERENT+APV	COHERENT (New QF)	COHERENT (New QF)+APV (New β)
R_n^{CsI}[fm]	$5.5^{+0.9}_{-1.1}\ (1\sigma)$	$5.42 \pm 0.31\ (1\sigma)$	$5.0 \pm 0.7(1\sigma)$	$5.04 \pm 0.31\ (1\sigma)$
ΔR_{np}^{Cs}[fm]	$0.7^{+0.9}_{-1.1}\ (1\sigma)$	0.62 ± 0.31	$0.2 \pm 0.7(1\sigma)$	0.23 ± 0.31

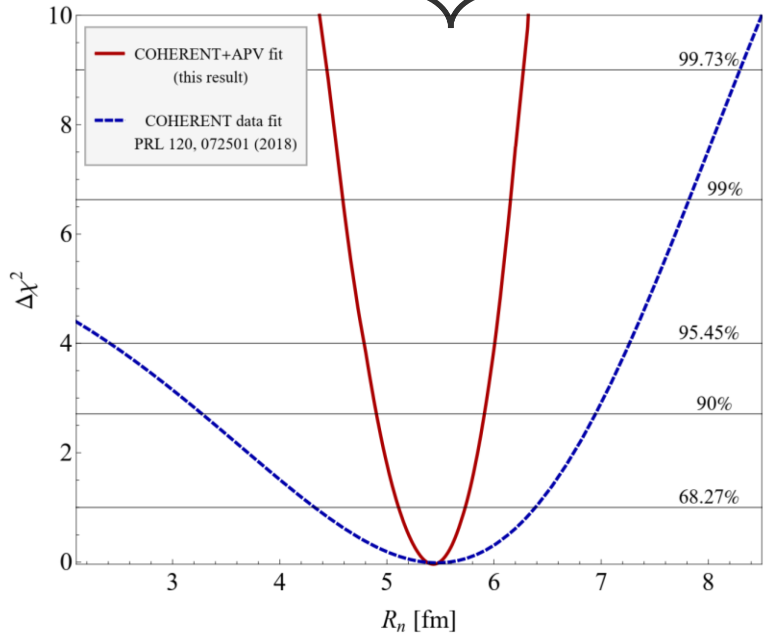

[C.M., Dordei F. PRD 99, 033010 (2019)]

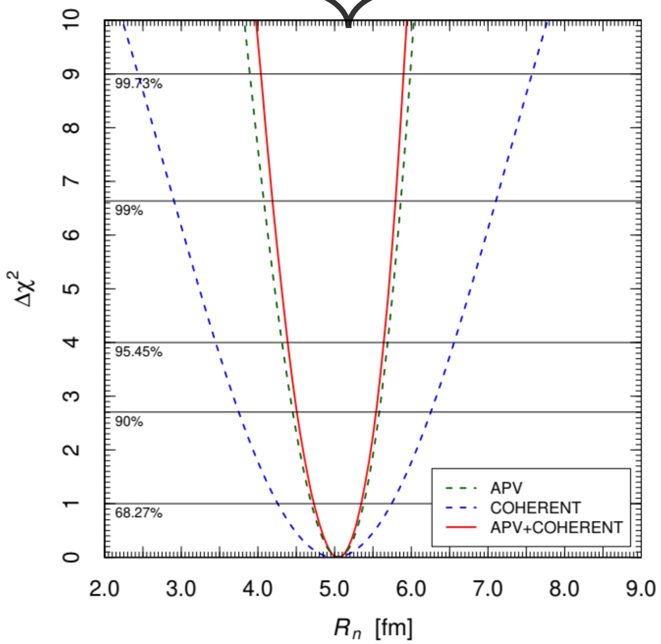

[C. M. Dordei F. et al., ArXiv:1908.06045]

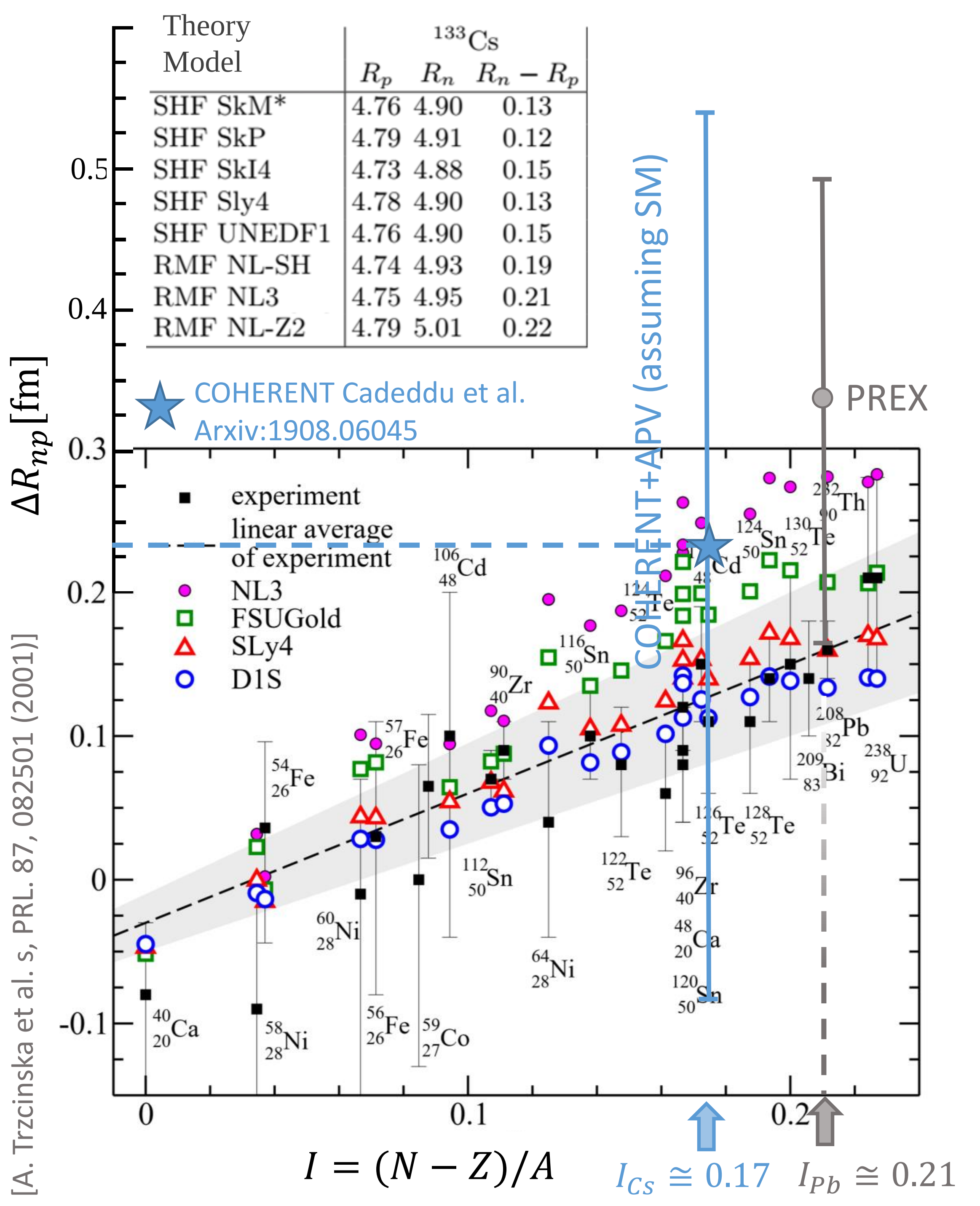

Theory Model	^{133}Cs R_p	R_n	$R_n - R_p$
SHF SkM*	4.76	4.90	0.13
SHF SkP	4.79	4.91	0.12
SHF SkI4	4.73	4.88	0.15
SHF Sly4	4.78	4.90	0.13
SHF UNEDF1	4.76	4.90	0.15
RMF NL-SH	4.74	4.93	0.19
RMF NL3	4.75	4.95	0.21
RMF NL-Z2	4.79	5.01	0.22

Cs NEUTRON SKIN MEASUREMENT USING COHERENT AND APV

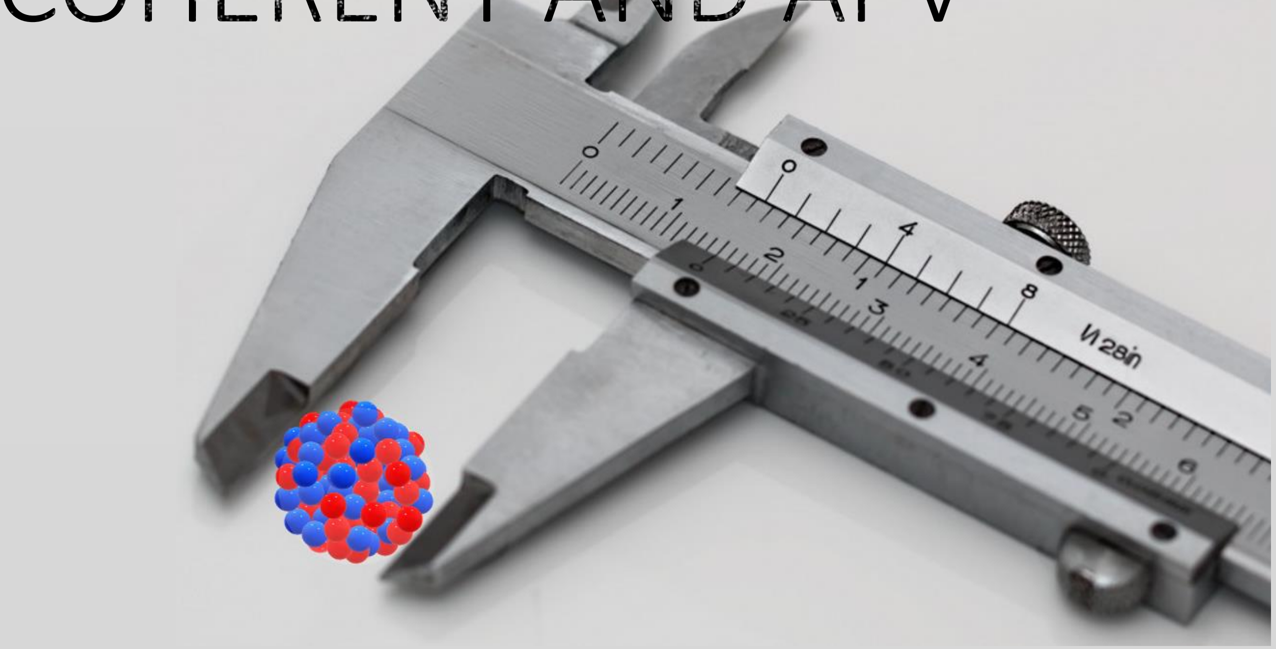

$$\Delta R_{np}^{Cs} = 0.62 \pm 0.31 \text{ fm}$$

COHERENT+APV (Old β)

$$\Delta R_{np}^{Cs} = 0.23 \pm 0.31 \text{ fm}$$

COHERENT (with different QF) + APV (New β)

Unique measurements for Cs

The COHERENT experiment

August 2017: First observation of CEnNS after 40 year from its prediction!

The CEnNS has eluded detection for **four decades**, even though its predicted cross-section is the largest by far of all low-energy neutrino couplings.

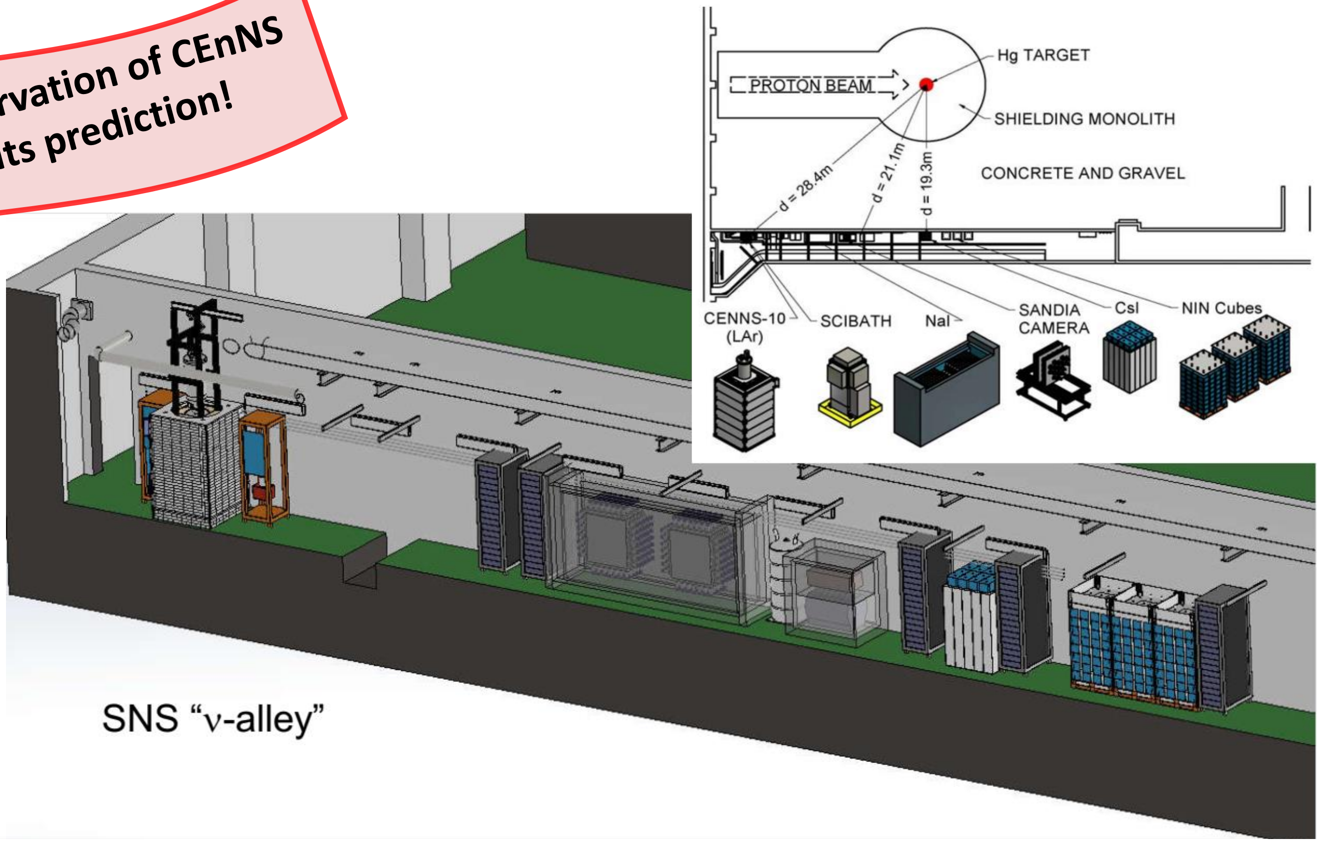

D. Akimov et al. "Observation of Coherent Elastic Neutrino-Nucleus Scattering" ***Science*** *357.6356 (2017)*

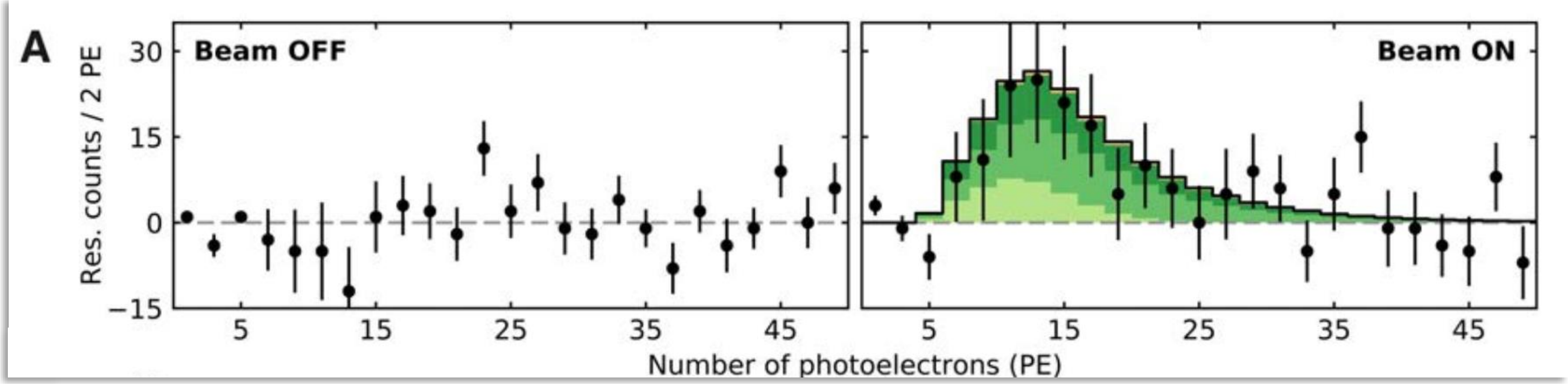

They observe this process at a 6.7σ CL, using a low-background, 14.6-kg CsI scintillator exposed to the neutrino emissions from the Spallation Neutron Source at Oak Ridge National Laboratory.

The COHERENT experiment (result)

- The Likelihood analysis, using the standard CEnNS cross section (**with a unique nuclear form factor**) showed that the best-fit value is **134 ± 22 CEnNS** events.

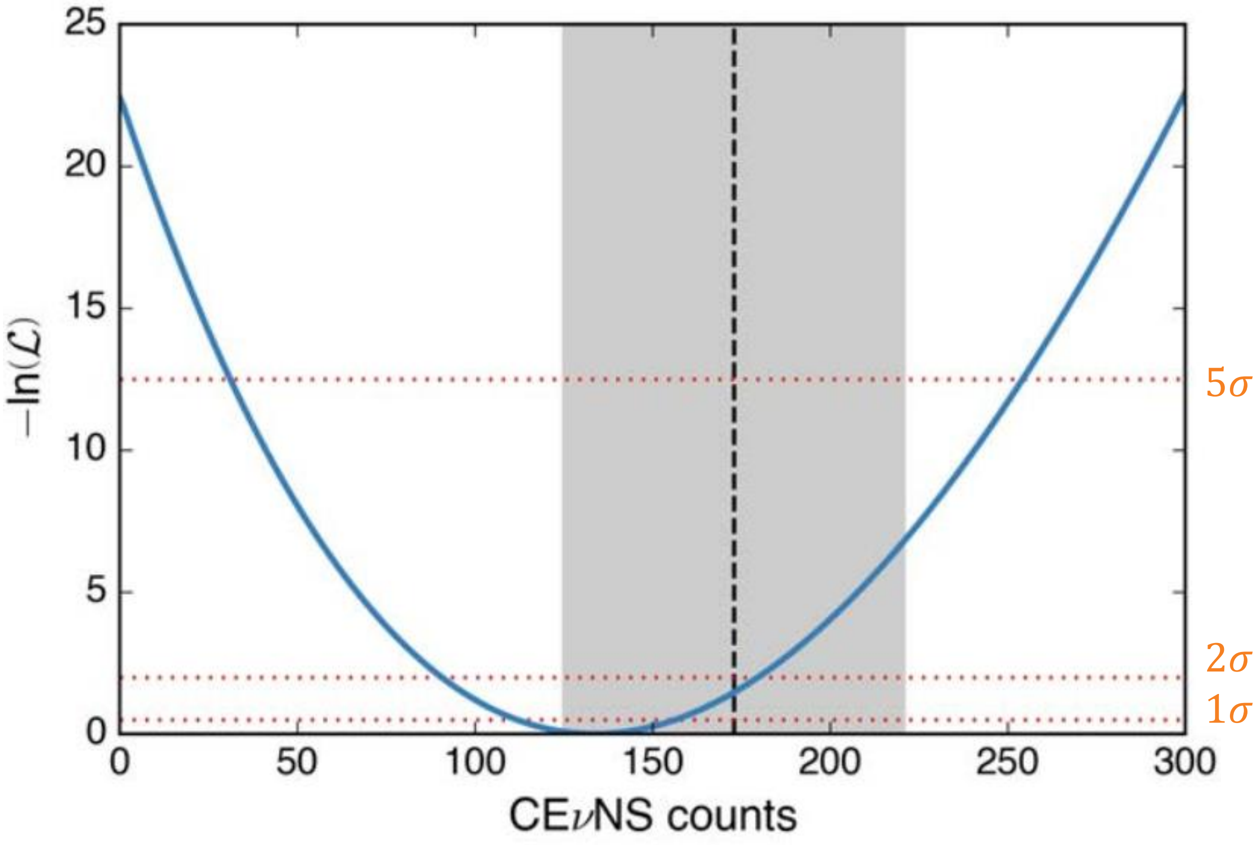

The result is within the 68% confidence band of the Standard Model prediction of **173 events**, shown as a shaded region and a vertical dashed line.

Comparison of log-likelihood values at counts of 0 and 134 indicates that the null hypothesis, corresponding to an absence of CEnNS events, is rejected at a level of 6.7-sigma, relative to the best fit.

This small discrepancy has been interpreted invoking **non standard interactions** between neutrinos and quarks (*arXiv:1712.09667, arXiv:1711.09773, arXiv:1710.09360, PLB 775 54-57, PRD 96 11, 115007 and many more…*) *however **relaxing the approximation of a unique form factor** for protons and neutrons it is possible to better fit the data.*

The CEnNS process as unique probe of the neutron density distribution of nuclei

The CEnNS process itself can be used to provide the first **model independent measurement of the neutron distribution radius**, which is basically unknown for most of the nuclei.

Even if it sounds strange, spatial distribution of neutrons inside nuclei is basically unknown!

The rms neutron distribution radius Rn and the difference between Rn and the rms radius Rp of the proton distribution (the so-called “**neutron skin**”)

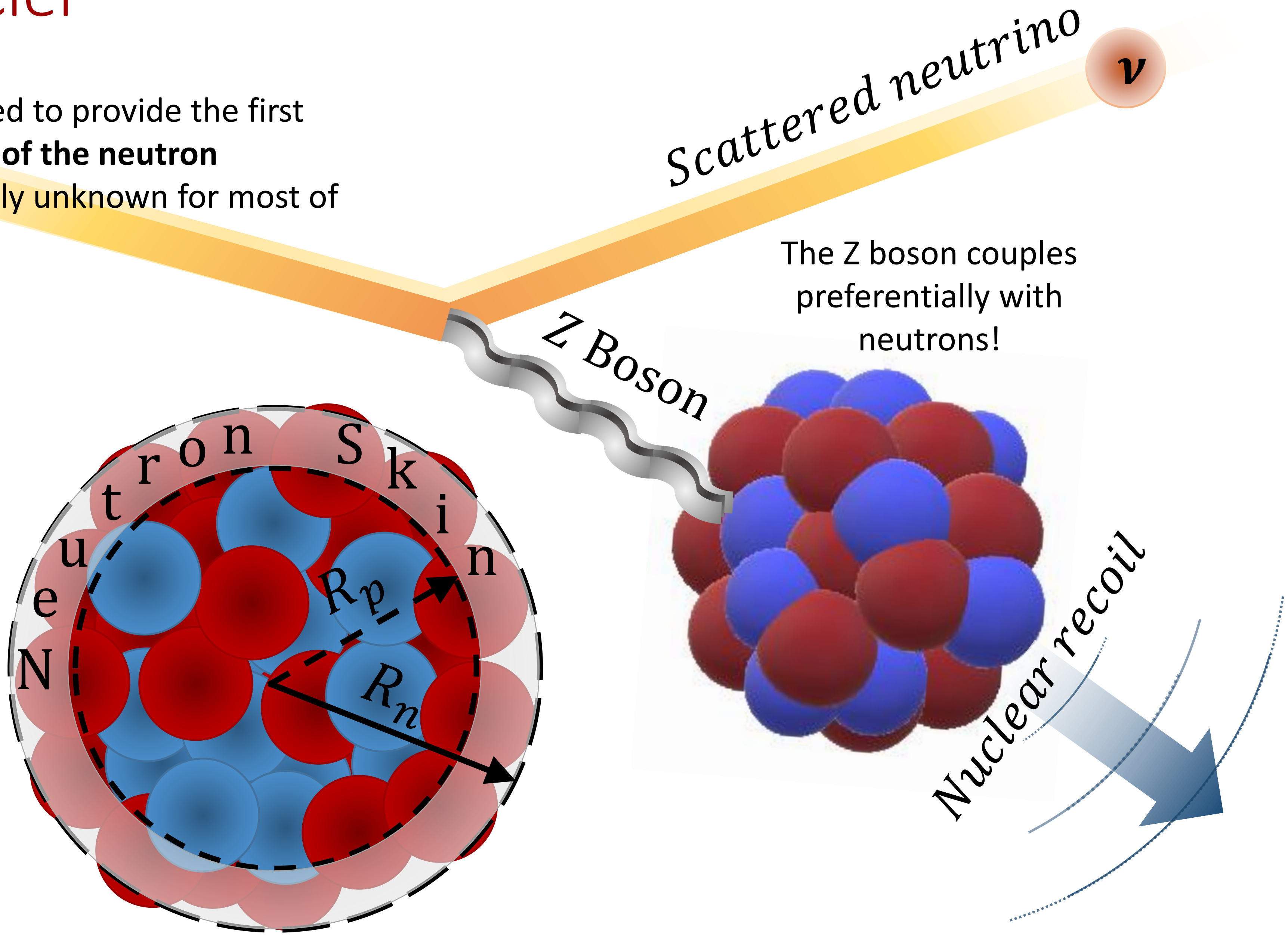

The Z boson couples preferentially with neutrons!

The proton form factor

$$\frac{d\sigma_{\nu-CsI}}{dT} = \frac{G_F^2 M}{4\pi}\left(1 - \frac{MT}{2E_\nu^2}\right)[N\, \boldsymbol{F_N(T, R_n)} - \varepsilon Z\, \boldsymbol{F_Z(T, R_p)}]^{\,2}$$

The proton structures of $^{133}_{55}Cs$ $(N = 78)$ and $^{127}_{53}I$ $(N = 74)$ have been studied with muonic spectroscopy and the data were fitted with **two-parameter Fermi density distributions** of the form

$$\rho_F(r) = \frac{\rho_0}{1 + e^{(r-c)/a}}$$

Where, the **half-density radius *c*** is related to the **rms radius** and the *a* parameter quantifies the **surface thickness** $t = 4\, a\, \ln 3$ (in the analysis fixed to 2.30 fm).

- Fitting the data they obtained

$R_p^{Cs} = 4.804$ fm (Caesium proton rms radius)
$R_p^{I} = 4.749$ fm (Iodine proton rms radius)

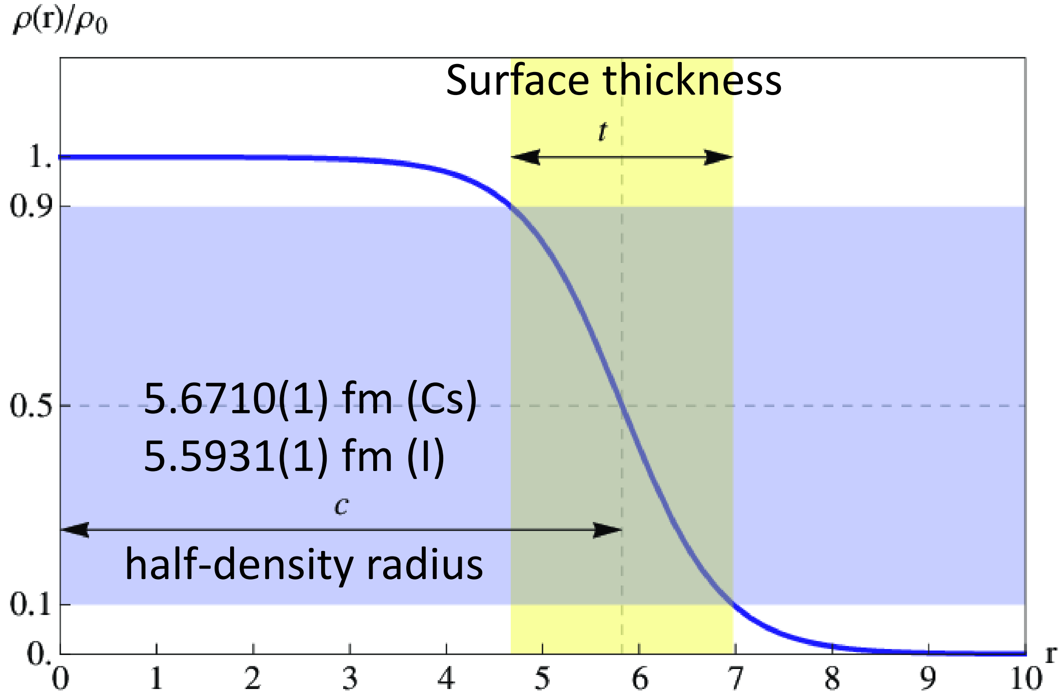

First average CsI neutron density distribution measurement

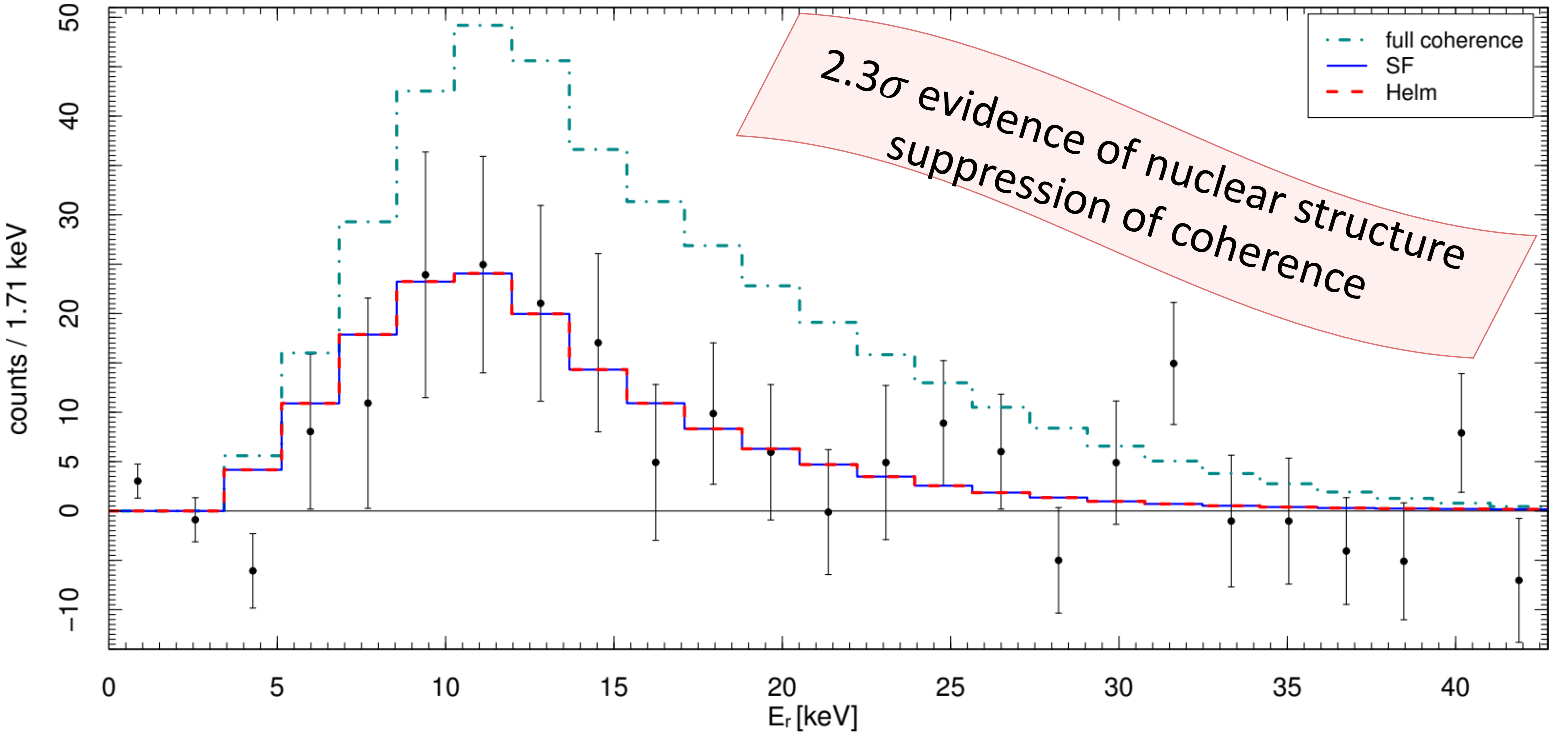

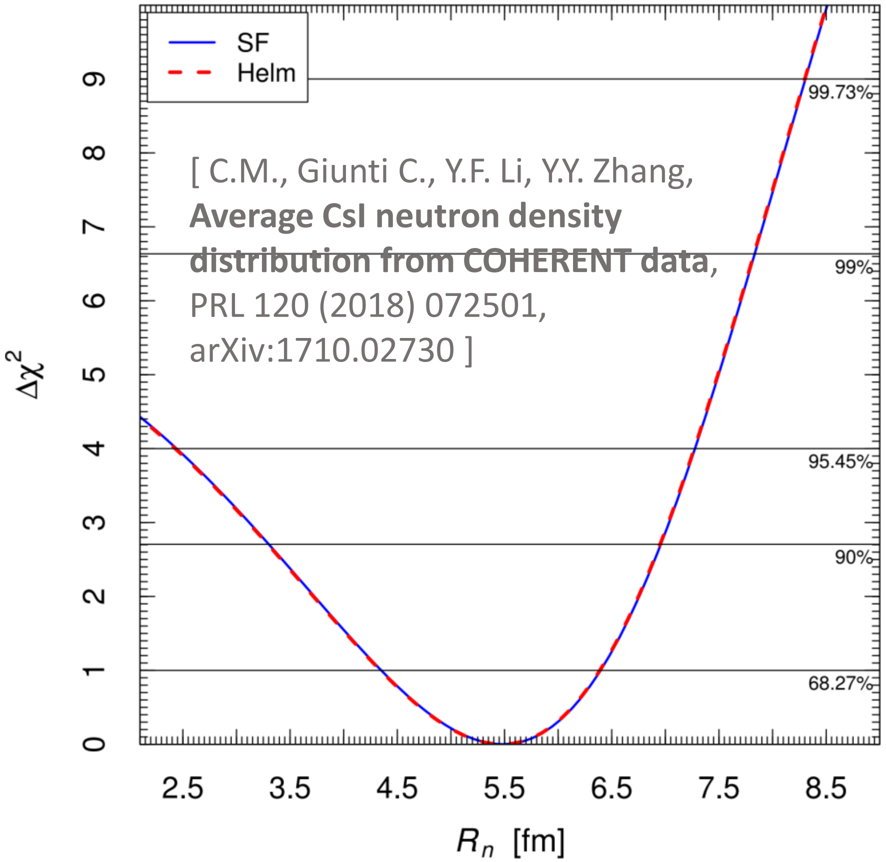

- We first compared the data with the predictions in the case of full coherence, i.e. all nuclear form factors equal to unity: **the corresponding histogram does not fit the data**.

- We fitted the COHERENT data in order to get information on the value of the neutron rms radius R_n, which is **determined by the minimization of the χ^2** using the **symmetrized Fermi** and **Helm form factors**.

This is the first model independent measurement of the CsI neutron radius

$$R_n^{CsI} = 5.5^{+0.9}_{-1.1}\ \text{fm}$$

The neutron skin

$$R_n^{CsI} = 5.5^{+0.9}_{-1.1}\ \text{fm}$$

Proton rms radius for Cs and I

$R_p^{Cs} = 4.804$ fm and
$R_p^{I} = 4.749$ fm
are around 4.78 fm, with a difference of about 0.05 fm

The neutron skin

$$\Delta R_{np}^{CsI} \equiv R_n - R_p \cong 0.7^{+0.9}_{-1.1}\ \text{fm}$$

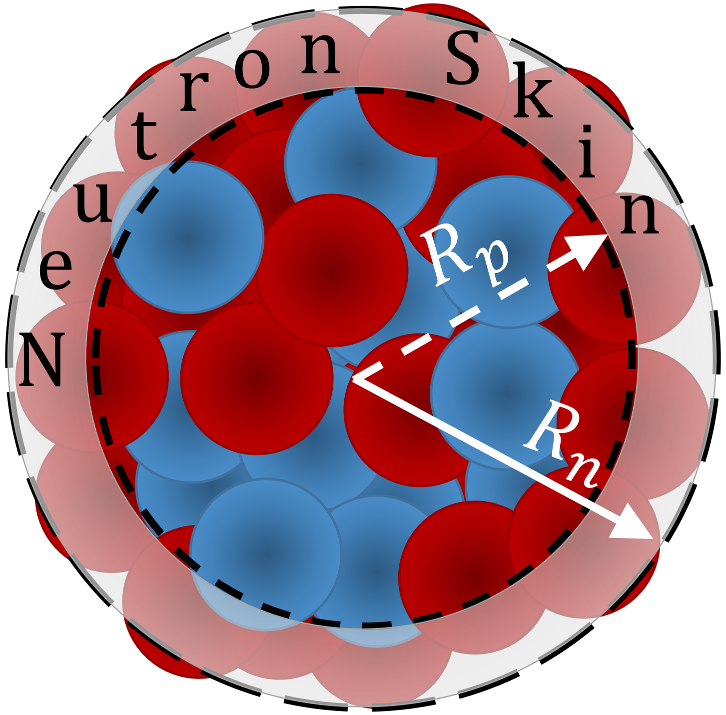

Theoretical values of the proton and neutron rms radii of Cs and I obtained with nuclear mean field models. The value is compatible with all the models...

	^{133}Cs			^{127}I			CsI		
Model	R_p	R_n	$R_n - R_p$	R_p	R_n	$R_n - R_p$	R_p	R_n	$R_n - R_p$
SHF SkM* [20]	4.76	4.90	0.13	4.71	4.84	0.13	4.73	4.86	0.13
SHF SkP [21]	4.79	4.91	0.12	4.72	4.84	0.12	4.75	4.87	0.12
SHF SkI4 [22]	4.73	4.88	0.15	4.67	4.81	0.14	4.70	4.83	0.14
SHF Sly4 [23]	4.78	4.90	0.13	4.71	4.84	0.13	4.73	4.87	0.13
SHF UNEDF1 [24]	4.76	4.90	0.15	4.68	4.83	0.15	4.71	4.87	0.15
RMF NL-SH [25]	4.74	4.93	0.19	4.68	4.86	0.19	4.71	4.89	0.18
RMF NL3 [26]	4.75	4.95	0.21	4.69	4.89	0.20	4.72	4.92	0.20
RMF NL-Z2 [27]	4.79	5.01	0.22	4.73	4.94	0.21	4.76	4.97	0.21

Neutrino charge radius

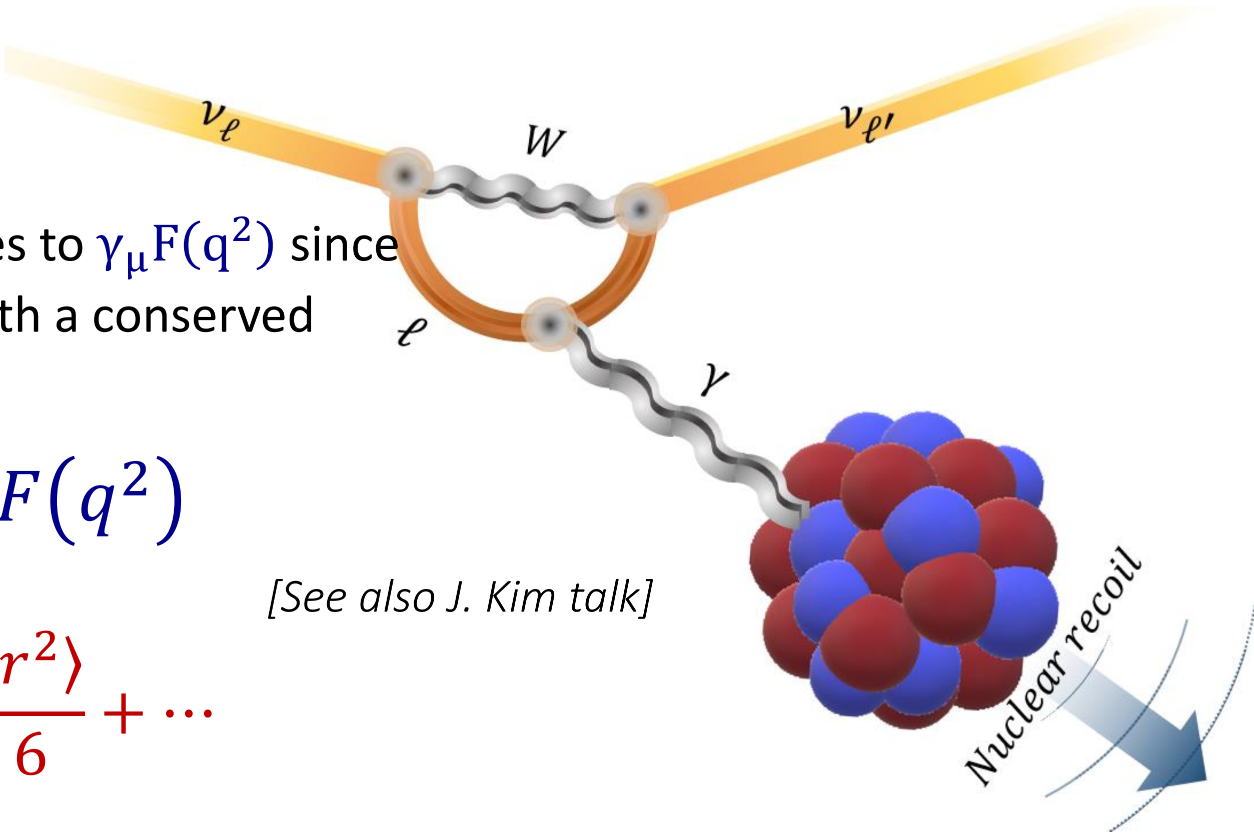

- In the Standard Model (SM) the effective vertex reduces to $\gamma_\mu F(q^2)$ since the contribution $q_\mu \gamma^\mu q_\mu / q^2$ vanishes in the coupling with a conserved current

$$\Lambda_\mu(q) = (\gamma_\mu - q_\mu \gamma^\mu q_\mu / q^2) F(q^2) \cong \gamma_\mu F(q^2)$$

[See also J. Kim talk]

$$F(q^2) = F(0) + q^2 \frac{\mathrm{d}F(q^2)}{\mathrm{d}q^2}\bigg|_{q^2=0} + \cdots = q^2 \frac{\langle r^2 \rangle}{6} + \cdots$$

- In the Standard Model $\langle r^2_{\nu_\ell} \rangle_{SM} = -\frac{G_F}{2\sqrt{2}\pi^2}\left[3 - 2\log\left(\frac{m_\ell^2}{m_W^2}\right)\right]$

$$\langle r^2_{\nu_e} \rangle_{SM} = -8.2 \times 10^{-33}\ cm^2$$
$$\langle r^2_{\nu_\mu} \rangle_{SM} = -4.8 \times 10^{-33}\ cm^2$$
$$\langle r^2_{\nu_\tau} \rangle_{SM} = -3.0 \times 10^{-33}\ cm^2$$

"A charge radius that is gauge-independent, finite is achieved by including additional diagrams in the calculation of $F(q^2)$"

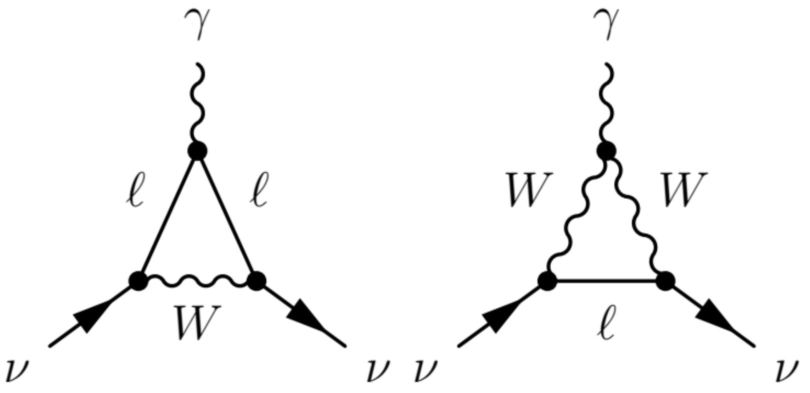

[Bernabeu et al, PRD 62 (2000) 113012, NPB 680 (2004) 450]

Neutrino charge radii contributions to ν_ℓ -$\mathcal{N}$ CEνNS

$$\frac{d\sigma_{\nu_{\ell}-\mathcal{N}}}{dT}(E_\nu,T)=\frac{G_F^2 M}{\pi}\left(1-\frac{MT}{2E_\nu^2}\right)\left\{\left[g_V^n N F_N(|q^2|)+\left(\overbrace{\frac{1}{2}-2\sin^2\vartheta_W}^{g_V^p}-\frac{2}{3}m_W^2\sin^2\vartheta_W\langle r_{\nu_{\ell\ell}}^2\rangle\right)Z F_Z(|q^2|)\right]^2\right.$$

$$\left.+\frac{4}{9}m_W^4\sin^4\vartheta_W\,Z^2F_Z^2(|q^2|)\sum_{\ell'\neq\ell}\left|\langle r_{\nu_{\ell'\ell}}^2\rangle\right|^2\right\}$$

- In the SM there are only diagonal charge radii $\langle r_{\nu_\ell}^2\rangle \equiv \langle r_{\nu_{\ell\ell}}^2\rangle$ because lepton numbers are conserved
- Diagonal charge radii generate the coherent shifts

$$\sin^2\vartheta_W \rightarrow \sin^2\vartheta_W\left(1+\frac{1}{3}m_W^2\langle r_{\nu_\ell}^2\rangle\right) \quad\Longleftrightarrow\quad \nu_\ell+\mathcal{N}\rightarrow\nu_\ell+\mathcal{N}$$

- Transition charge radii generate the incoherent contribution $\Longleftrightarrow$ $\nu_\ell+\mathcal{N}\rightarrow\sum_{\ell'\neq\ell}\nu_{\ell'\neq\ell}+\mathcal{N}$

$$\frac{4}{9}m_W^4\sin^4\vartheta_W\,Z^2F_Z^2(q^2)\sum_{\ell'\neq\ell}\left|\langle r_{\nu_{\ell'\ell}}^2\rangle\right|^2$$

Transition charge radii change the flavor of the neutrino in the final state of the elastic scattering process

[K. Kouzakov, A. Studenikin, PRD 95 (2017) 055013, arXiv:1703.00401]

Experimental bounds on neutrino charge radii

Elastic neutrino electron scattering $\nu_\ell + e^- \to \nu_\ell + e^-$

Method	Experiment	Limit [cm^2]	CL	Year
Reactor $\bar{\nu}_e\, e^-$	Krasnoyarsk	$\lvert\langle r^2_{\nu_e}\rangle\rvert < 7.3 \times 10^{-32}$	90%	1992
	TEXONO	$-4.2 \times 10^{-32} < \langle r^2_{\nu_e}\rangle < 6.6 \times 10^{-32}$	90%	2009
Accelerator $\nu_e\, e^-$	LAMPF	$-7.12 \times 10^{-32} < \langle r^2_{\nu_e}\rangle < 10.88 \times 10^{-32}$	90%	1992
	LSND	$-5.94 \times 10^{-32} < \langle r^2_{\nu_e}\rangle < 8.28 \times 10^{-32}$	90%	2001
Accelerator $\nu_\mu\, e^-$	BNL-E734	$-5.7 \times 10^{-32} < \langle r^2_{\nu_\mu}\rangle < 1.1 \times 10^{-32}$	90%	1990
	CHARM-II	$\lvert\langle r^2_{\nu_\mu}\rangle\rvert < 1.2 \times 10^{-32}$	90%	1994

[see the review Giunti, Studenikin, RMP 87 (2015) 531, arXiv:1403.6344]

For small recoil energies the effect of the neutrino charge radii in the case of elastic neutrino-electron scattering turns out to be smaller by a factor of the order of $M/m_e \sim 2 \times 10^5$ with respect to CEνNS

[update in Cadeddu, Giunti, Kouzakov, Li, Studenikin, Zhang, PRD 98 (2018) 113010, arXiv:1810.05606]

Fit of COHERENT time+energy data*

*from COHERENT data release available at http://doi.org/10.5281/zenodo.1286927 Arxiv:1804.09459

➢ Fixed neutron distribution radii (RMF NL-Z2):

$R_n(^{133}Cs) = 5.01$ fm
$R_n(^{133}I) = 4.94$ fm

$\chi^2_{min} = 154.2$
$NDF = 139 \quad GoF = 18\%$

Marginal 90% CL bounds
$[10^{-32}\ cm^2]$

$-63 < \langle r^2_{\nu_e} \rangle < 12$

$-7 < \langle r^2_{\nu_\mu} \rangle < 9$

$|\langle r^2_{\nu_{e\mu}} \rangle| < 22 \quad |\langle r^2_{\nu_{e\tau}} \rangle| < 37$

$|\langle r^2_{\nu_{\mu\tau}} \rangle| < 26$

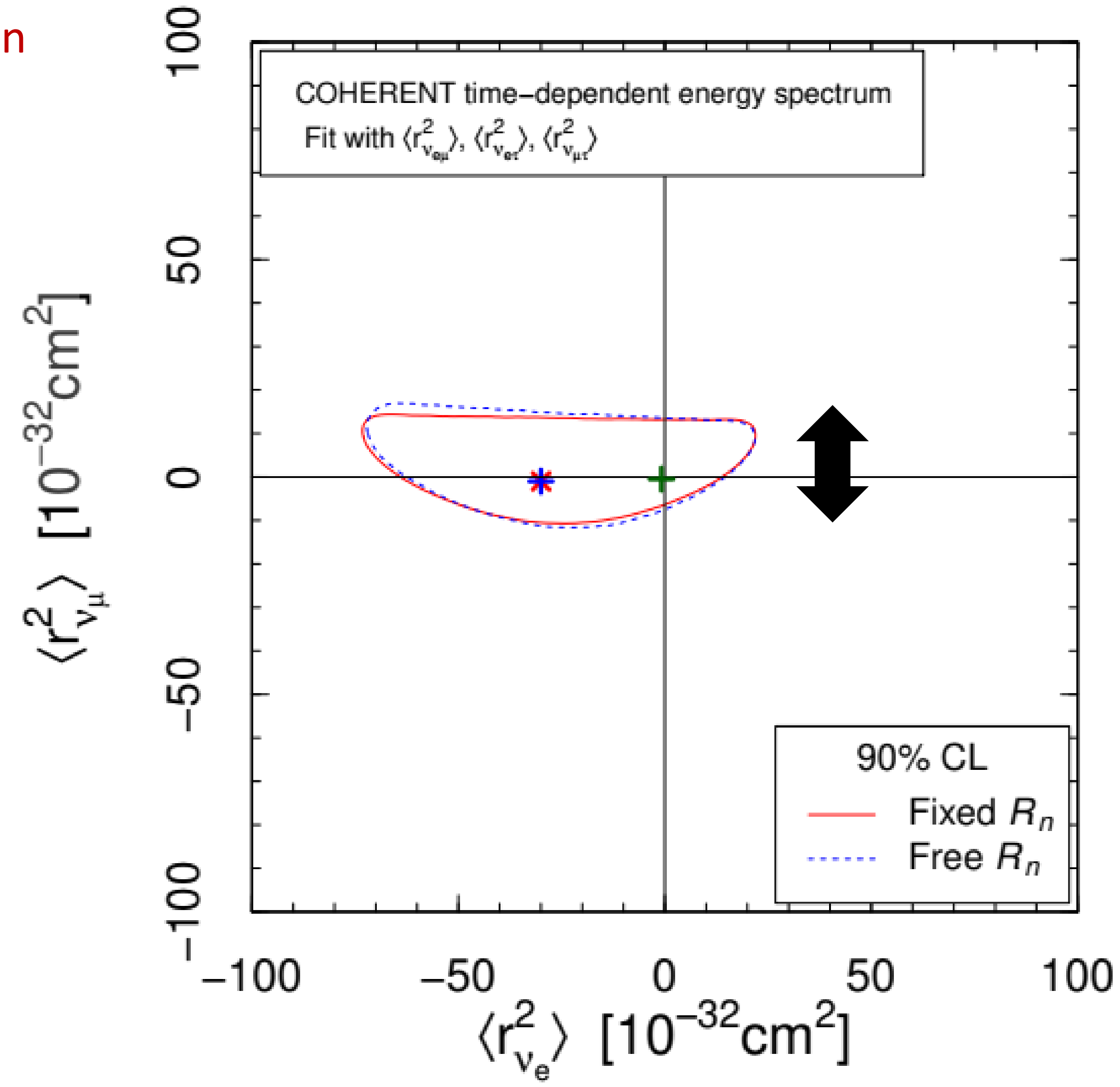

➢ Free neutron distribution radii:

$\chi^2_{min} = 154.2$
$NDF = 137$
$GoF = 15\%$

Marginal 90% CL bounds
$[10^{-32}\ cm^2]$

$-63 < \langle r^2_{\nu_e} \rangle < 12$

$\mathbf{-8 < \langle r^2_{\nu_\mu} \rangle < 11}$

$|\langle r^2_{\nu_{e\mu}} \rangle| < 22 \quad |\langle r^2_{\nu_{e\tau}} \rangle| < 38$

$|\langle r^2_{\nu_{\mu\tau}} \rangle| < 27$

Our results on PDG 2019

We have shown that the time information of the COHERENT data allows us to restrict the allowed ranges of the charge radii, especially that of $\langle r^2_{\nu_\mu} \rangle$, for which we obtained the 90% CL allowed interval

$$-8 \times 10^{-32}\ cm^2 < \langle r^2_{\nu_\mu} \rangle < 11 \times 10^{-32}\ cm^2$$

marginalizing over reliable allowed intervals of the rms radii of the neutron distributions of ${}^{133}_{55}Cs$ and ${}^{127}_{53}I$.

This limit is comparable with the BNL-E734 and CHARM-I.

[M. Cadeddu, C. Giunti, K. A. Kouzakov, Y. F. Li, A. I. Studenikin, Y.Y. Zhang, PRD 98 (2018) 113010, Editor' Suggestion, arXiv:1810.05606]

PHYSICAL REVIEW D

covering particles, fields, gravitation, and cosmology

Highlights Recent Accepted Authors Referees Search Press About

Editors' Suggestion Open Access Acce

Neutrino charge radii from COHERENT elastic neutrino-nucleus scattering

M. Cadeddu, C. Giunti, K. A. Kouzakov, Y. F. Li, A. I. Studenikin, and Y. Y. Zhang

Phys. Rev. D **98**, 113010 – Published 26 December 2018

NEUTRINO CHARGE RADIUS SQUARED

We report limits on the so-called neutrino charge radius squared. While the straight-forward definition of a neutrino charge radius has been proven to be gauge-dependent and, hence, unphysical (LEE 77C), there have been recent attempts to define a physically observable neutrino charge radius (BERNABEU 00, BERNABEU 02). The issue is still controversial (FUJIKAWA 03, BERNABEU 03). A more general interpretation of the experimental results is that they are limits on certain nonstandard contributions to neutrino scattering.

VALUE (10^{-32} cm^2)	CL%	DOCUMENT ID		TECN	COMMENT
−2.1 to 3.3	90	[1] DENIZ	10	TEXO	Reactor $\overline{\nu}_e\, e$
−4 to 5.5	90	[2] CADEDDU	18		ν_μ coherent scat. on CsI
−0.53 to 0.68	90	[3] HIRSCH	03		$\nu_\mu\, e$ scat.
−8.2 to 9.9	90	[4] HIRSCH	03		anomalous $e^+ e^- \to \nu \overline{\nu} \gamma$
−2.97 to 4.14	90	[5] AUERBACH	01	LSND	$\nu_e\, e \to \nu_e\, e$
−0.6 to 0.6	90	VILAIN	95B	CHM2	$\nu_\mu\, e$ elastic scat.
0.9 ±2.7		ALLEN	93	CNTR	LAMPF $\nu\, e \to \nu\, e$
< 2.3	95	MOURAO	92	ASTR	HOME/KAM2 ν rates
< 7.3	90	[6] VIDYAKIN	92	CNTR	Reactor $\overline{\nu} e \to \overline{\nu} e$
1.1 ±2.3		ALLEN	91	CNTR	Repl. by ALLEN 93
−1.1 ±1.0		[7] AHRENS	90	CNTR	$\nu_\mu\, e$ elastic scat.
−0.3 ±1.5		[7] DORENBOS...	89	CHRM	$\nu_\mu\, e$ elastic scat.
		[8] GRIFOLS	89B	ASTR	SN 1987A

[1] DENIZ 10 observe reactor $\overline{\nu}_e\, e$ scattering with recoil kinetic energies 3–8 MeV using CsI(Tl) detectors. The observed rate and spectral shape are consistent with the Standard Model prediction, leading to the reported constraint on $\overline{\nu}_e$ charge radius.

[2] CADEDDU 18 use the data of the COHERENT experiment, AKIMOV 18. The limit is $\langle r^2_\nu \rangle$ for ν_μ obtained from the time-dependent data. Weaker limits were obtained for charge radii of ν_e and for transition charge radii. The published value was divided by 2 to conform to the convention of this table.

[M. Tanabashi et al. (Particle Data Group), Phys. Rev. D 98, 030001 (2018) and 2019 update]